



HAL
open science

Speciation and distribution of chromium (III) in rice root tip and mature zone: The significant impact of root exudation and iron plaque on chromium bioavailability

Peiman Zandi, Xing Xia, Jianjun Yang, Jin Liu, Laurent Remusat, Cornelia Rumpel, Elke Bloem, Beata Barabasz Krasny, Ewald Schnug

► To cite this version:

Peiman Zandi, Xing Xia, Jianjun Yang, Jin Liu, Laurent Remusat, et al.. Speciation and distribution of chromium (III) in rice root tip and mature zone: The significant impact of root exudation and iron plaque on chromium bioavailability. *Journal of Hazardous Materials*, 2023, 448, pp.130992. 10.1016/j.jhazmat.2023.130992 . hal-04034436

HAL Id: hal-04034436

<https://cnrs.hal.science/hal-04034436v1>

Submitted on 17 Mar 2023

HAL is a multi-disciplinary open access archive for the deposit and dissemination of scientific research documents, whether they are published or not. The documents may come from teaching and research institutions in France or abroad, or from public or private research centers.

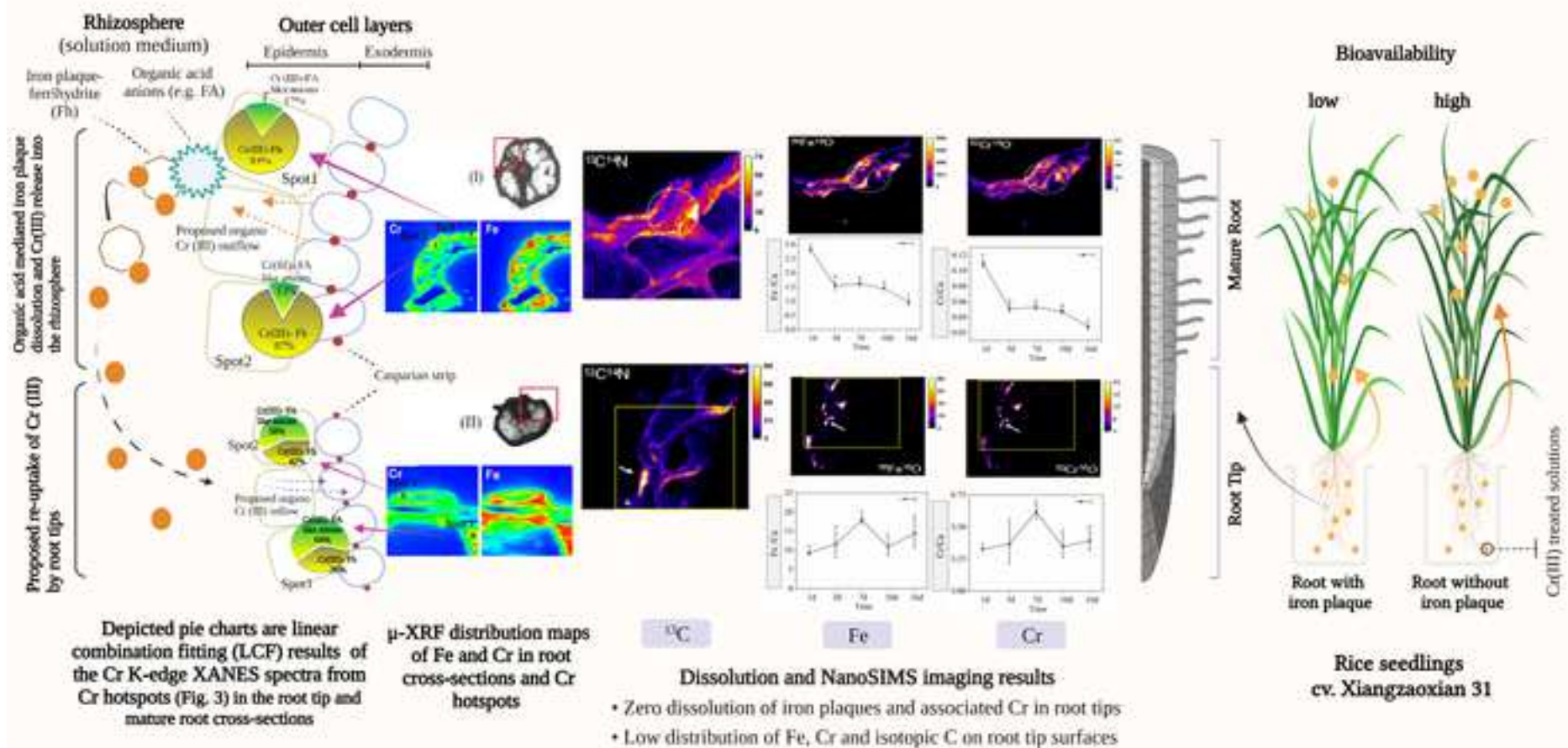
L'archive ouverte pluridisciplinaire **HAL**, est destinée au dépôt et à la diffusion de documents scientifiques de niveau recherche, publiés ou non, émanant des établissements d'enseignement et de recherche français ou étrangers, des laboratoires publics ou privés.

Copyright

Journal of Hazardous Materials

Speciation and distribution of chromium (Cr) in rice root tip and mature zone: the importance and impact of root exudation and iron plaque in Cr bioavailability --Manuscript Draft--

Manuscript Number:	HAZMAT-D-22-13168R1
Article Type:	Research Paper
Keywords:	Cr-speciation; Iron-plaque dissolution; NanoSIMS analysis; phytometabolites; root morphology
Corresponding Author:	Jianjun Yang, Prof. PhD. Chinese Academy of Agricultural Sciences Institute of Environment and Sustainable Development in Agriculture Beijing, CHINA
First Author:	Peiman Zandi, Assistant Prof.
Order of Authors:	Peiman Zandi, Assistant Prof. Xing Xia, PhD Jianjun Yang, Prof. PhD. Jin Liu, Associate Prof. Remusat Laurent, PhD Cornelia Rumpel, Prof. Elke Bloem, PhD Beata Barabasz Krasny, Associate Prof. Ewald Schnug, Prof. Dr
Suggested Reviewers:	Hamid Madani, PhD Prof., Islamic Azad University Arak Branch h-madani@iau-arak.ac.ir Ameer Hussain Jarwar, PhD Agricultural Research Institute jhomper@gmail.com Donald Spark, PhD Prof., University of Delaware dlsparks@udel.edu



Speciation and distribution of chromium (Cr) in rice root tip and mature zone: the importance and impact of root exudation and iron plaque in Cr bioavailability

Peiman Zandi^{a#,b}, Xing Xia^{a#}, Jianjun Yang^{a*}, Jin Liu^c, Remusat Laurent^d, Cornelia Rumpel^e, Elke Bloem^f, Beata Barabasz Krasny^g, Ewald Schnug^h

^a Institute of Environment and Sustainable Development in Agriculture, Chinese Academy of Agricultural Science, Beijing 100081, P. R. China

^b International Faculty of Applied Technology, Yibin University, Yibin 644000, China

^c College of Agronomy and Biotechnology, China Agricultural University, Beijing 100094, China

^d Muséum National d'Histoire Naturelle, Institut de Minéralogie, Physique des Matériaux et Cosmochimie, CNRS UMR 7590, Sorbonne Université, 75005 Paris, France

^e CNRS, Institute of Ecology and Environmental Sciences of Paris, IEES, UMR (CNRS-INRA-UPMC-UPEC-IRD), Thiverval-Grignon, 78850, France

^f Julius Kühn-Institut, Federal Research Centre for Cultivated Plants, Institute for Crop and Soil Sciences, Bundesallee 69, 38116 Braunschweig, Germany

^g Institute of Biology, Pedagogical University of Krakow, Podchorążych 2 St., 30-084 Kraków, Poland

^h Institute for Plant Biology, Department of Life Sciences, Technical University of Braunschweig, 38106 Braunschweig, Germany

[#]Xing Xia and Peiman Zandi equally contributed to this work.

* Corresponding author.

E-mail address: yangjianjun@caas.cn; yangjianjun-caas@outlook.com (J. Yang)

1 **Speciation and distribution of chromium (Cr) in rice root tip and mature** 2 **zone: the importance and impact of root exudation and iron plaque in Cr** 3 **bioavailability**

4 **Abstract**

5 Evidence on the contribution of root regions with varied maturity levels in iron plaque (IP) formation
6 and root exudation of metabolites and their consequences for uptake and bioavailability of chromium
7 (Cr) remains unknown. Therefore, we applied combined nanoscale secondary ion mass spectrometry
8 (NanoSIMS) and synchrotron-based techniques, micro-X-ray fluorescence (μ -XRF) and micro-X-ray
9 absorption near-edge structure (μ -XANES) to examine the speciation and localisation of Cr and the
10 distribution of (micro-) nutrients in rice root tip and mature region. μ -XRF mapping revealed that the
11 distribution of Cr and (micro-) nutrients varied between root regions. Cr K-edge XANES analysis at
12 Cr hotspots attributed the dominant speciation of Cr in outer (epidermal and sub-epidermal) cell
13 layers of the root tips and mature root to Cr(III)-FA (fulvic acid-like anions) (58-64%) and Cr(III)-Fh
14 (amorphous ferrihydrite) (83-87%) complexes, respectively. The co-occurrence of a high proportion
15 of Cr(III)-FA species and strong co-location signals of $^{52}\text{Cr}^{16}\text{O}$ and $^{13}\text{C}^{14}\text{N}$ in the mature root
16 epidermis relative to the sub-epidermis indicated an association of Cr with active root surfaces, where
17 the dissolution of IP and release of their associated Cr are likely subject to the mediation of organic
18 anions. The results of NanoSIMS (poor $^{52}\text{Cr}^{16}\text{O}$ and $^{13}\text{C}^{14}\text{N}$ signals), dissolution (no IP dissolution)
19 and μ -XANES (64% in sub-epidermis >58% in the epidermis for Cr(III)-FA species) analyses of root
20 tips may be indicative of the possible re-uptake of Cr by this region. The results of this research work
21 highlight the significance of IP and organic anions in rice root systems on the bioavailability and
22 dynamics of Cr.

23
24 **Keywords:** Cr-speciation, Iron-plaque dissolution, NanoSIMS analysis, phytometabolites, root
25 morphology

26 **Environmental Implications**

27 Considering how different root regions with varied iron plaque presence, dissolution rate, and
28 diverse root metabolites and their exudations may affect the fate of Cr uptake and bioavailability in
29 rice plants, the present study has, for the first time, set the stage for holistic investigation of two
30 critical parts of the root (tip/mature root) system at a molecular level using combined NanoSIMS and
31 synchrotron-based (μ -XRF/ μ -XANES) techniques. The findings of this study appear to be significant
32 for current and future studies on suppressing heavy metal bioavailability in contaminated paddy soil
33 systems.

34

35 **1. Introduction**

36 Soil contamination with heavy metals, especially chromium (Cr), is a widespread problem that
37 poses threats to human health risks through the food chain (Yang et al., 2019a; Ali et al., 2022).
38 In China, Cr is one of the eight heavy metals most strongly affecting agricultural soils, with a
39 contamination rate exceeding 1.1% (Zhao et al., 2015). Based on the China National Food Hygiene
40 Standard (GB 2762-2017), the bioaccessibility of Cr in rice grain should not exceed the Cr threshold
41 value of 1.0 mg.kg⁻¹ (Geng et al., 2020; Ali et al., 2022) to avoid adverse health complications (e.g.,
42 oxidative stress and DNA damage) associated with dietary Cr intake (Nickens et al., 2010; Khan et al.,
43 2012). Therefore, controlling Cr transfer in the soil-rice system is crucial for food safety.

44 Root uptake in rice is considered to be the major entry route of soil Cr into edible rice grains. The
45 root system of rice plants consists of seminal, nodal (primary), and lateral roots (Gu et al., 2017).
46 Among them, primary roots are classified into root tips and mature root regions according to the level
47 of development (Seyferth et al., 2010; Zandi et al., 2022). Root tips have underdeveloped vascular
48 systems, lacking the complete formation of the aerenchyma and Casparian bands (CBs). They account
49 only for a small fraction of the overall mineral element uptake in rice plants, while mature rice roots
50 have a fully developed anatomical structure with the cortex (exodermis, aerenchyma, endodermis) and
51 stele (xylem) that support the influx and transport of mineral nutrients (Yamaji and Ma, 2007;
52 Coudert et al., 2010; Fukao et al., 2019).

53 Similarly to many aquatic or semi-aquatic plants, rice is a hydrophyte species grown in flooded
54 paddy fields. Rice has to cope with anaerobic conditions by radial oxygen diffusion from the root
55 aerenchyma towards the root surface and adjacent rhizosphere (Deng et al., 2010; Xu et al., 2018),
56 where it mediates iron oxidation [Fe (II) to Fe (III)] and development of an amorphous coating of iron
57 (hydr)oxides (known as iron plaque, IP) on the root surface (Cheng et al., 2014; Tripathi et al., 2014;
58 Zandi et al., 2022). Moreover, continuous flooding was indicated to create a favourable rhizosphere
59 environment for IP formation (Xiao et al., 2021). The physical barrier of IP has been proposed to
60 serve as a natural protection mechanism against excess heavy metal concentration in plant parts (Khan
61 et al., 2016).

62 There is consensus that root capacity for aerobic respiration is the main factor in the oxidising
63 power of the rhizoplane zone (Wu et al., 2012; Holzschuh et al., 2014), and consequently the degree
64 of IP formation (Zandi et al., 2022). Rice root tips with no discernible aerenchyma structures were
65 found to have a higher oxygen discharge in comparison to the basal part of the root (Nishiuchi et al.,
66 2012). Nonetheless, IP was shown to be less frequent around the root tips (Williams et al., 2014) due
67 to their rapid development (Nishiuchi et al., 2012), possibly affecting heavy metal speciation and
68 mobility in this region compared to the basal root region.

69 Many studies concerning the whole root system have shown that iron (hydr)oxides have a strong
70 binding affinity for metal(loid) ions on the root surface and reduce their mobility and bioavailability,
71 thereby inhibiting the uptake and transport of toxic metals, including Cr (Hu et al., 2014; Cao et al.,
72 2018; Zandi et al., 2022). Previous studies have shown that in the absence or weak presence of IP,
73 higher concentrations of Cr were accumulated in root cells rather than in shoots of rice (Xu et al.,
74 2018; Zandi et al., 2020, 2021), suggesting that Cr mainly deposited in root cell walls hindered its
75 transport to the aerial organs (Zeng et al., 2011). The hydroponic and soil culture experiments have
76 demonstrated that an appropriate amount of IP on root surfaces could effectively adsorb Cr(III) and
77 Cr(VI) species and reduce their transfer to the rice roots and shoots, thus decreasing Cr concentrations
78 in rice tissues (Xu et al., 2018; Yu et al., 2017; Zandi et al., 2020).

79 In addition to the inhibition of iron (hydr)oxides, other factors such as root exudates, which
80 mainly consist of low or fairly low molecular weight (LMW) organic anion metabolites, with various

81 chemical functional groups (e.g., $-\text{COOH}$, $-\text{OH}$) (Seal et al., 2004), have been proposed to interact
82 with iron (hydr)oxides during sorption and chelation of heavy metals in the soil (Zhang et al., 2020)
83 and plant systems (Wang et al., 2019). Moreover, earlier studies have shown that these metabolites
84 can enhance the dissolution of iron (hydr)oxides bound to heavy metals, leading to their release into
85 the rhizosphere (Sebastian and Prasad, 2016; Luo et al., 2017; Saad et al., 2017). Studies on the entire
86 root system in environments contaminated with cadmium (Cd), aluminium (Al) and Cr have indicated
87 that organic anion secretions are highly associated with increased heavy metal tolerance through their
88 efflux into the rhizosphere (Yang et al., 2013; Saad et al., 2017; Yang et al., 2019b; Bali et al., 2020).
89 This efficient exclusion mechanism reduces metal uptake and accumulation in plants (Montiel-Rozas
90 et al., 2016).

91 In the rice root system, these metabolites may also act as a defensive barrier for the roots by
92 forming stable complexes with Cr (Uren, 2000; Zeng et al., 2008) or affecting their reduction and
93 immobilisation in the root (Xiao et al., 2023). Therefore, the contribution of root exudates to increased
94 Cr accumulation in rice roots could be related to the tolerance mechanism through chelation (Hayat et
95 al., 2012; Agnello et al., 2014). The rate and composition of metabolites released in response to Cr
96 stress correlate with plant genotype (Zeng et al., 2008) and metal speciation of Cr (Pradas del Real et
97 al., 2014).

98 Previous studies on the importance of IP or root exudation in suppressing the bioavailability of
99 heavy metal Cr in rice plants mainly focused on the evaluation of the entire root system (Zandi et al.,
100 2020; Xiao et al., 2023). This study has addressed for the first time how individual root regions with
101 varied maturity levels (e.g., less developed tips) may differ in the degree of IP formation or in the
102 secretion of organic anions in response to Cr stress. Further, the issues concerning the correlation of
103 these secretions with IP dissolution and Cr release, and whether IP dissolution mediated by root
104 metabolites can alter Cr mobility and bioavailability have also been analysed. Moreover, it remains
105 unclear whether the main root regions vary in their contribution to Cr chelation and immobilisation,
106 and reduced Cr accumulation in tissues under the influence of iron plaque and root exudation.
107 To bridge the gap, the present study explicitly proposed the combined application of state-of-the-art
108 high-sensitivity ion mass spectrometry (NanoSIMS) and synchrotron-based microprobe techniques,

109 such as micro-X-ray absorption near-edge structure spectroscopy (μ -XANES) and micro-beam X-ray
110 fluorescence (μ -XRF), to investigate the distribution and/or speciation of elements of interest (X) in
111 different root regions (root tips/ mature root) of rice at submicro- and microspatial scales, and their
112 association with ^{13}C -labelled root exudates on the active root surface.

113 The objectives of this study were to (1) explain/assess the interaction between Cr and Fe and its
114 effect on Cr uptake and translocation in rice plants, (2) elucidate the molecular speciation of Cr and
115 binding mechanisms of Cr species in different root regions, and (3) to localise the active root surface
116 with exudate release and its impact on Cr uptake by different root regions. We expected that these
117 results would provide a theoretical basis for understanding heavy metal sequestration and dynamics
118 on iron plaques and their benefits to human health by reducing rice contamination. We expected that
119 these results would provide a theoretical basis for understanding heavy metal sequestration and
120 dynamics on iron plaques and their benefit to human health by reducing rice contamination.

121

122 **2. Materials and methods**

123 2.1. Plant culture, treatments and metal extraction

124 Rice seed (*Oryza sativa* L. Var. Xiangzaoxian 31) germination (7 days on moist gauze in plastic
125 Petri dishes in the dark at 28°C) and initial growth (21 days in black plastic containers) were
126 conducted under controlled sterile conditions in half-strength nutrient solution (Table Supplementary
127 (S) 1-S1), as previously described (Zandi et al., 2021). The variety was a high-quality, early-maturing,
128 hybrid-based (Chen et al., 2000; Yu, 2018) model crop for bioremediation studies used at the Institute
129 of Environment and Sustainable Development in Agriculture, Chinese Academy of Agricultural
130 Sciences in Beijing.

131 The seedlings of the first group, intended for iron plaque (IP) formation (Fe80-CK; Fig. S1),
132 were transferred to solutions spiked with 80 mg L⁻¹ ferrous iron (FeSO₄·7H₂O), incubated for 24 h
133 and subsequently transferred into quarter strength and total strength nutrient solution for 2 and 3 days,
134 respectively. The second group (Fe0-Cr(III)) was not subjected to IP induction, but was grown in a
135 nutrient solution containing 1.0 mg L⁻¹ CrCl₃·6H₂O for 3 days, and then transferred to a quarter-

136 strength nutrient solution for 2 days. The first two groups were exclusively designed for
137 bioavailability analysis and were not included in the follow-up investigations described in sections 2.2,
138 2.3 and 2.4. The third group (Fe80-Cr(III)) was a combination of the two aforementioned treatments,
139 where seedlings with IP were exposed to Cr(III)-spiked solutions for 3 days. Each treatment was
140 performed in three replicates. Replenishment of depleted nutrients in culture solutions was carried out
141 every three days, and manual adjustment of the solutions to a suitable pH of 5.5 was done using 0.1 M
142 HCl and NaOH (Zandi et al., 2020). All seedlings were grown in a controlled plant growth chamber
143 (PGX-350D, NSEI Co., Ltd., China) with a relative humidity of 70% dedicated to predetermined
144 periodic dark (10 h, 20 °C) and light (14 h, 28 °C, 300-350 $\mu\text{mol m}^{-2}\text{s}^{-1}$) regimes. The selected Fe and
145 Cr concentrations were based on recommendations and results of earlier studies (Hu et al. 2014; Li et
146 al., 2015; Yu et al., 2017; Zandi et al., 2020).

147 The seedlings were collected, split into roots and shoots and rinsed with deionised water. Fresh
148 roots with IP were initially divided into the tip (from the root cap to the zone without root hair; ~2-3
149 cm) and mature (from the root hair zone to the base of primary roots) sections, and subsequently
150 incubated for 30 min at room temperature (25°C) in 30 mL of cold DCB (dithionite–citrate–
151 bicarbonate) solution containing NaHCO_3 (0.125 M), $\text{Na}_3\text{C}_6\text{H}_5\text{O}_7$ (0.03 M) and $\text{Na}_2\text{S}_2\text{O}_4$ (0.5 g) (Liu
152 et al., 2004). After incubation, the sections were thoroughly washed with deionised water and
153 removed from incubation tubes. The remaining extracts were initially filled up with deionised water to
154 a volume of 50 mL and subsequently passed through a 0.45- μm filter to remove root debris.

155 The digestion of plant materials was carried out according to Hu et al. (2014) with some
156 modifications. Briefly, plaque-free root sections were oven-dried (similar to shoot samples) and
157 homogenised, pre-digested overnight in heat-proof tubes (100 mL) in 5 mL of concentrated HNO_3
158 (~65-68%). Digestion was completed in a digester heating block at 160°C for ~3 h and after cooling
159 to room temperature, diluted in 25 mL of deionised water and filtered. A reagent blank and a series of
160 external standard solutions (e.g., GBW07605) from certified reference materials in China were
161 utilised to validate the quality control and accuracy of the entire digestion procedure. Fe and Cr
162 contents in the digestion solutions and DCB extracts were quantified using ICP-OES (Agilent 5110,
163 Agilent Technologies, Inc., USA).

164 2.2. Synchrotron-based microprobe analysis

165 Freshly sectioned root specimens were stored at -30°C until synchrotron-based microprobe
166 analyses. For $\mu\text{-XRF}$ imaging of root surfaces using the VESPERS beamline at the Canadian Light
167 Source (CLS), the roots were sectioned and flatly fixed on a Kapton tape. For $\mu\text{-XRF}/\mu\text{-XANES}$
168 analyses of root cross sections using the 15U beamline at the Shanghai Synchrotron Radiation Facility
169 (SSRF, Shanghai), the corresponding root sections were cut into 60- μm -thick slices by a microtome,
170 and subsequently mounted onto a Kapton tape for freeze-drying and stored at -20°C (Tian et al., 2010;
171 Lu et al., 2017). As described in previous studies (Yang et al., 2015; Wang et al., 2021), the $\mu\text{-XRF}$
172 method of both beamlines was similar, except that the data in VESPERS were analysed using SMRK
173 software, thus here we have only reported the experimental details for the 15U beamline at the SSRF.

174 X-rays with an incident energy of 10 keV were monochromatised using a Si (111) double-crystal
175 monochromator. The spot size of the X-ray beam was micro-focused to $10\ \mu\text{m} \times 5\ \mu\text{m}$ using a
176 Kirkpatrick-Baez (K-B) mirror system for scanning. The root samples were placed at an angle of 45°
177 to the beam incidence perpendicular to a 7-element Si(Li) detector (e2v, USA). After selecting the
178 region of interest by the microscope, the region was scanned step by step by moving the sample stage
179 with a step size of 5 and 10 μm for x and y direction, respectively. First, the whole fluorescence
180 spectrum was acquired, and then the fluorescence signals of the elements of interest, including K (3.3
181 keV), Ca (3.6 keV), Cr (5.4 keV), Mn (5.9 keV), Fe (6.4 keV) were selected and applied to all pixel
182 spectra to obtain multi-elemental 2D mapping with a dwell time of 1.5 s per pixel. After analysing the
183 $\mu\text{-XRF}$ images using Igor Pro 6.0 software (IGOR), the spots of interest were selected for Cr K-edge
184 $\mu\text{-XANES}$ spectra collection in the fluorescence mode at 25°C . The energy range and step were set to
185 5931-6080 eV and 0.5 eV, respectively. Several scans were collected from each spot and later
186 averaged to obtain a merged spectrum with a better signal-to-noise ratio. At least 2 hotspots from
187 cross-sections of the root tips and mature root regions were considered for $\mu\text{-XANES}$ spectrum
188 collection. Cr foil was also used to calibrate the beamline (X-ray) energy.

189 Cr K edge $\mu\text{-XANES}$ spectra of Cr(III) adsorbed on ferrihydrite (Cr(III)-Fh) and organo-Cr(III)
190 complexes (Cr(III)-FA) (synthesised by the interaction of CrCl_3 with fulvic acid) (Yang et al., 2020)
191 were acquired in the fluorescence mode and Cr(III) acetate in the total electron yield mode, and were

192 referred to as Cr reference standards. Since root iron plaques induced in a short 24-h period were
193 poorly crystallised and mostly amorphous (Xu and Yu, 2013), ferrihydrite, a typical amorphous iron
194 (hydr)oxide formed during iron hydrolysis (Yang et al., 2020), was considered as the principal sorbent
195 for Cr (III) sequestration in rice root IP in this study. Athena software (Ver. 2.1.1) was used for
196 fingerprint and linear combination fitting (LCF) analysis of sample μ -XANES spectra (Ravel and
197 Newville, 2005). Cr speciation and the percentage of each Cr species were determined based on the
198 LCF of Cr K-edge μ -XANES spectra of the hotspots using the spectra of the reference compounds as
199 end-members (Peng et al., 2015). The goodness of data fitting was assessed using the R-factor.

200 It should be noted that the limited root samples (one sample/ root section) and spots (2 hotspots/
201 root cross-sections) measured during the μ -XRF and μ -XANES analyses may not be representative of
202 the whole root samples. However, earlier studies used a similar method and have demonstrated that
203 the output result could account for most of the sample variation (Lombi and Susini, 2009; Seyfferth et
204 al., 2010; Frommer et al., 2011; Li et al., 2015; Yang et al., 2015).

205

206 2.3. ^{13}C labelling of rice and NanoSIMS analysis

207 The procedure for uniform ^{13}C labelling of rice was as described earlier (Ge et al., 2012; Yuan et al.,
208 2016) with some modifications. Briefly, rice seedlings belonging to the third treatment group (Fe80-
209 Cr (III)) were first exposed to CrCl_3 treatment for 24 h and subsequently transferred to normal (Cr-
210 free) nutrient solution and kept in transparent airtight perspex ^{13}C labelling and non-labelling
211 control boxes (40 cm long \times 50 cm wide \times 60 cm high; Fig. S2) for 24 h. During this period, the
212 concentration of ^{13}C inside the labelling box atmosphere was maintained at approximately
213 $400 \mu\text{L L}^{-1}$ (ppm) by controlled injection of 0.1 M $\text{Na}_2^{13}\text{CO}_3$ solution (^{13}C -enriched $> 99\%$) into 1 M
214 HCl solution. A CO_2 detector spectrometer (IRMS, RS-CO2WS-N01-2, Shandong Renke Control
215 Technol. Co., Ltd., China) was used to monitor CO_2 concentration inside the labelling boxes (Kaiser
216 et al., 2015). Isotopic labelling of rice seedlings with ^{13}C was performed by photosynthetic fixation of
217 ^{13}C in the aforementioned labelling boxes. Seedlings incubated in unlabelled control boxes served
218 as the reference factor for excess ^{13}C in shoots and roots after DCB extraction. The environmental
219 growth conditions in the perspex boxes were identical to those described in section 2.1.

220 Rice seedlings were harvested and separated into roots and shoots before IP dissolution could
221 occur, e.g., as a result of the secretion of ^{13}C -labelled and/or unlabelled metabolites by the roots.
222 Afterwards, root and shoot samples from both labelled and unlabelled control seedlings were ground
223 to determine ^{13}C abundance in the respective plant samples using a C/N element analyser coupled to
224 an isotope ratio mass spectrometer to verify successful labelling with ^{13}C (Isoprime 100, Elementar's
225 PYE cube, UK). Freshly sectioned root specimens were immersed in a tissue freezing medium
226 (SAKURA Tissue-Tek OCT) for rapid freezing at -30°C . Root sections were then axially frozen-cut
227 into 60- μm -thick slices using a microtome (Reichert-Jung, Germany). The slices were collected and
228 mounted onto a Si_3N_4 wafer and coated with gold (20 nm thick) for NanoSIMS analysis.

229 Cross-sections of mature roots and root tips were imaged using Cameca NanoSIMS 50 installed at
230 the Museum National d'Histoire Naturelle, Paris, France. The surfaces of the root samples were
231 scanned with a 16 keV Cs^+ (caesium) primary beam, set to 1 pA, leading to a spatial resolution of
232 approximately 150 nm. Secondary ions were collected in multicollection mode: $^{12}\text{C}^-$, $^{16}\text{O}^-$, $^{12}\text{C}^{14}\text{N}^-$
233 and $^{13}\text{C}^{14}\text{N}^-$ in the first run (for C isotope and N/C mapping), and $^{16}\text{O}^-$, $^{12}\text{C}^{14}\text{N}^-$, $^{13}\text{C}^{14}\text{N}^-$, $^{52}\text{Cr}^{16}\text{O}^-$ and
234 $^{56}\text{Fe}^{16}\text{O}^-$ in the second run (to determine associations of organic matter and heavy metals). Image
235 processing and data analysis were carried out using the freeware package OpenMIMS (multi-isotope
236 imaging mass spectrometry, freely available at <http://nrims.harvard.edu>). In total, more than eight
237 NanoSIMS images were acquired from the labelled samples. More detailed information on ^{13}C
238 isotopic maps and NanoSIMS image processing are provided in Supporting Information (SI)-A.

239

240 2.4. Fe plaque dissolution experiment

241 The function of root exudates in the dissolution of iron (hydr)oxides and release of their associated
242 Cr into the medium was investigated in a time-lapse experiment. To this end, another set of plaque-
243 bearing rice seedlings was exposed to Cr treatment ($\text{Fe}80 \times \text{Cr(III)}$) and allowed to grow in the same
244 nutrient solution for another 16 days. The sampling schedule was established for days 1, 3, 7, 10 and
245 16. Root samples at each sampling stage were subjected to DCB extraction for ICP readings of Fe, Cr
246 and calcium (Ca).

247

248 2.5.Data analysis and statistics

249 All Cr-based computations were based on previously described equations (Liu et al., 2004; Zandi
250 et al., 2020). The R statistical package (ver. 2.12.1) was used for all statistical analyses, and statistical
251 differences between treatment means were assessed using the least significant difference (LSD) test at
252 the 0.05 probability level (Data presented here are means \pm SD, n=3).

253

254 3. Results

255 3.1.Fe and Cr concentrations in different root regions

256 Regardless of the examined root regions, the quantities of Fe and Cr adsorbed on IP (DCB extracts)
257 in the roots treated with Cr were significantly higher than in the non-treated roots ($p < 0.05$) (Fig.1a,b).
258 The observed discrepancies between Cr concentrations in DCB solutions extracted from different root
259 sections were statistically significant ($p < 0.05$; DCB-Cr in mature root $>$ root tip). Similarly, Cr
260 concentrations in root tissues were in the following order: Root-Cr mature $>$ Root-Cr tip ($p < 0.05$)
261 (Fig.1b). Seedlings treated with Cr (+Cr seedlings) had higher Fe and Cr contents in their root tissues
262 compared to non-treated counterparts, with markedly increased Fe accumulation in both the tip (2.25-
263 fold) and mature root (1.72-fold) sections. It was also found that the overall Fe sequestration in IP
264 (DCB-Fe) on the mature root surface was significantly higher compared to the tip region both under
265 stress (Fe80-Cr(III)) and stress-free (Fe80-CK) conditions. Fe content in the root tip was significantly
266 higher than in the mature root under Cr stress conditions (Fig.1a).

267

268 3.2. Fe and Cr concentrations/proportions in different rice parts

269 The respective concentrations of Cr and Fe in shoots, plaque-free roots, and DCB extracts differed
270 in their distribution pattern. While the concentration (or relative proportion) of Cr in roots (53%) was
271 significantly higher than that accumulated in IP (\sim 37%) and shoots (\sim 10%), the relative
272 concentration of Fe in individual rice components was in the following order: DCB-extractable Fe $>$
273 Root-Fe $>$ Shoot-Fe (Table 1). Fe mainly accumulated in IP on the root surface under both stress
274 (\sim 89%) and stress-free (\sim 91%) conditions. Irrespective of Cr levels applied, Fe concentration in

275 shoots did not show any significant differences, whereas Fe concentration in IP and roots of Cr-
276 treated seedlings (Fe80-Cr(III)) was significantly (~ 1.52 to 1.98 times, respectively; $p < 0.05$) higher
277 compared to non-Cr treated seedlings (Fe80-CK) (Table 1; Fig. S5a). Only 1.5% of the total Cr
278 contents in roots translocated to shoots, with an 8.8% root-to-shoot Fe translocation efficiency
279 observed in rice exposed to Cr treatment (Table 1).

280

281 3.3. Elemental distribution in rice root

282 3.3.1. Two-dimensional surface view of the root tip and mature root sections

283 The results of *in vivo* scanning of Fe and Cr deposits on the epidermal surface of the root tip (Fig.
284 2a₁₋₂) and mature root (Fig. 2a₄₋₅) sections were partially consistent with ICP-OES analyses
285 concerning elemental distribution (Fig.1). The distribution patterns of Fe, Cr, and Ca fluorescence
286 signals in the root tips after Fe80-Cr(III) treatment were relatively weak (low-intensity spots), with
287 their hotspots scattered and located in slightly distant positions (Fig. 2a₄₋₆). Such distribution of
288 elemental intensities was considerably different from that observed in the mature section of the root,
289 where the intensity of elemental distribution mostly ranged from moderate (green), upper-moderate
290 (yellow) to high (red) levels.

291 According to the results of correlation analysis, the element Cr showed a slightly low ($R^2 = 0.57$) to
292 rather high ($R^2 = 0.77$) associations with high Fe intensities (~ 45 - 80 kilo-counts s^{-1}) and a range of
293 low to moderate associations with Ca (~ 0.2 - 2.3 kilo-counts s^{-1}) intensities, respectively, in IP
294 deposited in the tip zone of rice roots (Fig. 2b₄₋₅). Ca distribution pattern appeared to be similar to that
295 of Fe in the mature root zone, signifying a strong linear association between Fe (~ 5 - 55 kilo-counts s^{-1})
296 and Ca (~ 0.15 - 25 kilo-counts s^{-1}) concentration intensities ($R^2 = 0.90$; Fig. 2b₃). Similarly, Cr
297 concentration was the highest in the mature root zone (Fig. 2a₁), and greatly co-localised with Ca ($R^2 =$
298 0.91) and Fe ($R^2 = 0.90$) intensities observed in the same root zone (Fig. 2b₁₋₂). The majority of Cr
299 deposits in the mature zone of rice root was strongly correlated with a wide range of moderate (>50
300 kilo-counts s^{-1}) to high Fe intensities (<550 kilo-counts s^{-1}). Therefore, Cr was suggested to have a
301 strong association with Fe concentration intensities in the mature zone of rice roots, and this mostly
302 occurred in the Cr intensity range of ~ 10 - 38 kilo-counts s^{-1} (Fig. 2b₁).

303 For Cr signals emitted from the upper surface of the root tip and mature root sections, several
304 hotspots of moderate to high intensity were found, which were thought to be related to significant
305 fractions of Cr sequestered in IP. As outlined above, the concentrations of Cr, Fe and Ca tended to be
306 more intense in the mature root zone than in root tips. The majority of low to high Cr counts (~ 1.3 to
307 32.5 kilo-counts s^{-1}) correlated mostly with a low to moderate (~ 0.2 - 2.6 kilo-counts s^{-1}) counts of Ca
308 intensities in the tip zone of rice roots after Cr treatment (Fig. 2b₅). Ca was mainly distributed on the
309 epidermal surface of the mature root zone and this signal was reproduced by the element Fe. The
310 lower correlation of Cr with Fe (Fig. 2b₄) to Ca (Fig. 2b₅) could also be attributed to the co-
311 distribution of these two elements at hotspots, with no apparent correlation (or overlap) in their
312 moderate-intensity spots. The result indicated that the correlation between the intensities of Fe and Ca
313 fluorescence counts in root tips ($R^2 = 0.37$) was considerably lower than that in mature roots ($R^2 = 0.90$)
314 under Fe80-Cr(III) treatment (Fig. 2b₃₋₆). The low correlation between Fe and Ca counts in root tips
315 could be explained by a partial overlap of Fe hotspots in root tips in regions where Ca fluorescence
316 intensity was high.

317

318 3.3.2. Two-dimensional cross-section views of the root tip and mature root tissues

319 Cr was mainly localised in the epidermal and exodermal layers of both rice root sections. A higher
320 concentration of Cr was observed in the internal portion of sclerenchyma cells in the root tips in
321 comparison to the mature root section (Fig. 3a₁₋₂). In other words, Cr was enriched (with more
322 noticeable Cr spots) in the outer epidermis of mature roots. As shown in Fig. 3b₁, high-intensity Fe
323 spots could be observed on the most distal sides of epidermal and exodermal cells, while moderate-
324 intensity Fe spots were dispersed in sclerenchyma cells. In contrast, the inner portions of the
325 exodermal layer in the tip section showed a higher Fe content than the epidermis (Fig. 3b₂). Moreover,
326 Fe distribution was visible in root tip vessels, which likely corresponded to the vascular tissues of the
327 root, implying that Fe could penetrate the root tip surface into the stele and move upward. However,
328 there was no clear signal of Fe presence in the inner tissues of the mature root zone. Higher Fe
329 concentrations were recorded on the epidermal surface of the mature root zone, as opposed to the root

330 tip zone after Fe80-Cr(III) treatment. This result was consistent with our root surface μ -XRF analysis,
331 where an Fe-enrichment zone was observed on the dorsal surface of the mature root zone.

332 The co-occurrence of Fe and Cr in the epidermal and sclerenchyma cells was found in both root
333 regions (Fig. 3a₁₋₂, b₁₋₂). The correlation of Fe and Cr deposition was more pronounced in the mature
334 zone than the root tip zone, where, unlike the moderate amounts of Fe present in the root stele, no Cr
335 was located in this region (Fig. S3). It can be suggested based on the overlapping Fe and Cr signals
336 that there was a close correlation between Cr and Fe deposits in the epidermal and exodermal cell
337 layers in both sections of rice roots.

338 Fig. 3c₁₋₂ illustrates the effect of Cr on S distribution in the root tip and mature root cross-sections.
339 It is shown in Fig. 3c₁ that S was mainly dispersed in the outer cell layers (along the epidermis and
340 exodermis), in the ground tissues (across the cortex and endodermis) and the stele (pericycle and
341 vascular bundles) of the rice root. With the exception of the middle and central tissues, moderate-
342 intensity S spots in the epidermis and exodermis layers correlated well with Fe hotspots (Fig. 3b₁₋₂;
343 not marked), followed by Cr moderate-intensity spots. In comparison to Fig. 3c₁, a significant
344 decrease in S accumulation was found across the epidermis and exodermis tissues of rice root tips
345 (Fig. 3c₂). However, S distribution in the endodermis, pericycle, and stele of root tips was more
346 extensive than in the mature root zone. This suggested that a considerable proportion of S could
347 penetrate the stele in both sections of rice roots. Fig. 3a₂,b₂,c₂ demonstrated that S distribution did not
348 follow the pattern observed for Fe and Cr in the outer cell layers of the root tip cross-section.

349 Potassium (K) and Ca primarily accumulated in the internal cell layers of both root sections,
350 including endodermis, pericycle and vascular cylinder, as determined by high K and Ca fluorescence
351 intensities (Fig. 3e₁₋₂,f₁₋₂). This observation suggested successful penetration of both elements into the
352 root xylem and their subsequent possible translocation to the shoot. Images e₁,f₁ and e₂,f₂ in Fig. 3
353 clearly demonstrated that the cortex tissue in the mature root of Cr-exposed rice contained a limited
354 degree of an irregular radial dispersion/gradient of K and Ca relative to the root tip zone. This result
355 suggested that K and Ca tended to accumulate in vascular tissues. The distribution pattern of K was
356 analogous to that of Ca in rice roots from both regions. Regardless of the Mn-free region in the cortex
357 and Mn-enriched region in the stele, Mn concentration in the outer cell layers approximately

358 resembled Cr concentration in the rice root maturation region (Fig. 3a₁,d₁). Mn distribution in the rice
359 root tip region was not only limited to the outer cell layers and stele, but also included parts of cortical
360 tissues (Fig. 3d₂).

361

362 3.4. Cr K-edge μ -XANES analysis

363 One main peak and two shoulders, resolved at ~5999.0 eV (peak- 1), ~6005.0 eV (shoulder- 2) and
364 ~6015.0 eV (shoulder- 3), respectively, were recorded in the Cr K-edge XANES spectra associated
365 with spots of interest (SOIs) in the mature and tip region of the root (Fig. 4a). These features were
366 more similar to Cr(III)-Fh and Cr(III)-FA standards rather than the Cr(III) acetate standards with a
367 broader peak 1. The first derivative spectrum of Cr(III) acetate showed an apparently lower energy
368 position of peak b compared to other standards and samples (Fig. 4b). In addition, peak b for all
369 hotspot first derivative spectra displayed a similar shape to Cr(III)-Fh. However, peak c, which
370 appeared in the first derivative spectra of Cr(III)-FA and all hotspots, was absent in Cr(III)-Fh.
371 Therefore, Cr could co-exist and/or form complexes with fulvic acid-like (~FA) substances as an
372 organic metabolite with more diverse functional groups (Qin et al., 2016; Wang et al., 2019; Zhang et
373 al., 2020) and/or ferrihydrite as a typical amorphous form of iron (hydr)oxide in the outer cell layers
374 of rice roots (Tripathi et al., 2014; Zandi et al., 2020).

375 LCF analysis based on spectral features (Fig. 4a) revealed that Cr(III) bound to FA-like anions
376 accounted for 58-64% (spot 2-spot 1) and 13-17% (spot 2-spot 1) of total Cr in the tip and mature
377 regions of rice roots, respectively (Fig. 4c). In other words, the epidermal layer (spot 1) of the mature
378 root and the sub-epidermal layer (spot 1) in the root tip contained the highest proportion of Cr(III)-FA
379 species compared to spot 2 in the corresponding layers. The outer cell layers of the root tip (spot 1 and
380 spot 2) contained mainly Cr(III)-FA species, whereas Cr was mainly present as Fh-bound Cr(III) in
381 the IP of the mature root outer cell layers (83-87% of total Cr). This result suggested that the
382 immobilisation of Cr through complexation with ferrihydrite in IP on the outer cell layers of the
383 mature root was more important than the immobilisation of Cr species by complexation with phyto-
384 /organic metabolite compounds. More than 83% of total Cr was present as Cr(III)-Fh species in spot 1

385 and spot 2 of the mature root zone, which was considerably higher compared to spot 1 and spot 2 of
386 the root tip zone.

387

388 3.5. Carbon isotope results

389 The mean $\delta^{13}\text{C}$ values showed a remarkable disparity between the plaque-free ^{13}C -labelled (515.04‰)
390 and non-labelled (-30.00‰) root samples (Table S2), indicating that the downward flux of
391 photosynthetically processed $^{13}\text{CO}_2$ was significant (successful ^{13}C labelling) during the short period
392 of our experiment. However, in terms of C concentrations in labelled/non-labelled roots, this
393 discrepancy was not that robust since ~1.1% ^{13}C in the C pool of the non-labelled root samples was
394 partially similar to ~1.7% ^{13}C in the C pool of the ^{13}C -labelled roots. The results demonstrated that
395 plants with IP on their roots tended to assimilate less ^{13}C out of $^{13}\text{CO}_2$ than plants devoid of plaque.
396 We therefore found small differences between the ^{13}C abundance values in ^{13}C -enriched root cells
397 with or without IP induction. The severe reduction in C mass percentage (C%) in plaque-bearing roots
398 compared to plaque-free roots was likely caused by the contribution of Fe (III) precipitates to the
399 mass balance disturbance, regardless of whether roots were labelled or not.

400 The labelled shoot samples had a 3 times higher $^{13}\text{C}/^{12}\text{C}$ ratio (and ^{13}C abundance) compared to the
401 non-labelled shoot samples. It should be noted that the existing differences in $\delta^{13}\text{C}$ and ^{13}C abundance
402 between the labelled root and shoot samples did not significantly affect the mass percentage of C in
403 the corresponding samples. In comparison with shoot tissues, root tissue (with or without IP) samples
404 exposed to isotopically labelled $^{13}\text{CO}_2$ showed a lower proportion of ^{13}C isotope abundance, ranging
405 from 49.9% to 51.9%. Another noteworthy aspect to consider was whether the presence of IP on the
406 root surface altered C content in ^{13}C -labelled roots. In this regards, our results demonstrated a
407 substantial decrease (to about 49%) in C content of the plaque-bearing roots (^{13}C -root) compared to
408 plaque-free roots (^{13}C -root). It was assumed that the observed differences between the above samples
409 could be associated with the release of metabolites into the culture medium, or even their lower
410 production in the aerial parts, and thus decreased metabolic activity when IP was present.

411

412 3.6. Distribution mapping of metals and ^{13}C by NanoSIMS

413 NanoSIMS was used to map the relationship between metabolically active ^{13}C -enriched root
414 epidermal cells and metal complexes such as CrO and FeO (hereinafter referred to as iron (oxy)
415 hydroxide mineral) in both the tip and mature root regions. Two selected areas of root tips (Fig. 5b)
416 and mature roots (Fig. 5a) were analysed and colour composite images specifically showed the
417 epidermal cell layer of the roots treated with ferrous-spiked solutions and Cr(III). Regions of interest
418 in the two sections were defined based on whether iron (oxy) hydroxide minerals were present on (or
419 within) the epidermal cell membrane. Comparison of the tip with the mature region allowed for
420 accurate tracking of ^{13}C -enriched metabolites in these two areas. The presence of ^{13}C -enriched cells
421 was more abundant in the epidermal cell layers of mature roots than in the root tips (Fig. 5).

422 Based on composite images showing relative locations of species, such as $^{52}\text{Cr}^{16}\text{O}$, $^{13}\text{C}^{14}\text{N}$ and
423 $^{56}\text{Fe}^{16}\text{O}$, metabolically active epidermal cells in the mature root region were more enriched in ^{13}C
424 metabolites compared to the root tip. The location of ^{13}C -enriched metabolites was confined to the
425 epidermal cell walls (area 1 in Fig. 5a,b) and apoplastic spaces (area 2 in Fig. S4a₁). It was also
426 established that ^{13}C -labelled metabolites in the above-specified spots co-localised with Fe and Cr.
427 Moreover, $^{56}\text{Fe}^{16}\text{O}$ hotspots were always associated with a somewhat similar accumulation of $^{52}\text{Cr}^{16}\text{O}$.
428 The $^{56}\text{Fe}^{16}\text{O}$ signal indicated that Fe was mainly located on the root epidermal surface, irrespective of
429 the root zone. This phenomenon was more pronounced in the mature than in the immature (tip) region
430 of the root, with the outer (excluding epidermis) and inner cell (ground tissues and stele) layers of the
431 latter zone markedly associated with strong $^{56}\text{Fe}^{16}\text{O}$ signals (Fig. 3b₂).

432 The distribution of $^{56}\text{Fe}^{16}\text{O}$ in the two studied zones was heterogeneous with distinct regions of
433 accumulation along the outer edge of the root epidermis (area 2 in Fig. 5a,b). The ^{16}O images in the
434 two analysed zones clearly demonstrated that O signals were more evident in the mature root zone
435 than in the root tips (Fig. S4). The general pattern of O distribution in ^{16}O images resembled the
436 distribution observed in $^{56}\text{Fe}^{16}\text{O}$ and $^{52}\text{Cr}^{16}\text{O}$ images. Regardless of the root zone, the strongest
437 $^{56}\text{Fe}^{16}\text{O}$ and ^{16}O signals originating from the outer epidermal cell wall layer were tightly linked with
438 each other, implying that Fe was likely associated with oxide or oxy-hydroxide on the root surface.
439 The presence of overlapping signals of $^{56}\text{Fe}^{16}\text{O}$ and $^{13}\text{C}^{14}\text{N}$ or $^{12}\text{C}^{14}\text{N}$ (organic carbons, OCs) in

440 specific locations on the root surface suggested the occurrence of organo-Fe oxyhydroxide co-
441 precipitates (OFC) complexes in the examined root regions (SI-B).

442

443 3.7. Cr release during iron plaque dissolution

444 The mature root region appeared to have a lower Cr to Ca ratio compared to the root tips,
445 regardless of the sampling time (Fig. 6). This discrepancy was attributed to the higher intensity of Ca
446 distribution on the mature root surface (Fig. 2a₃₋₆). Fluctuations in the Fe/Ca ratios observed in the
447 root tip were not statistically significant ($p > 0.05$), while a significant difference between the Fe/Ca
448 ratios in the mature root zone (initial sharp decrease from day 1 to day 3) was recorded. The decrease
449 in this region was followed by a slight insignificant increase (day 3-day 7) and then another decrease
450 (day 7-day 10). This decline continued for the next 6 days (day 10-day 16). The trends in changes in
451 the Cr/Ca ratios in each of the root sections were identical to those observed for the Fe/Ca ratios,
452 suggesting that the release of immobilised Cr into the medium solution was consistent with IP
453 dissolution.

454

455 4. Discussion

456 The results of the present work supported the hypothesis that plant exposure to Cr stress further
457 stimulated Fe²⁺ exclusion and oxidation on the root surface (i.e., iron (hydr)oxide(s)/ IP formation)
458 due to elevated root oxygen release or enzymatic oxidation (Table 1 ; Fig. S5a) (Briat et al., 2010).
459 This effect was more confined to the mature zone of the rice root surface (Fig. 1a), presumably due to
460 the more developed structure (Nishiuchi et al., 2012). Thus, this region could better limit Cr's
461 bioavailability and mobility than immature root tips (Fig. 1b).

462 Iron (hydr)oxides serve not only as a physical barrier with a metal-sequestering ability (Amaral et
463 al. (2017) but also as metal-chelating ligands (e.g., DMA: 2'-deoxymugenic acid), which can bind
464 heavy metals (Banakar et al., 2017). This may explain why Fe accumulation in the tip zone was
465 slightly higher than in the mature root zone under Cr stress (Fig. 1a).

466 Root Cr content was higher than in DCB extracts and shoots (Fig. 1b; Fig. S5b). This suggests that
467 IP formation in conditions similar to flooded cultivation and its inhibitory effect on Cr uptake (Xiao et
468 al., 2021) is not necessarily limited to the root epidermal surface (Fig. 2a₂₋₅). This condition most
469 likely involves the apoplastic space in the outer layers of root cells (Fig. 3b₁₋₂) (Khan et al., 2016). It
470 appears that Cr-induced increased aerenchyma-rhizosphere oxygen outflux, coinciding with higher Fe
471 concentrations (Fig. 3b₁₋₂) (Becker et al., 2020), resulted in an increased amount of Cr precipitated on
472 the outer cell layers compared to internal cell tissues in the tip and mature zone of rice roots (Fig. 3a₁₋
473 ₂). It's worth noting that increased Cr retention in outer cell layers of plaque-bearing roots compared
474 to plaque-free roots was not associated with aerial uptake (Fig. S5b). This underlines the significance
475 of IP in Cr immobilisation (Zandi et al., 2020, 2021).

476 The observed correlation between Cr and Ca concentration intensities in surface μ -XRF imaging
477 of overlapping areas (Fig. 2a₁₋₃, a₄₋₆, b₂₋₅) indicated the importance of Ca as a critical factor in
478 rigidifying cell walls and providing structural integrity to cellular membranes (Hepler, 2005; Pathak et
479 al., 2021) in Cr cell wall sequestration by binding to it (Zeng et al., 2011). This effect was particularly
480 restricted to the outer surface (i.e., epidermal layer) of the mature root zone, where similar Cr (Fig.
481 2a₁), Fe (Fig. 2a₂) and Ca (Fig. 2a₃) concentration intensities indicated the co-precipitation of Fe with
482 Ca and Cr on epidermal root surfaces. It has been shown by sorption experiments that Ca (Gunnars et
483 al., 2002; van Genuchten et al., 2014) and Cr (Yu et al., 2017) can react with surface hydroxyl groups
484 and adsorb on iron oxides.

485 In the present study, Cr accumulation in the outer cell layers (except for the epidermis) was not
486 associated with Cr deposition on cell walls (Fig. 3a₁₋₂), as indicated by the low correlation between Ca
487 and Cr intensities ($R^2= 0.01$) in both root regions (Fig. S3). In contrast to our finding, in their research
488 on arsenic (As) and Cr (VI), respectively, Xu et al. (2022) and Zeng et al. (2011) attributed the
489 inhibitory role of cell walls to the entire root tissue. This difference might be related to the higher
490 mobility of metal species used in their studies.

491 The formation of Fe and Mn plaque on rice roots is indeed a ROL (radial oxygen loss)-mediated
492 exclusion strategy for limiting the absorption of potentially toxic elements (Yu et al., 2017; Li et al.,
493 2019). Consistently with Crowder and Coltman (1993), Ye et al. (2001) and Zhang et al. (2015), the

494 concentration of Fe deposits in the outer cell layers of both root regions in this work was also more
495 intense compared to Mn deposits (Fig. 3b₁₋₂,d₁₋₂). Therefore, it was not surprising that the co-
496 occurrence of Fe and Cr deposits in hotspot and non-hotspot regions was more pronounced than that
497 of Mn and Cr deposits in both regions of the root (Fig. 3; Fig. S3). It is generally accepted that the
498 functional groups in IP have the potential to form a more active substrate for metal sequestration (Cao
499 et al., 2018; Xu et al., 2018) than those in Mn plaque with its unique catalytic capacity and surface
500 activity (Ye et al., 2001; Liu and Zhu, 2005). In addition to Fe and Mn plaques, sulphur (S) containing
501 metabolites are also effective in Cr chelation and subcellular sequestration (Holland and Avery, 2011;
502 Zandi et al., 2021), as was evident in simultaneous S and Cr depositions in the examined root regions
503 (Fig.3a₁₋₂, c₁₋₂).

504 Exclusion and chelation mechanisms seem to co-occur in rice roots during Cr stress exposure,
505 which may lead to decreased Cr entry into the inner layers of root cells and hence lowered Cr uptake,
506 as seen in Fig. 3a₁₋₂ and Fig. S5b. This would confirm the hypothesis that root exudation of organic
507 metabolites effectively reduces heavy metal uptake by rice at the root-rhizosphere interface (exclusion
508 strategy) (Wang et al., 2019; Zhang et al., 2020).

509 The results of the XANES spectra of spots of interest (SOIs) in Cr μ -XRF mapping showed that
510 phytometabolites involved in Cr chelation and detoxification were likely LMW fulvic acid-like (~FA)
511 anions (Fig. 4c) (Wang et al., 2019; Zhang et al., 2020) which have not been reported for soil-free
512 plant systems. These compounds are supposed to form stable chelate compounds with certain heavy
513 metals (chelation strategy), such as Cd (Rashid et al., 2018) and Cr (Pradas del Real et al., 2014),
514 enabling plants to withstand Cr-induced toxicity (Chen et al., 2017). Besides, reports indicated the
515 high affinity of these metabolites for Fe(III) and other structurally similar trivalent metal cations,
516 including Mn (III) (Tang et al., 2010; Saad et al., 2017).

517 The proportion of Cr(III)-FA complexes varied between individual SOIs (spot 1 and spot 2) in
518 both root regions, proposing two different models (Fig. 4c). On the one hand, a higher percentage of
519 phytometabolites or FA-like anions was bound to Cr(III) species adjacent to the root surface compared
520 to the more internal tissues in the mature root (17% vs 13%), suggesting the existence of a resistance
521 mechanism through exclusion (Osmolovskaya et al., 2018; Bali et al., 2020). On the other hand, a

522 reverse trend (58% and 64% for epidermal and subepidermal layers, respectively) was observed for
523 organically bound Cr(III) in the root tip, suggesting the occurrence of a tolerance mechanism through
524 inclusion and chelation. The proposed models were consistent with our IP dissolution results (Fig. 6).
525 For instance, in the root tip zone with its unique trend of organo-Cr(III) species, neither IP dissolution
526 nor Cr release was found to occur (Figs. 4c and 6; SI-C), reinforcing the possibility of Cr re-uptake
527 from the root tip zone in the rhizosphere. Combining the proposed models with our ICP analysis (Fig.
528 S5b), it can be inferred that the binding of FA-like anions to Cr(III) species did not lead to increased
529 Cr mobility and accumulation in shoot tissues.

530 The limited IP build-up on the root surface (Fig. 2a₅) is assumed to have resulted in increased
531 binding of FA-like anions relative to Fh species to Cr ions at the adsorbing sites in the root tip
532 epidermis (58% vs 42%; T-Spot 2 in Fig. 4c). Consequently, the formed organo-Cr(III) species
533 transferred to the immobilising sites in the outer cell layers of the root tip (Fig. 3a₁). This assumption
534 was consistent with our carbon isotope results, where the absence (or scarcity) of root plaques
535 increased the biosynthesis and transport of ¹³C-labelled organic metabolites (isotopic organic carbons-
536 Ocs) to the root system (Table 2), thereby increasing the possibility of their binding to Cr. In a study
537 by Tao et al. (2020), it was demonstrated that a small portion of assimilated ¹³C was incorporated in
538 forming organic anion metabolites involved in Cd complexation.

539 The reduced abundance of isotopic OCs in rice roots with IP, compared to those stored in rice
540 roots without IP, indicated that root plaques effectively prevented the assimilation and transfer of
541 shoot-derived metabolites (Table 2) by Cr retention and stress alleviation. Studies on plaque-free roots
542 revealed that heavy metal stress increased the content of organic acid anions in the roots and root
543 exudates (Yang et al., 2000; Mariano Eduardo et al., 2005).

544 In contrast to being a more active site of organic anion metabolism and biosynthesis (Mariano
545 Eduardo et al., 2005), only a small fraction of total Cr in individual SOIs in the outer cell layers of the
546 mature root could be chelated (13-17%) or exuded by these metabolites compared to iron
547 (hydr)oxides (Fig. 4c). There was an obvious dominance of the Cr(III)-Fh complexes relative to
548 Cr(III)-FA complexes in individual SOIs in the mature root zone, indicating the substantial role
549 played by Fh composition of iron (hydr)oxides in conferring higher tolerance to Cr toxicity through

550 chelation and immobilisation (Yu et al., 2017; Zandi et al., 2020) in this region. The reduced
551 proportion of Cr(III)-Fh complexes in the epidermal layer of the mature root, relative to the
552 subepidermal layer of the mature root (83% vs 87%; Fig. 4c), could be explained by a higher IP
553 dissolution and its associated Cr under the influence of the supposed metabolites in this region (Fig. 6)
554 (Sebastian and Prasad, 2016; Saad et al., 2017).

555 Root surface NanoSIMS imaging demonstrated how Fe oxyhydroxide (FeO) and Cr-induced
556 isotopic/non-isotopic OCs were closely adherent to the epidermal surface and to each other (Fig. 5).
557 This proximity in turn indicated adsorption of organic anion metabolites or occlusion in the interstices
558 between amorphous Fh aggregates (Zeng et al., 2008). This co-occurrence not only inhibits the
559 growth of Fh, but also tends to form smaller amorphous aggregates, and is therefore believed to affect
560 aggregation behaviour, surface properties and solubility/accessibility of Fh (Eusterhues et al., 2014),
561 contributing to Fh removal and its associated Cr from the root epidermal layer (Fig. 6). Previous
562 dissolution studies showed that organic anion metabolites adsorbed on or co-precipitated with iron
563 (hydr)oxides were likely to weaken Cr(III)-Fe(III)-(oxy)hydroxide compositional bonds under
564 anaerobic conditions. This phenomenon enhanced the solubility and dissolution kinetics of iron
565 (hydr)oxides and associated dissolved Cr (Saad et al., 2017).

566 It is worth noting that the relationship between the secretion/exudation rate of organic anions and
567 their root concentrations is attributed to heavy metal-activated organic anion transporter channels in
568 the plasma membrane of root cells (Yang et al., 2012). The observed varied patterns of Cr-induced
569 secretion of phytometabolites (Fig. 5) and IP dissolutions (Fig. 6) between the examined root regions
570 (mature root > root tip) could be due to the fact that root exudates, regardless of their role in heavy
571 metal chelation (Montiel-Rozas et al., 2016), are secreted to promote solubility and absorption of
572 poorly available nutrients in the rhizosphere (Jones et al., 2004; Gojon, 2013). Indeed, the mature
573 zone of the root system is responsible for the majority of nutrient uptake in crop plants (Jones et al.,
574 2004; Wirth et al., 2007; Gojon, 2013), which in turn explains the absolute predominance of root
575 exudates and dissolution rate of iron (hydr)oxides in this region compared to the root tip region (Figs.
576 5 and 6). In other words, the increased secretion of organic anions from the mature region compared
577 to the immature (tip) region of the root, in addition to destabilising iron (hydr)oxides (Yang et al.,

578 2012, 2013) and possible release of their co-precipitated Cr ions (Fig. 6), can also be considered an
579 essential mechanism reducing the physical resistance of root plaques to nutrient absorption.

580 Considering the absence of IP dissolution and release of its Cr co-precipitates (Fig. 6) and limited
581 secretion of organic anions (Fig. 5) in the root tip region, the relatively higher proportion of organo-
582 Cr(III) species in more internal than external tissues (64% vs 58%) of the outer cell layers in this
583 region (Fig. 4c), likely reflected the importance of organic anions (i.e., FA-like anions) in capturing
584 and transferring the absorbed Cr in the form of organo-Cr(III) species to the root tip sub-epidermis.
585 The proposed model can also be construed as a possible direct or indirect re-uptake of Cr from the
586 solution medium after release from the mature region of rice roots (as outlined earlier) and its
587 subsequent immobilisation by a combination of Fh and FA-like chelators. The strong presence of
588 organo-Cr(III) (58-64%) complexes in relation to Cr(III)-Fh (36-42%) complexes in the root tip outer
589 cell layers (Fig. 4c) was an indirect reference to the reinforcing role of FA-like anions in Cr chelation
590 and immobilisation when the Fh chelator pool was insufficient. As indicated earlier, the accumulation
591 of ^{13}C -labelled organic metabolites was more intense in plaque-free roots (^{13}C -root) than in plaque-
592 bearing roots (Fe^{13}C -root) under Cr stress, regardless of the root section (Table 2). This indirectly
593 underscored the role played by these anions as complementary factors for Cr immobilisation.

594

595 **5. Concluding remarks**

596 The present study concludes that root plaques have a central role in Cr chelation and
597 immobilisation, especially in the mature root region. The uptake inhibiting function of IP was not only
598 confined to root epidermal surfaces but also stretched across the entire root outer cell layers. It
599 strongly suggested that an integration of both Cr resistance (exclusion) and tolerance (chelation)
600 strategies was directly involved in the mature region of the root, where iron (hydr)oxide precipitates
601 alone accounted for over 83% of total Cr (Cr(III)-Fh) species at Cr hotspots in the epidermal and sub-
602 epidermal layers of root cells. An uneven partnership in root Cr retention and inactivation was
603 actively present in root tissues; as such, none or limited IP coated roots contained an increased amount
604 of isotopic OCs or a higher percentage of Cr(III)-FA species (58-64% for root tips), respectively. The

605 proposed model concerning the outflow (Pos. mature root) or inflow (Neg. root tips) of metabolites
606 carrying Cr (organo-Cr (III)) in outer cell layers of both root regions was well consistent (positive-
607 Pos./ negative- Neg. effect) with signal intensities of ¹³C-labelled spots as active nano-scaled spots of
608 root exudates and iron (hydr)oxide dissolution.

609

610 **Data availability**

611 In addition to the **SI**, all other reasonable requests for data and research materials are available
612 via contacting the corresponding author.

613

614 **Funding**

615 The work was funded by the Top-Notch Young Talents Program of China, the National Natural
616 Science Foundation of China (U1632134), the Agricultural Science and Technology Innovation
617 Program of the Chinese Academy of Agricultural Science (2021-2025) and the National Center for
618 Scientific Research (CNRS) in France (CNRS funded the NanoSIMS analyses). The National
619 NanoSIMS facility at the Muséum National d'Histoire Naturelle was established by funds from CNRS,
620 Région Ile de France, Ministère délégué à l'Enseignement Supérieur et à la Recherche, and the
621 Muséum National d'Histoire Naturelle. Synchrotron-based microprobe analysis was conducted at the
622 Canadian Light Source, a national research facility of the University of Saskatchewan, which is
623 supported by the Canada Foundation for Innovation, the Natural Sciences and Engineering Research
624 Council of Canada, the National Research Council of Canada, the Canadian Institutes of Health
625 Research, the Province of Saskatchewan, and the University of Saskatchewan.

626

627 **CRedit authorship contribution statement**

628 #XX and PZ equally contributed to this work.

629 **JY**: designed the experiments. **XX** and **PZ**: performed the lab experiments with the kind
630 guidance of **JY**. **JY**, **XX** and **PZ**: performed the XRF, XANES and SEM measurements and data
631 analysis. **JY**, **JL**, **RL** and **CR**: conducted the NanoSIMS experiments. **JY**, **JL** and **XX**: performed the

632 NanoSIMS data analysis. **PZ**, **XX**, **JY** and **JL**: analysed the data and drafted the manuscript. **JY**, **PZ**,
633 **BE**, **ES** and **BBK**: participated in the interpretation of results. **JY**, **CR**, **RL**, **PZ**, **BE**, **ES** and **BBK**:
634 improved the grammar and corrected spelling mistakes. **PZ**, **JY**, **XX**, **BE**, **BBK** and **ES**: edited and
635 thoroughly revised the manuscripts. All authors read, corrected and approved the final submitted
636 version of the manuscript.

637

638 **Declaration of Competing Interest**

639 The authors declare that they have no known competing financial interests or personal
640 relationships that could have appeared to influence the work reported in this paper.

641

642 **References**

- 643 Agnello, A., Huguenot, D., Van Hullebusch, E., Esposito, G., 2014. Enhanced phytoremediation: a
644 review of low molecular weight organic acids and surfactants used as amendments. *Crit. Rev.*
645 *Environ. Sci. Technol.* 44, 2531e2576. <https://dx.doi.org/10.1080/10643389.2013.829764>.
- 646 Ali, W., Zhang, H., Mao, K., Shafeeque, M., Aslam, M.W., Yang, X., Zhong, L., Feng, X., Podgorski,
647 J., 2022. Chromium contamination in paddy soil-rice systems and associated human health risks
648 in Pakistan. *Sci. Total Environ.* 826,153910. <https://doi.org/10.1016/j.scitotenv.2022.153910>.
- 649 Amaral, D.C., Lopes, G., Guilherme, L.R.G., Seyfferth, A.L., 2017. A new approach to sampling
650 intact Fe plaque reveals Si-induced changes in Fe mineral composition and shoot as in rice.
651 *Environ. Sci. Technol.* 51, 38–45. <https://doi.org/10.1021/acs.est.6b03558>
- 652 Assimakopoulou, A., Kotsiras, A., Nifakos, K., 2013. Incidence of lettuce tipburn as related to
653 hydroponic system and cultivar. *J. Plant Nutr.* 36(9), 1383–1400.
654 <https://doi.org/10.1080/01904167.2013.793709>
- 655 Bali, A.S., Sidhu, G.P.S., Kumar, V., 2020. Root exudates ameliorate cadmium tolerance in plants: A
656 review. *Environ. Chem. Lett.* 18, 1243–1275. <https://doi.org/10.1007/s10311-020-01012-x>
- 657 Banakar, R., Fernandez, A.A., Díaz-Benito, P., Abadía, J., Capell, T., Christou, P., 2017.
658 Phytosiderophores determine thresholds for iron and zinc accumulation in biofortified rice

659 endosperm while inhibiting the accumulation of cadmium. *J. Exp. Bot.* 68(17), 4983–
660 4995. <https://doi.org/10.1093/jxb/erx304>

661 Becker, M., Ngo, N.S., Schenk, M.K.A., 2020. Silicon reduces the iron uptake in rice and induces
662 iron homeostasis related genes. *Sci. Rep.* 10, 5079. <https://doi.org/10.1038/s41598-020-61718-4>

663 Briat, J.F., Ravet, K., Arnaud, N., Duc, C., Boucherez, J., Touraine, B., Cellier, F., Gaymard, F., 2010.
664 New insights into ferritin synthesis and function highlight a link between iron homeostasis and
665 oxidative stress in plants. *Ann. Bot.* 105, 811–822. <https://doi.org/10.1093/aob/mcp128>

666 Cao, Z.Z., Qin, M.L., Lin, X.Y., Zhu, Z.W., Chen, M.X., 2018. Sulfur supply reduces cadmium
667 uptake and translocation in rice grains (*Oryza sativa* L.) by enhancing iron plaque formation,
668 cadmium chelation vacuolar sequestration. *Environ. Pollut.* 238, 76–84.
669 <https://doi.org/10.1016/j.envpol.2018.02.083>

670 Chen, K., Li, B., He, G., 2000. High-yielding cultivation techniques for a new high-quality rice
671 variety Xiangzaoxian No. 31. *Crop Res.* 4, 43. [https://doi.org/10.16848/j.cnki.issn.1001-](https://doi.org/10.16848/j.cnki.issn.1001-5280.2000.04.017)
672 5280.2000.04.017. [in Chinese]

673 Chen, Y.T., Wang, Y., Yeh, K.C., 2017. Role of root exudates in metal acquisition and tolerance.
674 *Curr. Opin. Plant Biol.* 39, 66–72. <https://doi.org/10.1016/j.pbi.2017.06.004>

675 Cheng, H., Wang, M., Wong, M.H., Ye, Z., 2014. Do radial oxygen loss and iron plaque formation
676 on roots alter Cd and Pb uptake and distribution in rice plant tissues? *Plant Soil* 375, 137–148.
677 <https://doi.org/10.1007/s11104-013-1945-0>

678 Coudert, Y., Périn, C., Courtois, B., Khong, N.G., Gantet, P., 2010. Genetic control of root
679 development in rice, the model cereal. *Trend Plant Sci.* 15(4), 219–226. [https://doi.org/](https://doi.org/10.1016/j.tplants.2010.01.008)
680 10.1016/j.tplants.2010.01.008.

681 Crowder, A.A., Coltman, D.W., 1993. Formation of manganese oxide plaque on rice roots in solution
682 culture under varying pH and manganese (Mn^{2+}) concentration conditions. *J. Plant Nutr.* 16 (4),
683 589–599. <https://doi.org/10.1080/01904169309364559>

684 Deng, D., Wu, S.C., Wu, F.Y., Deng, H., Wong, M.H., 2010. Effects of root anatomy and Fe plaque
685 on arsenic uptake by rice seedlings grown in solution culture. *Environ. Pollut.* 158, 2589–2595.
686 <https://doi.org/10.1016/j.envpol.2010.05.015>.

687 Eusterhues, K., Hädrich, A., Neidhardt, J., Küsel, K., Keller, T.F., Jandt, K.D., Totsche, K.U., 2014.
688 Reduction of ferrihydrite with adsorbed and coprecipitated organic matter: microbial reduction
689 by *Geobacter bremensis* vs. Abiotic reduction by Na-dithionite. *Biogeosciences* 11, 4953–4966.
690 <https://doi.org/10.5194/bg-11-4953-2014>

691 Frommer, J., Voegelin, A., Dittmar, J., Marcus, M.A., Kretzschmar, R., 2011. Biogeochemical
692 processes and arsenic enrichment around rice roots in paddy soil: results from micro-focused X-
693 ray spectroscopy. *Eur. J. Soil Sci.* 62, 305–317. [https://doi.org/10.1111/j.1365-
694 2389.2010.01328.x](https://doi.org/10.1111/j.1365-2389.2010.01328.x)

695 Fukao, T., Barrera-Figueroa, B.E., Juntawong, P., Peña-Castro, J.M., 2019. Submergence and
696 waterlogging stress in plants: a review highlighting research opportunities and understudied
697 aspects. *Front. Plant Sci.* 10, 340. <https://doi.org/10.3389/fpls.2019.00340>

698 Ge, T., Yuan, H., Zhu, H., Wu, X., Nie, S., Liu, C., Tong, C., Wu, J., Brookes, P., 2012. Biological
699 carbon assimilation and dynamics in a flooded rice–soil system. *Soil Biol. Biochem.* 48, 39–46.
700 <https://doi.org/10.1016/j.soilbio.2012.01.009>

701 Geng, Z., Wang, P., Fu, Y., Liu, W., Cui, Y., 2020. Bioaccessibility of chromium in rice and Its
702 human health risk assessment, *Asian J. Ecotoxicol.* (6), 205–211.
703 <https://doi.org/10.7524/AJE.1673-5897.20190610002>

704 Gojon, A., 2013. Inorganic Nitrogen acquisition and signalling. In: Eshel, A., Beeckman, T. (Eds.),
705 *Plant Roots*. CRC Press, Boca Rotan, pp. 1–14.

706 Gu, D., Zhen, F., Hannaway, D.B., Zhu, Y., Liu, L., Cao, W., Tang, L., 2017. Quantitative
707 classification of rice (*Oryza sativa* L.) root length and diameter using image analysis. *PLoS One*
708 12(1), e0169968. <https://doi.org/10.1371/journal.pone.0169968>.

709 Gunnars, A., Blomqvist, S., Johansson, P., Andersson, C., 2002. Formation of Fe (III) oxyhydroxide
710 colloids in fresh water and brackish seawater, with incorporation of phosphate and calcium.
711 *Geochim. Cosmochim. Acta* 66, 745–758. [https://doi.org/10.1016/S0016-7037\(01\)00818-3](https://doi.org/10.1016/S0016-7037(01)00818-3)

712 Hayat, S., Khaliq, G., Irfan, M., Wani, A.S., Tripathi, B.N., Ahmad, A., 2012. Physiological
713 changes induced by chromium stress in plants: an overview. *Protoplasma* 249, 599–611.
714 <https://doi.org/10.1007/s00709-011-0331-0>

- 715 Hepler, P.K., 2005. Calcium: A central regulator of plant growth and development. *Plant Cell*. 17(8),
716 2142–2155. <https://doi.org/10.1105/tpc.105.032508>
- 717 Holland, S.L., Avery, S.V., 2011. Chromate toxicity and the role of sulfur. *Metallomics* 3, 1119–1123.
718 <https://doi.org/10.1039/c1mt00059d>
- 719 Holzschuh, M.J., Carlos, F.S., Carmona, F.C., Bohnen, H., Anghinoni, I., 2014. Iron oxidation on the
720 surface of adventitious roots and its relation to aerenchyma formation in rice genotypes. *Revista*
721 *Brasileira de Ciência do Solo* 38 (1), 185–192. [https://doi.org/10.1590/S0100-](https://doi.org/10.1590/S0100-06832014000100018)
722 [06832014000100018](https://doi.org/10.1590/S0100-06832014000100018)
- 723 Hu, Y., Huang, Y.Z., Liu Y.X., 2014. Influence of iron plaque on chromium accumulation and
724 translocation in three rice (*Oryza sativa* L.) cultivars grown in solution culture. *Chem. Ecol.* 30
725 (1), 29–38. <https://doi.org/10.1080/02757540.2013.829050>
- 726 Jones, D.L., Hodge, A., Kuzyakov, Y., 2004. Plant and mycorrhizal regulation of
727 rhizodeposition. *New Phytol.* 163 (3), 459–480. [https://doi.org/10.1111/j.1469-](https://doi.org/10.1111/j.1469-8137.2004.01130.x)
728 [8137.2004.01130.x](https://doi.org/10.1111/j.1469-8137.2004.01130.x)
- 729 Kaiser, C., Kilburn, M.R., Clode, P.L., Fuchslueger, L., Koranda, M., Cliff, J.B., Solaiman, Z.M.,
730 Murphy, D.V., 2015. Exploring the transfer of recent plant photosynthates to soil microbes:
731 mycorrhizal pathway vs. direct root exudation. *New Phytol.* 205, 1537–1551.
732 <https://doi.org/10.1111/nph.13138>
- 733 Khan, F.H., Ambreen, K., Fatima, G. and Kumar, S., 2012. Assessment of health risks with reference
734 to oxidative stress and DNA damage in chromium exposed population. *Sci. Total Environ.* 430,
735 68–74. <https://doi.org/10.1016/j.scitotenv.2012.04.063>
- 736 Khan, N., Seshadri, B., Bolan, N., Saint, C.P., Kirkham, N.B., Chowdhury, S., Yamaguchi, N., Lee,
737 D.Y., Li, G., Kunhikrishnan, A., Qi, F., Karunanithi, R., Qiu, R., Zhu, Y.G., Syu, C.H., 2016.
738 Root iron plaque on wetland plants as a dynamic pool of nutrients and contaminants. *Adv. Agron.*
739 138, 1–96. <https://doi.org/10.1016/bs.agron.2016.04.002>
- 740 Li, J., Jia, Y., Dong, R., Huang, R., Liu, P., Li, X., Wang, Z., Liu, G., Chen, Z., 2019. Advances in the
741 mechanisms of plant tolerance to manganese toxicity. *Int. J. Mol. Sci.* 20(20), 5096.

742 <https://doi.org/10.3390/ijms20205096>

743 Li, Y., Zhao, J., Zjang, B., Liu, Y., Xu, X., Li, Y.F., Li, B., Gao, Y., Chai, Z., 2015. The influence of
744 iron plaque on the absorption, translocation and transformation of mercury in rice (*Oryza sativa*
745 L.) seedlings exposed to different mercury species. *Plant Soil* 398, 87–97.
746 <https://doi.org/10.1007/s11104-015-2627-x>

747 Liu, W.J., Zhu, Y.G., 2005. Iron and Mn plaques on the surface of roots of wetland plants. *Acta Ecol.*
748 *Sin.* 25 (2), 358–363. (In Chinese)

749 Liu, W.J., Zhu, Y.G., Smith, F.A., Smith, S.E., 2004. Do phosphorus nutrition and iron plaque alter
750 arsenate (As) uptake by rice seedlings in hydroponic culture? *New Phytol.* 162, 481–488.
751 <https://doi.org/10.1111/j.1469-8137.2004.01035.x>

752 Lombi, E., Susini, J., 2009. Synchrotron-based techniques for plant and soil science: opportunities,
753 challenges and future perspectives. *Plant Soil* 320, 1–35. [https://doi.org/10.1007/s11104-008-](https://doi.org/10.1007/s11104-008-9876-x)
754 [9876-x](https://doi.org/10.1007/s11104-008-9876-x)

755 Lu, L., Xie, R., Liu, T., Wang, H., Hou, D., Du, Y., He, Z., Yang, X., Sun, H., Tian, S., 2017. Spatial
756 imaging and speciation of Cu in rice (*Oryza sativa* L.) roots using synchrotron-based X-ray
757 microfluorescence and X-ray absorption spectroscopy. *Chemosphere* 175, 356–364.
758 <https://doi.org/10.1016/j.chemosphere.2017.02.082>.

759 Luo, Q., Wang, S., Sun, L., Wang, H., 2017. Metabolic profiling of root exudates from two ecotypes
760 of *Sedum alfredii* treated with Pb based on GC-MS. *Sci. Rep.* 7, 39878.
761 <https://doi.org/10.1038/srep39878>

762 Mariano Eduardo, D., Jorge Renato, A., Keltjens Willem, G., Marcelo, M., 2005. Metabolism and
763 root exudation of organic acid anions under aluminium stress. *Braz. J. Plant Physiol.* 17,
764 157–172. <https://doi.org/10.1590/S1677-04202005000100013>.

765 Montiel-Rozas, M.M., Madejón, E., Madejón, P., 2016. Effect of heavy metals and organic matter on
766 root exudates of herbaceous species: An assessment in sand and soil conditions under different
767 levels of contamination. *Environ. Pollut.* 216, 273–281.
768 <https://doi.org/10.1016/j.envpol.2016.05.080>

769 Nickens, K.P., Patierno, S.R. and Ceryak, S., 2010. Chromium genotoxicity: a double-edged sword.

770 Chem. Biol. Interact., 188(2), 276–288. <https://doi.org/10.1016/j.cbi.2010.04.018>

771 Nishiuchi, S., Yamauchi, T., Takahashi, H., Kotula, L., Nakazono, M., 2012. Mechanisms for coping
772 with submergence and waterlogging in rice. *Rice* 5, 2. <https://doi.org/10.1186/1939-8433-5-2>

773 Osmolovskaya, N., Dung, V.V., Kuchaeva, L., 2018. The role of organic acids in heavy metal
774 tolerance in plants. *Bio. Comm.* 63 (1), 9–16. <https://doi.org/10.21638/spbu03.2018.103>

775 Pathak, R.K., Singh, D.B., Sharma, H., Pandey, D., Dwivedi, S., 2021. Calcium uptake and
776 translocation in plants. In: Upadhyay, S.K. (Ed.), *Calcium Transport Elements in Plants*, 1st, ed.
777 Academic Press, New York, pp. 373–386.

778 Peng, C., Duan, D., Xu, C., Chen, Y., Sun, L., Zhang, H., Yuan, X., Zheng, L., Yang, Y., Yang, J.,
779 Zhen, X., Chen, Y., Shi, J., 2015. Translocation and biotransformation of CuO nanoparticles in
780 rice (*Oryza sativa* L.) plants. *Environ. Pollut.* 197, 99–107.
781 <https://doi.org/10.1016/j.envpol.2014.12.008>.

782 Pradas del Real, A.E., García-Gonzalo, P., Lobo, M.C., Pérez-Sanz, A., 2014. Chromium speciation
783 modifies root exudation in two genotypes of *Silene vulgaris*. *Environ. Exp. Bot.* 107, 1–6.
784 <https://doi.org/10.1016/j.envexpbot.2014.05.002>

785 Qin, Y., Zhu, H., Zhang, M., Zhang, H., Xiang, C., Li, B., 2016. GC-MS analysis of membrane-
786 graded fulvic acid and Its activity on promoting wheat seed germination. *Molecules* 21(10), 1363.
787 <https://doi.org/10.3390/molecules21101363>

788 Rashid, I., Murtaza, G., Zahir, Z.A., Farooq, M., 2018. Effect of humic and fulvic acid transformation
789 on cadmium availability to wheat cultivars in sewage sludge amended soil. *Environ. Sci. Pollut.*
790 *Res.* 25, 16071–16079. <https://doi.org/10.1007/s11356-018-1821-9>.

791 Ravel, B., Newville, M., 2005. Athena, Artemis, Hephaestus: data analysis for X-ray absorption
792 spectroscopy using IFEFFIT. *J. Synchrotron Rad.* 12, 537–541.
793 <https://doi.org/10.1107/S0909049505012719>

794 Saad, E.M., Sun, J., Chen, S., Borkiewicz, O.J., Zhu, M., Duckworth, O.W., Tang, Y., 2017.
795 Siderophore and organic acid promoted dissolution and transformation of Cr(III)-Fe (III)-(oxy)
796 hydroxides. *Environ. Sci. Technol.* 51 (6), 3223–3232. <https://doi.org/10.1021/acs.est.6b05408>

797 Seal, A.N., Haig, T., Pratley, J.E., 2004. Evaluation of putative allelochemicals in rice root exudates
798 for their role in the suppression of Arrowhead root growth. *J. Chem. Ecol.* 30, 1663–1678.
799 <https://doi.org/10.1023/B:JOEC.0000042075.96379.71>

800 Sebastian, A., Prasad, M.N.V., 2016. Iron plaque decreases cadmium accumulation in *Oryza sativa* L.
801 and serves as a source of iron. *Plant Biol.* 18 (6), 1008–1015. <https://doi.org/10.1111/plb.12484>.

802 Seyfferth, A.L., Webb, S.M., Andrews, J.C., Fendorf, S., 2010. Arsenic localization, speciation, and
803 co-occurrence with iron on rice (*Oryza sativa* L.) roots having variable Fe coatings. *Environ. Sci.*
804 *Technol.* 44, 8108–8113. <https://doi.org/10.1021/es101139z>

805 Somenahally, A.C., Hollister, E.B., Yan, W., Gentry, T.J., Loeppert, R.H., 2011. Water management
806 impacts on arsenic speciation and iron-reducing bacteria in contrasting rice-rhizosphere
807 compartments. *Environ. Sci. Technol.* 45, 8328–8335. <https://doi.org/10.1021/es2012403>

808 Tang, Y.Z., Michel, F.M., Zhang, L.H., Harrington, R., Parise, J.B., Reeder, R.J., 2010. Structural
809 properties of the Cr(III)-Fe(III) (oxy)hydroxide compositional series: Insights for a Nanomaterial
810 "solid solution". *Chem. Mat.* 22 (12), 3589–3598. <https://doi.org/10.1021/cm1000472>

811 Tao, Q., Zhao, J., Jinxing, L., Liu, Y., Luo, J., Yuan, S., Li, B., Li, Q., Xu, Q., Yu, X., Huang, H., Li,
812 T., 2020. Unique root exudate tartaric acid enhanced cadmium mobilization and uptake in Cd-
813 hyperaccumulator *Sedum alfredii*. 383, 121177. <https://doi.org/10.1016/j.jhazmat.2019.121177>

814 Tian, S., Lu, L., Yang, X., Webb, S.M., Du, Y., Brown, P.H., 2010. Spatial imaging and speciation of
815 lead in the accumulator plant *Sedum alfredii* by microscopically focused synchrotron X-ray
816 investigation. *Environ. Sci. Technol.* 44(15), 5920–5926. <https://doi.org/10.1021/es903921t>

817 Tripathi, R.D., Tripathi, P., Dwivedi, S., Kumar, A., Mishra, A., Chauhan, P.S., Norton, G.J.,
818 Nautiyal, C.S., 2014. Roles for root iron plaque in sequestration and uptake of heavy metals and
819 metalloids in aquatic and wetland plants. *Metallomics* 6, 1789–1800.
820 <https://doi.org/10.1039/c4mt00111g>

821 Uren, N.C., 2000. Types, amount, and possible functions of compounds released into the
822 rhizosphere by soil-grown plants. In: Pinton, R., Varanini, Z., Nannipieri, P. (Eds.), *The*

823 Rhizosphere: Biochemistry and Organic Substances at the Soil–Plant Interface. Marcel
824 Dekker, New York, pp. 19–40.

825 van Genuchten, C.M., Gadgil, A.J., Peña, J., 2014. Fe (III) nucleation in the presence of bivalent 12
826 cations and oxyanions leads to subnanoscale 7 Å polymers. *Environ. Sci. Technol.* 48, 11828–
827 11836. <https://doi.org/10.1021/es503281a>

828 Wang, Y., Yang, J., Han, H., Hu, Y., Wang, J., Feng, Y., Yua, B., Xia, X., Darma, A., 2021.
829 Differential transformation mechanisms of exotic Cr(VI) in agricultural soils with contrasting
830 physio-chemical and biological properties. *Chemosphere* 729, 130546
831 <https://doi.org/10.1016/j.chemosphere.2021.130546>

832 Wang, Y., Yang, R., Zheng, J., Shen, Z., Xu, X., 2019. Exogenous foliar application of fulvic acid
833 alleviate cadmium toxicity in lettuce (*Lactuca sativa* L.). *Ecotoxicol. Environ Saf.* 167,10–19.
834 <https://doi.org/10.1016/j.ecoenv.2018.08.064>.

835 Williams, P.N., Santner, J., Larsen, M., Lehto, N.J., Oburger, E., Wenzel, W., Glud, R.N., Davison,
836 W., Zhang, H., 2014. Localised flux maxima of arsenic, lead, and iron around root apices in
837 flooded lowland rice. *Environ. Sci. Technol.* 48 (15), 8498–8506.
838 <https://doi.org/10.1021/es501127k>

839 Wirth, J., Chopin, F., Santoni, V., Viennois, G., Tillard, P., Krapp, A., Lejay, L., Daniel-Vedele, F.,
840 Gojon, A., 2007. Regulation of root nitrate uptake at the NRT2.1 protein level in *Arabidopsis*
841 *thaliana*. *J. Biol. Chem.* 282, 23541–23552. <https://doi.org/10.1074/jbc.M700901200>

842 Wu, C., Ye, Z., Li, H., Wu, S., Deng, D., Zhu, Y., Wong, M., 2012. Do radial oxygen loss and
843 external aeration affect iron plaque formation and arsenic accumulation and speciation in rice? *J.*
844 *Exp. Bot.* 63, 2961–2970. <https://doi.org/10.1093/jxb/ers017>.

845 Xiao, W., Ye, X., Zhu, Z., Zhang, Q., Zhao, S., Chen, D., Gao, N., Hu, J., 2021. Continuous flooding
846 stimulates root iron plaque formation and reduces chromium accumulation in rice (*Oryza sativa*
847 L.). *Sci. Total Environ.* 788,147786. <https://doi.org/10.1016/j.scitotenv.2021.147786>

848 Xiao, W., Zhang, Q., Zhao, S., Chen, D., Gao, N., Huang, M., Ye, X., 2023. Citric acid
849 secretion from rice roots contributes to reduction and immobilization of Cr(VI) by

850 driving microbial sulfur and iron cycle in paddy soil. *Sci. Total Environ.* 16,158832.
851 <https://doi.org/10.1016/j.scitotenv.2022.158832>.

852 Xu, B., Wang, F., Zhang, Q., Lan, Q., Liu, C., Guo, X., Cai, Q., Chen, Y., Wang, G., Ding, J., 2018.
853 Influence of iron plaque on the uptake and accumulation of chromium by rice (*Oryza sativa* L.)
854 seedlings: Insights from hydroponic and soil cultivation. *Ecotoxicol Environ. Saf.* 162, 51–58.
855 <https://doi.org/10.1016/j.ecoenv.2018.06.063>

856 Xu, B., Yu, S., 2013. Root iron plaque formation and characteristics under N₂ flushing and its effects
857 on translocation of Zn and Cd in paddy rice seedlings (*Oryza sativa*). *Ann. Bot.*, 111(6):1189–
858 1195. doi:10.1093/aob/mct072

859 Xu, M., Gao, P., Wu, J., Ma, J., Zhang, X., Yang, G., Long, L., Chen, C., Song, C., Xiao, Y., 2022.
860 Biochar promotes arsenic sequestration on iron plaques and cell walls in rice roots. *Chemosphere*
861 288, 132422. <https://doi.org/10.1016/j.chemosphere.2021.132422>

862 Yamaji, N., Ma, J.F., 2007. Spatial distribution and temporal variation of the rice silicon transporter
863 Lsi1. *Plant Physiol.* 143, 1306–1313. <https://doi.org/10.1104/pp.106.093005>

864 Yang, J., Xia, X., Liu, J., Wang, J., Hu, Y., 2020. Molecular mechanisms of chromium (III)
865 immobilization by organo–ferrihydrite co-precipitates: The significant roles of ferrihydrite and
866 carboxyl. *Environ. Sci. Technol.* 54 (8), 4820–4828. <https://doi.org/10.1021/acs.est.9b06510>

867 Yang, J., Zhu, S., Zheng, C., Sun, L., Liu, J., Shi, J., 2015. Impact of S fertilizers on pore-water Cu
868 dynamics and transformation in a contaminated paddy soil with various flooding periods. *J.*
869 *Hazard. Mater.* 286, 432–439. <https://doi.org/10.1016/j.jhazmat.2015.01.035>

870 Yang, L.T., Jiang, H.X., Qi, Y.P., Chen, L.S., 2012. Differential expression of genes involved in
871 alternative glycolytic pathways, phosphorus scavenging and recycling in response to aluminium
872 and phosphorus interactions in citrus roots. *Mol. Biol. Rep.* 39 (5), 6353–6366.
873 <https://doi.org/10.1007/s11033-012-1457-7>.

874 Yang, L.T., Qi, Y.P., Jiang, H.X., Chen, L.S., 2013. Roles of organic acid anion secretion in
875 aluminium tolerance of higher plants. *Biomed. Res. Int.* 2013, 173682.
876 <https://doi.org/10.1155/2013/173682>

877 Yang, S., Zhao, J., Chang, S.X., Collins, C., Xu, J., Liu, X., 2019a. Status assessment and
878 probabilistic health risk modeling of metals accumulation in agriculture soils across China: A
879 synthesis. *Environ. Int.* 128, 165–174. <https://doi.org/10.1016/j.envint.2019.04.044>

880 Yang, Y., Yang, Z., Yu, S., Chen, H., 2019b. Organic acids exuded from roots increase the available
881 potassium content in the rhizosphere soil: a rhizobag experiment in *Nicotiana tabacum*. *Hort. Sci.*
882 *54*, 23–27. <https://doi.org/10.21273/HORTSCI13569-18>

883 Yang, Y.Y., Jung, J.Y., Song, W.Y., Suh, H.S., Lee, Y., 2000. Identification of rice varieties with
884 high tolerance or sensitivity to lead and characterization of the mechanism of tolerance. *Plant*
885 *Physiol.* 124, 1019–1026. <https://doi.org/10.1104/pp.124.3.1019>

886 Ye, Z.H., Cheung, K.C., Wong, M.H., 2001. Copper uptake in *Typha latifolia* as affected by iron and
887 manganese plaque on the root surface. *Can. J. Bot.* 79, 314–320. <https://doi.org/10.1139/b01-012>

888 Yu, X.Z., Lu, M.R., Zhang, X.H., 2017. The role of iron plaque in transport and distribution of
889 chromium by rice seedlings. *Cereal Res. Commun.* 45 (4), 598–609.
890 <https://doi.org/10.1556/0806.45.2017.040>

891 Yu, Y., 2018. *History of Chinese Rice Varieties (Hunan Conventional Rice Rolls)*, first ed. China
892 Agriculture Press, China.

893 Yuan, H., Zhu, Z., Liu, S., Ge, T., Jing, H., Li, B., Liu, Q., Lynn, T.M., Wu, J., Kuzyakov, Y., 2016.
894 Microbial utilization of rice root exudates: ¹³C labeling and PLFA composition. *Biol. Fertil.*
895 *Soils* 52, 615–627. <https://doi.org/10.1007/s00374-016-1101-0>

896 Zandi, P., Yang, J., Darma, A., Bloem, E., Xia, X., Wang, Y., Li, Q., Schnug, E., 2022. Iron plaque
897 formation, characteristics, and its role as a barrier and/or facilitator to heavy metal uptake in
898 hydrophyte rice (*Oryza sativa* L.). *Environ. Geochem. Health.* [https://doi.org/10.1007/s10653-](https://doi.org/10.1007/s10653-022-01246-4)
899 [022-01246-4](https://doi.org/10.1007/s10653-022-01246-4).

900 Zandi, P., Yang, J., Xia, X., Barabasz-Krasny, B., Mozdzeń, K., Puła, J., Elke, B., Wang, Y.,
901 Hussain, S., Hashemi, S.M., Rózanowski, B., Qian, L., 2021. Sulphur nutrition and iron plaque
902 formation on roots of rice seedlings and their consequences for immobilisation and uptake of
903 chromium in solution culture. *Plant Soil* 462, 365–388. [https://doi.org/10.1007/s11104-021-](https://doi.org/10.1007/s11104-021-04870-8)
904 [04870-8](https://doi.org/10.1007/s11104-021-04870-8)

- 905 Zandi, P., Yang, J.J., Xin, X., Yu, T., Li, Q., Mozdzeń, K., Barabasz-Krasny, B., Yaosheng, W., 2020.
906 Do sulfur addition and rhizoplane iron plaque affect chromium uptake by rice (*Oryza sativa* L.)
907 seedlings in culture solution? J. Hazard. Mater. 2020, 121803.
908 <https://doi.org/10.1016/j.jhazmat.2019.121803>
- 909 Zeng, F., Chen, S., Miao, Y., Wu, F., Zhang, G., 2008. Changes of organic acid exudation and
910 rhizosphere pH in rice plants under chromium stress. Environ. Pollut. 155 (2), 284–289.
911 <https://doi.org/10.1016/j.envpol.2007.11.019>
- 912 Zeng, F., Zhou, W., Qiu, B., Ali, S., Wu, F., Zhang, G., 2011. Subcellular distribution and chemical
913 forms of chromium in rice plants suffering from different levels of chromium toxicity. J. Plant
914 Nutr. Soil Sci. 174, 249–256. <https://doi.org/10.1002/jpln.200900309>
- 915 Zhang, Q., Liu, J., Lu, H., Zhao, S., Wang, W., Du, J., Yan, C., 2015. Effects of silicon on growth,
916 root anatomy, radial oxygen loss (ROL) and Fe/Mn plaque of *Aegiceras corniculatum* (L.)
917 Blanco seedlings exposed to cadmium. Environ. Nanotechnol. Monitor. Manag. 4, 6–11.
918 <https://doi.org/10.1016/j.enmm.2015.04.001>
- 919 Zhang, Z., Shi, W., Ma, H., Zhou, B., Li, H., Lü, C., He, J., 2020. Binding mechanism between fulvic
920 acid and heavy metals: integrated interpretation of binding experiments, fraction
921 characterizations, and models. Water Air Soil Pollut. 231,184. [https://doi.org/10.1007/s11270-](https://doi.org/10.1007/s11270-020-04558-2)
922 [020-04558-2](https://doi.org/10.1007/s11270-020-04558-2)
- 923 Zhao, F., Ma, Y., Zhu, Y.G., Tang, Z., Mcgrath, S.P., 2015. Soil contamination in China, current
924 status and mitigation strategies. Environ. Sci. Technol. 49 (2), 750–759.
925 <https://doi.org/10.1021/es5047099>

Speciation and distribution of chromium (Cr) in rice root tip and mature zone: the importance and impact of root exudation and iron plaque in Cr bioavailability

Peiman Zandi^{a#,b}, Xing Xia^{a#}, Jianjun Yang^{a*}, Jin Liu^c, Remusat Laurent^d, Cornelia Rumpel^e, Elke Bloem^f, Beata Barabasz Krasny^g, Ewald Schnug^h

^a Institute of Environment and Sustainable Development in Agriculture, Chinese Academy of Agricultural Science, Beijing 100081, P. R. China

^b International Faculty of Applied Technology, Yibin University, Yibin 644000, China

^c College of Agronomy and Biotechnology, China Agricultural University, Beijing 100094, China

^d Muséum National d'Histoire Naturelle, Institut de Minéralogie, Physique des Matériaux et Cosmochimie, CNRS UMR 7590, Sorbonne Université, 75005 Paris, France

^e CNRS, Institute of Ecology and Environmental Sciences of Paris, IEES, UMR (CNRS-INRA-UPMC-UPEC-IRD), Thiverval-Grignon, 78850, France

^f Julius Kühn-Institut, Federal Research Centre for Cultivated Plants, Institute for Crop and Soil Sciences, Bundesallee 69, 38116 Braunschweig, Germany

^g Institute of Biology, Pedagogical University of Krakow, Podchorążych 2 St., 30-084 Kraków, Poland

^h Institute for Plant Biology, Department of Life Sciences, Technical University of Braunschweig, 38106 Braunschweig, Germany

[#]Xing Xia and Peiman Zandi equally contributed to this work.

* Corresponding author.

E-mail address: yangjianjun@caas.cn; yangjianjun-caas@outlook.com (J. Yang)

Speciation and distribution of chromium (Cr) in rice root tip and mature zone: the importance and impact of root exudation and iron plaque in Cr bioavailability

Abstract

Evidence on the contribution of root regions with varied maturity levels in iron plaque (IP) formation and root exudation of metabolites and their consequences for uptake and bioavailability of chromium (Cr) remains unknown. Therefore, we applied combined nanoscale secondary ion mass spectrometry (NanoSIMS) and synchrotron-based techniques, micro-X-ray fluorescence (μ -XRF) and micro-X-ray absorption near-edge structure (μ -XANES) to examine the speciation and localisation of Cr and the distribution of (micro-) nutrients in rice root tip and mature region. μ -XRF mapping revealed that the distribution of Cr and (micro-) nutrients varied between root regions. Cr K-edge XANES analysis at Cr hotspots attributed the dominant speciation of Cr in outer (epidermal and sub-epidermal) cell layers of the root tips and mature root to Cr(III)-FA (fulvic acid-like anions) (58-64%) and Cr(III)-Fh (amorphous ferrihydrite) (83-87%) complexes, respectively. The co-occurrence of a high proportion of Cr(III)-FA species and strong co-location signals of $^{52}\text{Cr}^{16}\text{O}$ and $^{13}\text{C}^{14}\text{N}$ in the mature root epidermis relative to the sub-epidermis indicated an association of Cr with active root surfaces, where the dissolution of IP and release of their associated Cr are likely subject to the mediation of organic anions. The results of NanoSIMS (poor $^{52}\text{Cr}^{16}\text{O}$ and $^{13}\text{C}^{14}\text{N}$ signals), dissolution (no IP dissolution) and μ -XANES (64% in sub-epidermis >58% in the epidermis for Cr(III)-FA species) analyses of root tips may be indicative of the possible re-uptake of Cr by this region. The results of this research work highlight the significance of IP and organic anions in rice root systems on the bioavailability and dynamics of Cr.

Keywords: Cr-speciation, Iron-plaque dissolution, NanoSIMS analysis, phytometabolites, root morphology

Environmental Implications

27 Considering how different root regions with varied iron plaque presence, dissolution rate, and
28 diverse root metabolites and their exudations may affect the fate of Cr uptake and bioavailability in
29 rice plants, the present study has, for the first time, set the stage for holistic investigation of two
30 critical parts of the root (tip/mature root) system at a molecular level using combined NanoSIMS and
31 synchrotron-based (μ -XRF/ μ -XANES) techniques. The findings of this study appear to be significant
32 for current and future studies on suppressing heavy metal bioavailability in contaminated paddy soil
33 systems.

34

35 1. Introduction

36 Soil contamination with heavy metals, especially chromium (Cr), is a widespread problem that
37 poses threats to human health risks through the food chain (Yang et al., 2019a; Ali et al., 2022).
38 In China, Cr is one of the eight heavy metals most strongly affecting agricultural soils, with a
39 contamination rate exceeding 1.1% (Zhao et al., 2015). Based on the China National Food Hygiene
40 Standard (GB 2762-2017), the bioaccessibility of Cr in rice grain should not exceed the Cr threshold
41 value of 1.0 mg.kg⁻¹ (Geng et al., 2020; Ali et al., 2022) to avoid adverse health complications (e.g.,
42 oxidative stress and DNA damage) associated with dietary Cr intake (Nickens et al., 2010; Khan et al.,
43 2012). Therefore, controlling Cr transfer in the soil-rice system is crucial for food safety.

44 Root uptake in rice is considered to be the major entry route of soil Cr into edible rice grains. The
45 root system of rice plants consists of seminal, nodal (primary), and lateral roots (Gu et al., 2017).
46 Among them, primary roots are classified into root tips and mature root regions according to the level
47 of development (Seyferth et al., 2010; Zandi et al., 2022). Root tips have underdeveloped vascular
48 systems, lacking the complete formation of the aerenchyma and Casparian bands (CBs). They account
49 only for a small fraction of the overall mineral element uptake in rice plants, while mature rice roots
50 have a fully developed anatomical structure with the cortex (exodermis, aerenchyma, endodermis) and
51 stele (xylem) that support the influx and transport of mineral nutrients (Yamaji and Ma, 2007;
52 Coudert et al., 2010; Fukao et al., 2019).

53 Similarly to many aquatic or semi-aquatic plants, rice is a hydrophyte species grown in flooded
54 paddy fields. Rice has to cope with anaerobic conditions by radial oxygen diffusion from the root
55 aerenchyma towards the root surface and adjacent rhizosphere (Deng et al., 2010; Xu et al., 2018),
56 where it mediates iron oxidation [Fe (II) to Fe (III)] and development of an amorphous coating of iron
57 (hydr)oxides (known as iron plaque, IP) on the root surface (Cheng et al., 2014; Tripathi et al., 2014;
58 Zandi et al., 2022). Moreover, continuous flooding was indicated to create a favourable rhizosphere
59 environment for IP formation (Xiao et al., 2021). The physical barrier of IP has been proposed to
60 serve as a natural protection mechanism against excess heavy metal concentration in plant parts (Khan
61 et al., 2016).

62 There is consensus that root capacity for aerobic respiration is the main factor in the oxidising
63 power of the rhizoplane zone (Wu et al., 2012; Holzschuh et al., 2014), and consequently the degree
64 of IP formation (Zandi et al., 2022). Rice root tips with no discernible aerenchyma structures were
65 found to have a higher oxygen discharge in comparison to the basal part of the root (Nishiuchi et al.,
66 2012). Nonetheless, IP was shown to be less frequent around the root tips (Williams et al., 2014) due
67 to their rapid development (Nishiuchi et al., 2012), possibly affecting heavy metal speciation and
68 mobility in this region compared to the basal root region.

69 Many studies concerning the whole root system have shown that iron (hydr)oxides have a strong
70 binding affinity for metal(loid) ions on the root surface and reduce their mobility and bioavailability,
71 thereby inhibiting the uptake and transport of toxic metals, including Cr (Hu et al., 2014; Cao et al.,
72 2018; Zandi et al., 2022). Previous studies have shown that in the absence or weak presence of IP,
73 higher concentrations of Cr were accumulated in root cells rather than in shoots of rice (Xu et al.,
74 2018; Zandi et al., 2020, 2021), suggesting that Cr mainly deposited in root cell walls hindered its
75 transport to the aerial organs (Zeng et al., 2011). The hydroponic and soil culture experiments have
76 demonstrated that an appropriate amount of IP on root surfaces could effectively adsorb Cr(III) and
77 Cr(VI) species and reduce their transfer to the rice roots and shoots, thus decreasing Cr concentrations
78 in rice tissues (Xu et al., 2018; Yu et al., 2017; Zandi et al., 2020).

79 In addition to the inhibition of iron (hydr)oxides, other factors such as root exudates, which
80 mainly consist of low or fairly low molecular weight (LMW) organic anion metabolites, with various

81 chemical functional groups (e.g., $-\text{COOH}$, $-\text{OH}$) (Seal et al., 2004), have been proposed to interact
82 with iron (hydr)oxides during sorption and chelation of heavy metals in the soil (Zhang et al., 2020)
83 and plant systems (Wang et al., 2019). Moreover, earlier studies have shown that these metabolites
84 can enhance the dissolution of iron (hydr)oxides bound to heavy metals, leading to their release into
85 the rhizosphere (Sebastian and Prasad, 2016; Luo et al., 2017; Saad et al., 2017). Studies on the entire
86 root system in environments contaminated with cadmium (Cd), aluminium (Al) and Cr have indicated
87 that organic anion secretions are highly associated with increased heavy metal tolerance through their
88 efflux into the rhizosphere (Yang et al., 2013; Saad et al., 2017; Yang et al., 2019b; Bali et al., 2020).
89 This efficient exclusion mechanism reduces metal uptake and accumulation in plants (Montiel-Rozas
90 et al., 2016).

91 In the rice root system, these metabolites may also act as a defensive barrier for the roots by
92 forming stable complexes with Cr (Uren, 2000; Zeng et al., 2008) or affecting their reduction and
93 immobilisation in the root (Xiao et al., 2023). Therefore, the contribution of root exudates to increased
94 Cr accumulation in rice roots could be related to the tolerance mechanism through chelation (Hayat et
95 al., 2012; Agnello et al., 2014). The rate and composition of metabolites released in response to Cr
96 stress correlate with plant genotype (Zeng et al., 2008) and metal speciation of Cr (Pradas del Real et
97 al., 2014).

98 Previous studies on the importance of IP or root exudation in suppressing the bioavailability of
99 heavy metal Cr in rice plants mainly focused on the evaluation of the entire root system (Zandi et al.,
100 2020; Xiao et al., 2023). This study has addressed for the first time how individual root regions with
101 varied maturity levels (e.g., less developed tips) may differ in the degree of IP formation or in the
102 secretion of organic anions in response to Cr stress. Further, the issues concerning the correlation of
103 these secretions with IP dissolution and Cr release, and whether IP dissolution mediated by root
104 metabolites can alter Cr mobility and bioavailability have also been analysed. Moreover, it remains
105 unclear whether the main root regions vary in their contribution to Cr chelation and immobilisation,
106 and reduced Cr accumulation in tissues under the influence of iron plaque and root exudation.

107 To bridge the gap, the present study explicitly proposed the combined application of state-of-the-art
108 high-sensitivity ion mass spectrometry (NanoSIMS) and synchrotron-based microprobe techniques,

109 such as micro-X-ray absorption near-edge structure spectroscopy (μ -XANES) and micro-beam X-ray
110 fluorescence (μ -XRF), to investigate the distribution and/or speciation of elements of interest (X) in
111 different root regions (root tips/ mature root) of rice at submicro- and microspatial scales, and their
112 association with ^{13}C -labelled root exudates on the active root surface.

113 The objectives of this study were to (1) explain/assess the interaction between Cr and Fe and its
114 effect on Cr uptake and translocation in rice plants, (2) elucidate the molecular speciation of Cr and
115 binding mechanisms of Cr species in different root regions, and (3) to localise the active root surface
116 with exudate release and its impact on Cr uptake by different root regions. We expected that these
117 results would provide a theoretical basis for understanding heavy metal sequestration and dynamics
118 on iron plaques and their benefits to human health by reducing rice contamination. We expected that
119 these results would provide a theoretical basis for understanding heavy metal sequestration and
120 dynamics on iron plaques and their benefit to human health by reducing rice contamination.

121

122 2. Materials and methods

123 2.1. Plant culture, treatments and metal extraction

124 Rice seed (*Oryza sativa* L. Var. Xiangzaoxian 31) germination (7 days on moist gauze in plastic
125 Petri dishes in the dark at 28°C) and initial growth (21 days in black plastic containers) were
126 conducted under controlled sterile conditions in half-strength nutrient solution (Table Supplementary
127 (S) 1-S1), as previously described (Zandi et al., 2021). The variety was a high-quality, early-maturing,
128 hybrid-based (Chen et al., 2000; Yu, 2018) model crop for bioremediation studies used at the Institute
129 of Environment and Sustainable Development in Agriculture, Chinese Academy of Agricultural
130 Sciences in Beijing.

131 The seedlings of the first group, intended for iron plaque (IP) formation (Fe80-CK; Fig. S1),
132 were transferred to solutions spiked with 80 mg L⁻¹ ferrous iron (FeSO₄·7H₂O), incubated for 24 h
133 and subsequently transferred into quarter strength and total strength nutrient solution for 2 and 3 days,
134 respectively. The second group (Fe0-Cr(III)) was not subjected to IP induction, but was grown in a
135 nutrient solution containing 1.0 mg L⁻¹ CrCl₃·6H₂O for 3 days, and then transferred to a quarter-

136 strength nutrient solution for 2 days. The first two groups were exclusively designed for
137 bioavailability analysis and were not included in the follow-up investigations described in sections 2.2,
138 2.3 and 2.4. The third group (Fe80-Cr(III)) was a combination of the two aforementioned treatments,
139 where seedlings with IP were exposed to Cr(III)-spiked solutions for 3 days. Each treatment was
140 performed in three replicates. Replenishment of depleted nutrients in culture solutions was carried out
141 every three days, and manual adjustment of the solutions to a suitable pH of 5.5 was done using 0.1 M
142 HCl and NaOH (Zandi et al., 2020). All seedlings were grown in a controlled plant growth chamber
143 (PGX-350D, NSEI Co., Ltd., China) with a relative humidity of 70% dedicated to predetermined
144 periodic dark (10 h, 20 °C) and light (14 h, 28 °C, 300-350 $\mu\text{mol m}^{-2}\text{s}^{-1}$) regimes. The selected Fe and
145 Cr concentrations were based on recommendations and results of earlier studies (Hu et al., 2014; Li et
146 al., 2015; Yu et al., 2017; Zandi et al., 2020).

147 The seedlings were collected, split into roots and shoots and rinsed with deionised water. Fresh
148 roots with IP were initially divided into the tip (from the root cap to the zone without root hair; ~2-3
149 cm) and mature (from the root hair zone to the base of primary roots) sections, and subsequently
150 incubated for 30 min at room temperature (25°C) in 30 mL of cold DCB (dithionite–citrate–
151 bicarbonate) solution containing NaHCO_3 (0.125 M), $\text{Na}_3\text{C}_6\text{H}_5\text{O}_7$ (0.03 M) and $\text{Na}_2\text{S}_2\text{O}_4$ (0.5 g) (Liu
152 et al., 2004). After incubation, the sections were thoroughly washed with deionised water and
153 removed from incubation tubes. The remaining extracts were initially filled up with deionised water to
154 a volume of 50 mL and subsequently passed through a 0.45- μm filter to remove root debris.

155 The digestion of plant materials was carried out according to Hu et al. (2014) with some
156 modifications. Briefly, plaque-free root sections were oven-dried (similar to shoot samples) and
157 homogenised, pre-digested overnight in heat-proof tubes (100 mL) in 5 mL of concentrated HNO_3
158 (~65-68%). Digestion was completed in a digester heating block at 160°C for ~3 h and after cooling
159 to room temperature, diluted in 25 mL of deionised water and filtered. A reagent blank and a series of
160 external standard solutions (e.g., GBW07605) from certified reference materials in China were
161 utilised to validate the quality control and accuracy of the entire digestion procedure. Fe and Cr
162 contents in the digestion solutions and DCB extracts were quantified using ICP-OES (Agilent 5110,
163 Agilent Technologies, Inc., USA).

164 2.2. Synchrotron-based microprobe analysis

165 Freshly sectioned root specimens were stored at -30°C until synchrotron-based microprobe
166 analyses. For $\mu\text{-XRF}$ imaging of root surfaces using the VESPERS beamline at the Canadian Light
167 Source (CLS), the roots were sectioned and flatly fixed on a Kapton tape. For $\mu\text{-XRF}/\mu\text{-XANES}$
168 analyses of root cross sections using the 15U beamline at the Shanghai Synchrotron Radiation Facility
169 (SSRF, Shanghai), the corresponding root sections were cut into $60\text{-}\mu\text{m}$ -thick slices by a microtome,
170 and subsequently mounted onto a Kapton tape for freeze-drying and stored at -20°C (Tian et al., 2010;
171 Lu et al., 2017). As described in previous studies (Yang et al., 2015; Wang et al., 2021), the $\mu\text{-XRF}$
172 method of both beamlines was similar, except that the data in VESPERS were analysed using SMRK
173 software, thus here we have only reported the experimental details for the 15U beamline at the SSRF.

174 X-rays with an incident energy of 10 keV were monochromatised using a Si (111) double-crystal
175 monochromator. The spot size of the X-ray beam was micro-focused to $10\text{ }\mu\text{m} \times 5\text{ }\mu\text{m}$ using a
176 Kirkpatrick-Baez (K-B) mirror system for scanning. The root samples were placed at an angle of 45°
177 to the beam incidence perpendicular to a 7-element Si(Li) detector (e2v, USA). After selecting the
178 region of interest by the microscope, the region was scanned step by step by moving the sample stage
179 with a step size of 5 and $10\text{ }\mu\text{m}$ for x and y direction, respectively. First, the whole fluorescence
180 spectrum was acquired, and then the fluorescence signals of the elements of interest, including K (3.3
181 keV), Ca (3.6 keV), Cr (5.4 keV), Mn (5.9 keV), Fe (6.4 keV) were selected and applied to all pixel
182 spectra to obtain multi-elemental 2D mapping with a dwell time of 1.5 s per pixel. After analysing the
183 $\mu\text{-XRF}$ images using Igor Pro 6.0 software (IGOR), the spots of interest were selected for Cr K-edge
184 $\mu\text{-XANES}$ spectra collection in the fluorescence mode at 25°C . The energy range and step were set to
185 $5931\text{-}6080\text{ eV}$ and 0.5 eV , respectively. Several scans were collected from each spot and later
186 averaged to obtain a merged spectrum with a better signal-to-noise ratio. At least 2 hotspots from
187 cross-sections of the root tips and mature root regions were considered for $\mu\text{-XANES}$ spectrum
188 collection. Cr foil was also used to calibrate the beamline (X-ray) energy.

189 Cr K edge $\mu\text{-XANES}$ spectra of Cr(III) adsorbed on ferrihydrite (Cr(III)-Fh) and organo-Cr(III)
190 complexes (Cr(III)-FA) (synthesised by the interaction of CrCl_3 with fulvic acid) (Yang et al., 2020)
191 were acquired in the fluorescence mode and Cr(III) acetate in the total electron yield mode, and were

referred to as Cr reference standards. Since root iron plaques induced in a short 24-h period were poorly crystallised and mostly amorphous (Xu and Yu, 2013), ferrihydrite, a typical amorphous iron (hydr)oxide formed during iron hydrolysis (Yang et al., 2020), was considered as the principal sorbent for Cr (III) sequestration in rice root IP in this study. Athena software (Ver. 2.1.1) was used for fingerprint and linear combination fitting (LCF) analysis of sample μ -XANES spectra (Ravel and Newville, 2005). Cr speciation and the percentage of each Cr species were determined based on the LCF of Cr K-edge μ -XANES spectra of the hotspots using the spectra of the reference compounds as end-members (Peng et al., 2015). The goodness of data fitting was assessed using the R-factor.

It should be noted that the limited root samples (one sample/ root section) and spots (2 hotspots/ root cross-sections) measured during the μ -XRF and μ -XANES analyses may not be representative of the whole root samples. However, earlier studies used a similar method and have demonstrated that the output result could account for most of the sample variation (Lombi and Susini, 2009; Seyfferth et al., 2010; Frommer et al., 2011; Li et al., 2015; Yang et al., 2015).

2.3. ^{13}C labelling of rice and NanoSIMS analysis

The procedure for uniform ^{13}C labelling of rice was as described earlier (Ge et al., 2012; Yuan et al., 2016) with some modifications. Briefly, rice seedlings belonging to the third treatment group (Fe80-Cr (III)) were first exposed to CrCl_3 treatment for 24 h and subsequently transferred to normal (Cr-free) nutrient solution and kept in transparent airtight perspex ^{13}C labelling and non-labelling control boxes (40 cm long \times 50 cm wide \times 60 cm high; Fig. S2) for 24 h. During this period, the concentration of ^{13}C inside the labelling box atmosphere was maintained at approximately $400 \mu\text{L L}^{-1}$ (ppm) by controlled injection of 0.1 M $\text{Na}_2^{13}\text{CO}_3$ solution (^{13}C -enriched > 99%) into 1 M HCl solution. A CO_2 detector spectrometer (IRMS, RS-CO2WS-N01-2, Shandong Renke Control Technol. Co., Ltd., China) was used to monitor CO_2 concentration inside the labelling boxes (Kaiser et al., 2015). Isotopic labelling of rice seedlings with ^{13}C was performed by photosynthetic fixation of ^{13}C in the aforementioned labelling boxes. Seedlings incubated in unlabelled control boxes served as the reference factor for excess ^{13}C in shoots and roots after DCB extraction. The environmental growth conditions in the perspex boxes were identical to those described in section 2.1.

220 Rice seedlings were harvested and separated into roots and shoots before IP dissolution could
221 occur, e.g., as a result of the secretion of ^{13}C -labelled and/or unlabelled metabolites by the roots.
222 Afterwards, root and shoot samples from both labelled and unlabelled control seedlings were ground
223 to determine ^{13}C abundance in the respective plant samples using a C/N element analyser coupled to
224 an isotope ratio mass spectrometer to verify successful labelling with ^{13}C (Isoprime 100, Elementar's
225 PYE cube, UK). Freshly sectioned root specimens were immersed in a tissue freezing medium
226 (SAKURA Tissue-Tek OCT) for rapid freezing at -30°C . Root sections were then axially frozen-cut
227 into 60- μm -thick slices using a microtome (Reichert-Jung, Germany). The slices were collected and
228 mounted onto a Si_3N_4 wafer and coated with gold (20 nm thick) for NanoSIMS analysis.

229 Cross-sections of mature roots and root tips were imaged using Cameca NanoSIMS 50 installed at
230 the Museum National d'Histoire Naturelle, Paris, France. The surfaces of the root samples were
231 scanned with a 16 keV Cs^+ (caesium) primary beam, set to 1 pA, leading to a spatial resolution of
232 approximately 150 nm. Secondary ions were collected in multicollection mode: $^{12}\text{C}^-$, $^{16}\text{O}^-$, $^{12}\text{C}^{14}\text{N}^-$
233 and $^{13}\text{C}^{14}\text{N}^-$ in the first run (for C isotope and N/C mapping), and $^{16}\text{O}^-$, $^{12}\text{C}^{14}\text{N}^-$, $^{13}\text{C}^{14}\text{N}^-$, $^{52}\text{Cr}^{16}\text{O}^-$ and
234 $^{56}\text{Fe}^{16}\text{O}^-$ in the second run (to determine associations of organic matter and heavy metals). Image
235 processing and data analysis were carried out using the freeware package OpenMIMS (multi-isotope
236 imaging mass spectrometry, freely available at <http://nrims.harvard.edu>). In total, more than eight
237 NanoSIMS images were acquired from the labelled samples. More detailed information on ^{13}C
238 isotopic maps and NanoSIMS image processing are provided in Supporting Information (SI)-A.

239

240 2.4.Fe plaque dissolution experiment

241 The function of root exudates in the dissolution of iron (hydr)oxides and release of their associated
242 Cr into the medium was investigated in a time-lapse experiment. To this end, another set of plaque-
243 bearing rice seedlings was exposed to Cr treatment ($\text{Fe}80 \times \text{Cr(III)}$) and allowed to grow in the same
244 nutrient solution for another 16 days. The sampling schedule was established for days 1, 3, 7, 10 and
245 16. Root samples at each sampling stage were subjected to DCB extraction for ICP readings of Fe, Cr
246 and calcium (Ca).

247

248 2.5.Data analysis and statistics

249 All Cr-based computations were based on previously described equations (Liu et al., 2004; Zandi
250 et al., 2020). The R statistical package (ver. 2.12.1) was used for all statistical analyses, and statistical
251 differences between treatment means were assessed using the least significant difference (LSD) test at
252 the 0.05 probability level (Data presented here are means \pm SD, n=3).

253

254 3. Results

255 3.1.Fe and Cr concentrations in different root regions

256 Regardless of the examined root regions, the quantities of Fe and Cr adsorbed on IP (DCB extracts)
257 in the roots treated with Cr were significantly higher than in the non-treated roots ($p < 0.05$) (Fig.1a,b).
258 The observed discrepancies between Cr concentrations in DCB solutions extracted from different root
259 sections were statistically significant ($p < 0.05$; DCB-Cr in mature root > root tip). Similarly, Cr
260 concentrations in root tissues were in the following order: Root-Cr mature > Root-Cr tip ($p < 0.05$)
261 (Fig.1b). Seedlings treated with Cr (+Cr seedlings) had higher Fe and Cr contents in their root tissues
262 compared to non-treated counterparts, with markedly increased Fe accumulation in both the tip (2.25-
263 fold) and mature root (1.72-fold) sections. It was also found that the overall Fe sequestration in IP
264 (DCB-Fe) on the mature root surface was significantly higher compared to the tip region both under
265 stress (Fe80-Cr(III)) and stress-free (Fe80-CK) conditions. Fe content in the root tip was significantly
266 higher than in the mature root under Cr stress conditions (Fig.1a).

267

268 3.2. Fe and Cr concentrations/proportions in different rice parts

269 The respective concentrations of Cr and Fe in shoots, plaque-free roots, and DCB extracts differed
270 in their distribution pattern. While the concentration (or relative proportion) of Cr in roots (53%) was
271 significantly higher than that accumulated in IP (~37%) and shoots (~10%), the relative
272 concentration of Fe in individual rice components was in the following order: DCB-extractable Fe >
273 Root-Fe > Shoot-Fe (Table 1). Fe mainly accumulated in IP on the root surface under both stress
274 (~89%) and stress-free (~91%) conditions. Irrespective of Cr levels applied, Fe concentration in

275 shoots did not show any significant differences, whereas Fe concentration in IP and roots of Cr-
276 treated seedlings (Fe80-Cr(III)) was significantly (~ 1.52 to 1.98 times, respectively; $p < 0.05$) higher
277 compared to non-Cr treated seedlings (Fe80-CK) (Table 1; Fig. S5a). Only 1.5% of the total Cr
278 contents in roots translocated to shoots, with an 8.8% root-to-shoot Fe translocation efficiency
279 observed in rice exposed to Cr treatment (Table 1).

280

281 3.3. Elemental distribution in rice root

282 3.3.1. Two-dimensional surface view of the root tip and mature root sections

283 The results of *in vivo* scanning of Fe and Cr deposits on the epidermal surface of the root tip (Fig.
284 2a₁₋₂) and mature root (Fig. 2a₄₋₅) sections were partially consistent with ICP-OES analyses
285 concerning elemental distribution (Fig.1). The distribution patterns of Fe, Cr, and Ca fluorescence
286 signals in the root tips after Fe80-Cr(III) treatment were relatively weak (low-intensity spots), with
287 their hotspots scattered and located in slightly distant positions (Fig. 2a₄₋₆). Such distribution of
288 elemental intensities was considerably different from that observed in the mature section of the root,
289 where the intensity of elemental distribution mostly ranged from moderate (green), upper-moderate
290 (yellow) to high (red) levels.

291 According to the results of correlation analysis, the element Cr showed a slightly low ($R^2 = 0.57$) to
292 rather high ($R^2 = 0.77$) associations with high Fe intensities (~ 45 - 80 kilo-counts s^{-1}) and a range of
293 low to moderate associations with Ca (~ 0.2 - 2.3 kilo-counts s^{-1}) intensities, respectively, in IP
294 deposited in the tip zone of rice roots (Fig. 2b₄₋₅). Ca distribution pattern appeared to be similar to that
295 of Fe in the mature root zone, signifying a strong linear association between Fe (~ 5 - 55 kilo-counts s^{-1})
296 and Ca (~ 0.15 - 25 kilo-counts s^{-1}) concentration intensities ($R^2 = 0.90$; Fig. 2b₃). Similarly, Cr
297 concentration was the highest in the mature root zone (Fig. 2a₁), and greatly co-localised with Ca ($R^2 =$
298 0.91) and Fe ($R^2 = 0.90$) intensities observed in the same root zone (Fig. 2b₁₋₂). The majority of Cr
299 deposits in the mature zone of rice root was strongly correlated with a wide range of moderate (>50
300 kilo-counts s^{-1}) to high Fe intensities (<550 kilo-counts s^{-1}). Therefore, Cr was suggested to have a
301 strong association with Fe concentration intensities in the mature zone of rice roots, and this mostly
302 occurred in the Cr intensity range of ~ 10 - 38 kilo-counts s^{-1} (Fig. 2b₁).

303 For Cr signals emitted from the upper surface of the root tip and mature root sections, several
304 hotspots of moderate to high intensity were found, which were thought to be related to significant
305 fractions of Cr sequestered in IP. As outlined above, the concentrations of Cr, Fe and Ca tended to be
306 more intense in the mature root zone than in root tips. The majority of low to high Cr counts (~ 1.3 to
307 32.5 kilo-counts s^{-1}) correlated mostly with a low to moderate (~ 0.2 - 2.6 kilo-counts s^{-1}) counts of Ca
308 intensities in the tip zone of rice roots after Cr treatment (Fig. 2b₅). Ca was mainly distributed on the
309 epidermal surface of the mature root zone and this signal was reproduced by the element Fe. The
310 lower correlation of Cr with Fe (Fig. 2b₄) to Ca (Fig. 2b₅) could also be attributed to the co-
311 distribution of these two elements at hotspots, with no apparent correlation (or overlap) in their
312 moderate-intensity spots. The result indicated that the correlation between the intensities of Fe and Ca
313 fluorescence counts in root tips ($R^2 = 0.37$) was considerably lower than that in mature roots ($R^2 = 0.90$)
314 under Fe80-Cr(III) treatment (Fig. 2b₃₋₆). The low correlation between Fe and Ca counts in root tips
315 could be explained by a partial overlap of Fe hotspots in root tips in regions where Ca fluorescence
316 intensity was high.

317

318 3.3.2. Two-dimensional cross-section views of the root tip and mature root tissues

319 Cr was mainly localised in the epidermal and exodermal layers of both rice root sections. A higher
320 concentration of Cr was observed in the internal portion of sclerenchyma cells in the root tips in
321 comparison to the mature root section (Fig. 3a₁₋₂). In other words, Cr was enriched (with more
322 noticeable Cr spots) in the outer epidermis of mature roots. As shown in Fig. 3b₁, high-intensity Fe
323 spots could be observed on the most distal sides of epidermal and exodermal cells, while moderate-
324 intensity Fe spots were dispersed in sclerenchyma cells. In contrast, the inner portions of the
325 exodermal layer in the tip section showed a higher Fe content than the epidermis (Fig. 3b₂). Moreover,
326 Fe distribution was visible in root tip vessels, which likely corresponded to the vascular tissues of the
327 root, implying that Fe could penetrate the root tip surface into the stele and move upward. However,
328 there was no clear signal of Fe presence in the inner tissues of the mature root zone. Higher Fe
329 concentrations were recorded on the epidermal surface of the mature root zone, as opposed to the root

330 tip zone after Fe80-Cr(III) treatment. This result was consistent with our root surface μ -XRF analysis,
331 where an Fe-enrichment zone was observed on the dorsal surface of the mature root zone.

332 The co-occurrence of Fe and Cr in the epidermal and sclerenchyma cells was found in both root
333 regions (Fig. 3a₁₋₂, b₁₋₂). The correlation of Fe and Cr deposition was more pronounced in the mature
334 zone than the root tip zone, where, unlike the moderate amounts of Fe present in the root stele, no Cr
335 was located in this region (Fig. S3). It can be suggested based on the overlapping Fe and Cr signals
336 that there was a close correlation between Cr and Fe deposits in the epidermal and exodermal cell
337 layers in both sections of rice roots.

338 Fig. 3c₁₋₂ illustrates the effect of Cr on S distribution in the root tip and mature root cross-sections.
339 It is shown in Fig. 3c₁ that S was mainly dispersed in the outer cell layers (along the epidermis and
340 exodermis), in the ground tissues (across the cortex and endodermis) and the stele (pericycle and
341 vascular bundles) of the rice root. With the exception of the middle and central tissues, moderate-
342 intensity S spots in the epidermis and exodermis layers correlated well with Fe hotspots (Fig. 3b₁₋₂;
343 not marked), followed by Cr moderate-intensity spots. In comparison to Fig. 3c₁, a significant
344 decrease in S accumulation was found across the epidermis and exodermis tissues of rice root tips
345 (Fig. 3c₂). However, S distribution in the endodermis, pericycle, and stele of root tips was more
346 extensive than in the mature root zone. This suggested that a considerable proportion of S could
347 penetrate the stele in both sections of rice roots. Fig. 3a₂,b₂,c₂ demonstrated that S distribution did not
348 follow the pattern observed for Fe and Cr in the outer cell layers of the root tip cross-section.

349 Potassium (K) and Ca primarily accumulated in the internal cell layers of both root sections,
350 including endodermis, pericycle and vascular cylinder, as determined by high K and Ca fluorescence
351 intensities (Fig. 3e₁₋₂,f₁₋₂). This observation suggested successful penetration of both elements into the
352 root xylem and their subsequent possible translocation to the shoot. Images e₁,f₁ and e₂,f₂ in Fig. 3
353 clearly demonstrated that the cortex tissue in the mature root of Cr-exposed rice contained a limited
354 degree of an irregular radial dispersion/gradient of K and Ca relative to the root tip zone. This result
355 suggested that K and Ca tended to accumulate in vascular tissues. The distribution pattern of K was
356 analogous to that of Ca in rice roots from both regions. Regardless of the Mn-free region in the cortex
357 and Mn-enriched region in the stele, Mn concentration in the outer cell layers approximately

358 resembled Cr concentration in the rice root maturation region (Fig. 3a₁,d₁). Mn distribution in the rice
359 root tip region was not only limited to the outer cell layers and stele, but also included parts of cortical
360 tissues (Fig. 3d₂).

361

362 3.4. Cr K-edge μ -XANES analysis

363 One main peak and two shoulders, resolved at \sim 5999.0 eV (peak- 1), \sim 6005.0 eV (shoulder- 2) and
364 \sim 6015.0 eV (shoulder- 3), respectively, were recorded in the Cr K-edge XANES spectra associated
365 with spots of interest (SOIs) in the mature and tip region of the root (Fig. 4a). These features were
366 more similar to Cr(III)-Fh and Cr(III)-FA standards rather than the Cr(III) acetate standards with a
367 broader peak 1. The first derivative spectrum of Cr(III) acetate showed an apparently lower energy
368 position of peak b compared to other standards and samples (Fig. 4b). In addition, peak b for all
369 hotspot first derivative spectra displayed a similar shape to Cr(III)-Fh. However, peak c, which
370 appeared in the first derivative spectra of Cr(III)-FA and all hotspots, was absent in Cr(III)-Fh.
371 Therefore, Cr could co-exist and/or form complexes with fulvic acid-like (\sim FA) substances as an
372 organic metabolite with more diverse functional groups (Qin et al., 2016; Wang et al., 2019; Zhang et
373 al., 2020) and/or ferrihydrite as a typical amorphous form of iron (hydr)oxide in the outer cell layers
374 of rice roots (Tripathi et al., 2014; Zandi et al., 2020).

375 LCF analysis based on spectral features (Fig. 4a) revealed that Cr(III) bound to FA-like anions
376 accounted for 58-64% (spot 2-spot 1) and 13-17% (spot 2-spot 1) of total Cr in the tip and mature
377 regions of rice roots, respectively (Fig. 4c). In other words, the epidermal layer (spot 1) of the mature
378 root and the sub-epidermal layer (spot 1) in the root tip contained the highest proportion of Cr(III)-FA
379 species compared to spot 2 in the corresponding layers. The outer cell layers of the root tip (spot 1 and
380 spot 2) contained mainly Cr(III)-FA species, whereas Cr was mainly present as Fh-bound Cr(III) in
381 the IP of the mature root outer cell layers (83-87% of total Cr). This result suggested that the
382 immobilisation of Cr through complexation with ferrihydrite in IP on the outer cell layers of the
383 mature root was more important than the immobilisation of Cr species by complexation with phyto-
384 /organic metabolite compounds. More than 83% of total Cr was present as Cr(III)-Fh species in spot 1

385 and spot 2 of the mature root zone, which was considerably higher compared to spot 1 and spot 2 of
386 the root tip zone.

387

388 3.5. Carbon isotope results

389 The mean $\delta^{13}\text{C}$ values showed a remarkable disparity between the plaque-free ^{13}C -labelled (515.04‰)
390 and non-labelled (-30.00‰) root samples (Table S2), indicating that the downward flux of
391 photosynthetically processed $^{13}\text{CO}_2$ was significant (successful ^{13}C labelling) during the short period
392 of our experiment. However, in terms of C concentrations in labelled/non-labelled roots, this
393 discrepancy was not that robust since ~1.1% ^{13}C in the C pool of the non-labelled root samples was
394 partially similar to ~1.7% ^{13}C in the C pool of the ^{13}C -labelled roots. The results demonstrated that
395 plants with IP on their roots tended to assimilate less ^{13}C out of $^{13}\text{CO}_2$ than plants devoid of plaque.
396 We therefore found small differences between the ^{13}C abundance values in ^{13}C -enriched root cells
397 with or without IP induction. The severe reduction in C mass percentage (C%) in plaque-bearing roots
398 compared to plaque-free roots was likely caused by the contribution of Fe (III) precipitates to the
399 mass balance disturbance, regardless of whether roots were labelled or not.

400 The labelled shoot samples had a 3 times higher $^{13}\text{C}/^{12}\text{C}$ ratio (and ^{13}C abundance) compared to the
401 non-labelled shoot samples. It should be noted that the existing differences in $\delta^{13}\text{C}$ and ^{13}C abundance
402 between the labelled root and shoot samples did not significantly affect the mass percentage of C in
403 the corresponding samples. In comparison with shoot tissues, root tissue (with or without IP) samples
404 exposed to isotopically labelled $^{13}\text{CO}_2$ showed a lower proportion of ^{13}C isotope abundance, ranging
405 from 49.9% to 51.9%. Another noteworthy aspect to consider was whether the presence of IP on the
406 root surface altered C content in ^{13}C -labelled roots. In this regards, our results demonstrated a
407 substantial decrease (to about 49%) in C content of the plaque-bearing roots (^{13}C -root) compared to
408 plaque-free roots (^{13}C -root). It was assumed that the observed differences between the above samples
409 could be associated with the release of metabolites into the culture medium, or even their lower
410 production in the aerial parts, and thus decreased metabolic activity when IP was present.

411

412 3.6. Distribution mapping of metals and ^{13}C by NanoSIMS

413 NanoSIMS was used to map the relationship between metabolically active ^{13}C -enriched root
414 epidermal cells and metal complexes such as CrO and FeO (hereinafter referred to as iron (oxy)
415 hydroxide mineral) in both the tip and mature root regions. Two selected areas of root tips (Fig. 5b)
416 and mature roots (Fig. 5a) were analysed and colour composite images specifically showed the
417 epidermal cell layer of the roots treated with ferrous-spiked solutions and Cr(III). Regions of interest
418 in the two sections were defined based on whether iron (oxy) hydroxide minerals were present on (or
419 within) the epidermal cell membrane. Comparison of the tip with the mature region allowed for
420 accurate tracking of ^{13}C -enriched metabolites in these two areas. The presence of ^{13}C -enriched cells
421 was more abundant in the epidermal cell layers of mature roots than in the root tips (Fig. 5).

422 Based on composite images showing relative locations of species, such as $^{52}\text{Cr}^{16}\text{O}$, $^{13}\text{C}^{14}\text{N}$ and
423 $^{56}\text{Fe}^{16}\text{O}$, metabolically active epidermal cells in the mature root region were more enriched in ^{13}C
424 metabolites compared to the root tip. The location of ^{13}C -enriched metabolites was confined to the
425 epidermal cell walls (area 1 in Fig. 5a,b) and apoplastic spaces (area 2 in Fig. S4a₁). It was also
426 established that ^{13}C -labelled metabolites in the above-specified spots co-localised with Fe and Cr.
427 Moreover, $^{56}\text{Fe}^{16}\text{O}$ hotspots were always associated with a somewhat similar accumulation of $^{52}\text{Cr}^{16}\text{O}$.
428 The $^{56}\text{Fe}^{16}\text{O}$ signal indicated that Fe was mainly located on the root epidermal surface, irrespective of
429 the root zone. This phenomenon was more pronounced in the mature than in the immature (tip) region
430 of the root, with the outer (excluding epidermis) and inner cell (ground tissues and stele) layers of the
431 latter zone markedly associated with strong $^{56}\text{Fe}^{16}\text{O}$ signals (Fig. 3b₂).

432 The distribution of $^{56}\text{Fe}^{16}\text{O}$ in the two studied zones was heterogeneous with distinct regions of
433 accumulation along the outer edge of the root epidermis (area 2 in Fig. 5a,b). The ^{16}O images in the
434 two analysed zones clearly demonstrated that O signals were more evident in the mature root zone
435 than in the root tips (Fig. S4). The general pattern of O distribution in ^{16}O images resembled the
436 distribution observed in $^{56}\text{Fe}^{16}\text{O}$ and $^{52}\text{Cr}^{16}\text{O}$ images. Regardless of the root zone, the strongest
437 $^{56}\text{Fe}^{16}\text{O}$ and ^{16}O signals originating from the outer epidermal cell wall layer were tightly linked with
438 each other, implying that Fe was likely associated with oxide or oxy-hydroxide on the root surface.
439 The presence of overlapping signals of $^{56}\text{Fe}^{16}\text{O}$ and $^{13}\text{C}^{14}\text{N}$ or $^{12}\text{C}^{14}\text{N}$ (organic carbons, OCs) in

440 specific locations on the root surface suggested the occurrence of organo-Fe oxyhydroxide co-
441 precipitates (OFC) complexes in the examined root regions (SI-B).

442

443 3.7. Cr release during iron plaque dissolution

444 The mature root region appeared to have a lower Cr to Ca ratio compared to the root tips,
445 regardless of the sampling time (Fig. 6). This discrepancy was attributed to the higher intensity of Ca
446 distribution on the mature root surface (Fig. 2a₃₋₆). Fluctuations in the Fe/Ca ratios observed in the
447 root tip were not statistically significant ($p > 0.05$), while a significant difference between the Fe/Ca
448 ratios in the mature root zone (initial sharp decrease from day 1 to day 3) was recorded. The decrease
449 in this region was followed by a slight insignificant increase (day 3-day 7) and then another decrease
450 (day 7-day 10). This decline continued for the next 6 days (day 10-day 16). The trends in changes in
451 the Cr/Ca ratios in each of the root sections were identical to those observed for the Fe/Ca ratios,
452 suggesting that the release of immobilised Cr into the medium solution was consistent with IP
453 dissolution.

454

455 4. Discussion

456 The results of the present work supported the hypothesis that plant exposure to Cr stress further
457 stimulated Fe²⁺ exclusion and oxidation on the root surface (i.e., iron (hydr)oxide(s)/ IP formation)
458 due to elevated root oxygen release or enzymatic oxidation (Table 1 ; Fig. S5a) (Briat et al., 2010).
459 This effect was more confined to the mature zone of the rice root surface (Fig. 1a), presumably due to
460 the more developed structure (Nishiuchi et al., 2012). Thus, this region could better limit Cr's
461 bioavailability and mobility than immature root tips (Fig. 1b).

462 Iron (hydr)oxides serve not only as a physical barrier with a metal-sequestering ability (Amaral et
463 al. (2017) but also as metal-chelating ligands (e.g., DMA: 2'-deoxymugenic acid), which can bind
464 heavy metals (Banakar et al., 2017). This may explain why Fe accumulation in the tip zone was
465 slightly higher than in the mature root zone under Cr stress (Fig. 1a).

466 Root Cr content was higher than in DCB extracts and shoots (Fig. 1b; Fig. S5b). This suggests that
467 IP formation in conditions similar to flooded cultivation and its inhibitory effect on Cr uptake (Xiao et
468 al., 2021) is not necessarily limited to the root epidermal surface (Fig. 2a₂₋₅). This condition most
469 likely involves the apoplastic space in the outer layers of root cells (Fig. 3b₁₋₂) (Khan et al., 2016). It
470 appears that Cr-induced increased aerenchyma-rhizosphere oxygen outflux, coinciding with higher Fe
471 concentrations (Fig. 3b₁₋₂) (Becker et al., 2020), resulted in an increased amount of Cr precipitated on
472 the outer cell layers compared to internal cell tissues in the tip and mature zone of rice roots (Fig. 3a₁₋
473 ₂). It's worth noting that increased Cr retention in outer cell layers of plaque-bearing roots compared
474 to plaque-free roots was not associated with aerial uptake (Fig. S5b). This underlines the significance
475 of IP in Cr immobilisation (Zandi et al., 2020, 2021).

476 The observed correlation between Cr and Ca concentration intensities in surface μ -XRF imaging
477 of overlapping areas (Fig. 2a₁₋₃, a₄₋₆, b₂₋₅) indicated the importance of Ca as a critical factor in
478 rigidifying cell walls and providing structural integrity to cellular membranes (Hepler, 2005; Pathak et
479 al., 2021) in Cr cell wall sequestration by binding to it (Zeng et al., 2011). This effect was particularly
480 restricted to the outer surface (i.e., epidermal layer) of the mature root zone, where similar Cr (Fig.
481 2a₁), Fe (Fig. 2a₂) and Ca (Fig. 2a₃) concentration intensities indicated the co-precipitation of Fe with
482 Ca and Cr on epidermal root surfaces. It has been shown by sorption experiments that Ca (Gumars et
483 al., 2002; van Genuchten et al., 2014) and Cr (Yu et al., 2017) can react with surface hydroxyl groups
484 and adsorb on iron oxides.

485 In the present study, Cr accumulation in the outer cell layers (except for the epidermis) was not
486 associated with Cr deposition on cell walls (Fig. 3a₁₋₂), as indicated by the low correlation between Ca
487 and Cr intensities ($R^2=0.01$) in both root regions (Fig. S3). In contrast to our finding, in their research
488 on arsenic (As) and Cr (VI), respectively, Xu et al. (2022) and Zeng et al. (2011) attributed the
489 inhibitory role of cell walls to the entire root tissue. This difference might be related to the higher
490 mobility of metal species used in their studies.

491 The formation of Fe and Mn plaque on rice roots is indeed a ROL (radial oxygen loss)-mediated
492 exclusion strategy for limiting the absorption of potentially toxic elements (Yu et al., 2017; Li et al.,
493 2019). Consistently with Crowder and Coltman (1993), Ye et al. (2001) and Zhang et al. (2015), the

494 concentration of Fe deposits in the outer cell layers of both root regions in this work was also more
495 intense compared to Mn deposits (Fig. 3b₁₋₂, d₁₋₂). Therefore, it was not surprising that the co-
496 occurrence of Fe and Cr deposits in hotspot and non-hotspot regions was more pronounced than that
497 of Mn and Cr deposits in both regions of the root (Fig. 3; Fig. S3). It is generally accepted that the
498 functional groups in IP have the potential to form a more active substrate for metal sequestration (Cao
499 et al., 2018; Xu et al., 2018) than those in Mn plaque with its unique catalytic capacity and surface
500 activity (Ye et al., 2001; Liu and Zhu, 2005). In addition to Fe and Mn plaques, sulphur (S) containing
501 metabolites are also effective in Cr chelation and subcellular sequestration (Holland and Avery, 2011;
502 Zandi et al., 2021), as was evident in simultaneous S and Cr depositions in the examined root regions
503 (Fig. 3a₁₋₂, c₁₋₂).

504 Exclusion and chelation mechanisms seem to co-occur in rice roots during Cr stress exposure,
505 which may lead to decreased Cr entry into the inner layers of root cells and hence lowered Cr uptake,
506 as seen in Fig. 3a₁₋₂ and Fig. S3b. This would confirm the hypothesis that root exudation of organic
507 metabolites effectively reduces heavy metal uptake by rice at the root-rhizosphere interface (exclusion
508 strategy) (Wang et al., 2019; Zhang et al., 2020).

509 The results of the XANES spectra of spots of interest (SOIs) in Cr μ -XRF mapping showed that
510 phytometabolites involved in Cr chelation and detoxification were likely LMW fulvic acid-like (~FA)
511 anions (Fig. 4c) (Wang et al., 2019; Zhang et al., 2020) which have not been reported for soil-free
512 plant systems. These compounds are supposed to form stable chelate compounds with certain heavy
513 metals (chelation strategy), such as Cd (Rashid et al., 2018) and Cr (Pradas del Real et al., 2014),
514 enabling plants to withstand Cr-induced toxicity (Chen et al., 2017). Besides, reports indicated the
515 high affinity of these metabolites for Fe(III) and other structurally similar trivalent metal cations,
516 including Mn (III) (Tang et al., 2010; Saad et al., 2017).

517 The proportion of Cr(III)-FA complexes varied between individual SOIs (spot 1 and spot 2) in
518 both root regions, proposing two different models (Fig. 4c). On the one hand, a higher percentage of
519 phytometabolites or FA-like anions was bound to Cr(III) species adjacent to the root surface compared
520 to the more internal tissues in the mature root (17% vs 13%), suggesting the existence of a resistance
521 mechanism through exclusion (Osmolovskaya et al., 2018; Bali et al., 2020). On the other hand, a

522 reverse trend (58% and 64% for epidermal and subepidermal layers, respectively) was observed for
523 organically bound Cr(III) in the root tip, suggesting the occurrence of a tolerance mechanism through
524 inclusion and chelation. The proposed models were consistent with our IP dissolution results (Fig. 6).
525 For instance, in the root tip zone with its unique trend of organo-Cr(III) species, neither IP dissolution
526 nor Cr release was found to occur (Figs. 4c and 6; SI-C), reinforcing the possibility of Cr re-uptake
527 from the root tip zone in the rhizosphere. Combining the proposed models with our ICP analysis (Fig.
528 S5b), it can be inferred that the binding of FA-like anions to Cr(III) species did not lead to increased
529 Cr mobility and accumulation in shoot tissues.

530 The limited IP build-up on the root surface (Fig. 2a₅) is assumed to have resulted in increased
531 binding of FA-like anions relative to Fh species to Cr ions at the adsorbing sites in the root tip
532 epidermis (58% vs 42%; T-Spot 2 in Fig. 4c). Consequently, the formed organo-Cr(III) species
533 transferred to the immobilising sites in the outer cell layers of the root tip (Fig. 3a₁). This assumption
534 was consistent with our carbon isotope results, where the absence (or scarcity) of root plaques
535 increased the biosynthesis and transport of ¹³C-labelled organic metabolites (isotopic organic carbons-
536 Ocs) to the root system (Table 2), thereby increasing the possibility of their binding to Cr. In a study
537 by Tao et al. (2020), it was demonstrated that a small portion of assimilated ¹³C was incorporated in
538 forming organic anion metabolites involved in Cd complexation.

539 The reduced abundance of isotopic OCs in rice roots with IP, compared to those stored in rice
540 roots without IP, indicated that root plaques effectively prevented the assimilation and transfer of
541 shoot-derived metabolites (Table 2) by Cr retention and stress alleviation. Studies on plaque-free roots
542 revealed that heavy metal stress increased the content of organic acid anions in the roots and root
543 exudates (Yang et al., 2000; Mariano Eduardo et al., 2005).

544 In contrast to being a more active site of organic anion metabolism and biosynthesis (Mariano
545 Eduardo et al., 2005), only a small fraction of total Cr in individual SOIs in the outer cell layers of the
546 mature root could be chelated (13-17%) or exuded by these metabolites compared to iron
547 (hydr)oxides (Fig. 4c). There was an obvious dominance of the Cr(III)-Fh complexes relative to
548 Cr(III)-FA complexes in individual SOIs in the mature root zone, indicating the substantial role
549 played by Fh composition of iron (hydr)oxides in conferring higher tolerance to Cr toxicity through

550 chelation and immobilisation (Yu et al., 2017; Zandi et al., 2020) in this region. The reduced
551 proportion of Cr(III)-Fh complexes in the epidermal layer of the mature root, relative to the
552 subepidermal layer of the mature root (83% vs 87%; Fig. 4c), could be explained by a higher IP
553 dissolution and its associated Cr under the influence of the supposed metabolites in this region (Fig. 6)
554 (Sebastian and Prasad, 2016; Saad et al., 2017).

555 Root surface NanoSIMS imaging demonstrated how Fe oxyhydroxide (FeO) and Cr-induced
556 isotopic/non-isotopic OCs were closely adherent to the epidermal surface and to each other (Fig. 5).
557 This proximity in turn indicated adsorption of organic anion metabolites or occlusion in the interstices
558 between amorphous Fh aggregates (Zeng et al., 2008). This co-occurrence not only inhibits the
559 growth of Fh, but also tends to form smaller amorphous aggregates, and is therefore believed to affect
560 aggregation behaviour, surface properties and solubility/accessibility of Fh (Eusterhues et al., 2014),
561 contributing to Fh removal and its associated Cr from the root epidermal layer (Fig. 6). Previous
562 dissolution studies showed that organic anion metabolites adsorbed on or co-precipitated with iron
563 (hydr)oxides were likely to weaken Cr(III)-Fe(III)-(oxy)hydroxide compositional bonds under
564 anaerobic conditions. This phenomenon enhanced the solubility and dissolution kinetics of iron
565 (hydr)oxides and associated dissolved Cr (Saad et al., 2017).

566 It is worth noting that the relationship between the secretion/exudation rate of organic anions and
567 their root concentrations is attributed to heavy metal-activated organic anion transporter channels in
568 the plasma membrane of root cells (Yang et al., 2012). The observed varied patterns of Cr-induced
569 secretion of phytometabolites (Fig. 5) and IP dissolutions (Fig. 6) between the examined root regions
570 (mature root > root tip) could be due to the fact that root exudates, regardless of their role in heavy
571 metal chelation (Montiel-Rozas et al., 2016), are secreted to promote solubility and absorption of
572 poorly available nutrients in the rhizosphere (Jones et al., 2004; Gojon, 2013). Indeed, the mature
573 zone of the root system is responsible for the majority of nutrient uptake in crop plants (Jones et al.,
574 2004; Wirth et al., 2007; Gojon, 2013), which in turn explains the absolute predominance of root
575 exudates and dissolution rate of iron (hydr)oxides in this region compared to the root tip region (Figs.
576 5 and 6). In other words, the increased secretion of organic anions from the mature region compared
577 to the immature (tip) region of the root, in addition to destabilising iron (hydr)oxides (Yang et al.,

578 2012, 2013) and possible release of their co-precipitated Cr ions (Fig. 6), can also be considered an
579 essential mechanism reducing the physical resistance of root plaques to nutrient absorption.

580 Considering the absence of IP dissolution and release of its Cr co-precipitates (Fig. 6) and limited
581 secretion of organic anions (Fig. 5) in the root tip region, the relatively higher proportion of organo-
582 Cr(III) species in more internal than external tissues (64% vs 58%) of the outer cell layers in this
583 region (Fig. 4c), likely reflected the importance of organic anions (i.e., FA-like anions) in capturing
584 and transferring the absorbed Cr in the form of organo-Cr(III) species to the root tip sub-epidermis.
585 The proposed model can also be construed as a possible direct or indirect re-uptake of Cr from the
586 solution medium after release from the mature region of rice roots (as outlined earlier) and its
587 subsequent immobilisation by a combination of Fh and FA-like chelators.

588 The strong presence of organo-Cr(III) (58-64%) complexes in relation to Cr(III)-Fh (36-42%)
589 complexes in the root tip outer cell layers (Fig. 4c) was an indirect reference to the reinforcing role of
590 FA-like anions in Cr chelation and immobilisation when the Fh chelator pool was insufficient. As
591 indicated earlier, the accumulation of ¹³C-labelled organic metabolites was more intense in plaque-
592 free roots (¹³C-root) than in plaque-bearing roots (Fe¹³C-root) under Cr stress, regardless of the root
593 section (Table 2). This indirectly underscored the role played by these anions as complementary
594 factors for Cr immobilisation.

595

596 5. Concluding remarks

597 The present study concludes that root plaques have a central role in Cr chelation and
598 immobilisation, especially in the mature root region. The uptake inhibiting function of IP was not only
599 confined to root epidermal surfaces but also stretched across the entire root outer cell layers. It
600 strongly suggested that an integration of both Cr resistance (exclusion) and tolerance (chelation)
601 strategies was directly involved in the mature region of the root, where iron (hydr)oxide precipitates
602 alone accounted for over 83% of total Cr (Cr(III)-Fh) species at Cr hotspots in the epidermal and sub-
603 epidermal layers of root cells. An uneven partnership in root Cr retention and inactivation was
604 actively present in root tissues; as such, none or limited IP coated roots contained an increased amount

605 of isotopic OCs or a higher percentage of Cr(III)-FA species (58-64% for root tips), respectively. The
606 proposed model concerning the outflow (Pos. mature root) or inflow (Neg. root tips) of metabolites
607 carrying Cr (organo-Cr (III)) in outer cell layers of both root regions was well consistent (positive-
608 Pos./ negative- Neg. effect) with signal intensities of ¹³C-labelled spots as active nano-scaled spots of
609 root exudates and iron (hydr)oxide dissolution.

610

611 **Data availability**

612 In addition to the SI, all other reasonable requests for data and research materials are available
613 via contacting the corresponding author.

614

615 **Funding**

616 The work was funded by the Top-Notch Young Talents Program of China, the National Natural
617 Science Foundation of China (U1632134), the Agricultural Science and Technology Innovation
618 Program of the Chinese Academy of Agricultural Science (2021-2025) and the National Center for
619 Scientific Research (CNRS) in France (CNRS funded the NanoSIMS analyses). The National
620 NanoSIMS facility at the Muséum National d'Histoire Naturelle was established by funds from CNRS,
621 Région Ile de France, Ministère délégué à l'Enseignement Supérieur et à la Recherche, and the
622 Muséum National d'Histoire Naturelle. Synchrotron-based microprobe analysis was conducted at the
623 Canadian Light Source, a national research facility of the University of Saskatchewan, which is
624 supported by the Canada Foundation for Innovation, the Natural Sciences and Engineering Research
625 Council of Canada, the National Research Council of Canada, the Canadian Institutes of Health
626 Research, the Province of Saskatchewan, and the University of Saskatchewan.

627

628 **CRedit authorship contribution statement**

629 #XX and PZ equally contributed to this work.

630 **JY**: designed the experiments. **XX** and **PZ**: performed the lab experiments with the kind
631 guidance of **JY**. **JY**, **XX** and **PZ**: performed the XRF, XANES and SEM measurements and data

632 analysis. **JY, JL, RL** and **CR**: conducted the NanoSIMS experiments. **JY, JL** and **XX**: performed the
633 NanoSIMS data analysis. **PZ, XX, JY** and **JL**: analysed the data and drafted the manuscript. **JY, PZ,**
634 **BE, ES** and **BBK**: participated in the interpretation of results. **JY, CR, RL, PZ, BE, ES** and **BBK**:
635 improved the grammar and corrected spelling mistakes. **PZ, JY, XX, BE, BBK** and **ES**: edited and
636 thoroughly revised the manuscripts. All authors read, corrected and approved the final submitted
637 version of the manuscript.

638

639 **Declaration of Competing Interest**

640 The authors declare that they have no known competing financial interests or personal
641 relationships that could have appeared to influence the work reported in this paper.

642

643 **References**

644 **Agnello, A., Huguenot, D., Van Hullebusch, E., Esposito, G., 2014. Enhanced phytoremediation: a**
645 **review of low molecular weight organic acids and surfactants used as amendments. Crit. Rev.**
646 **Environ. Sci. Technol. 44, 2531e2576. <https://dx.doi.org/10.1080/10643389.2013.829764>.**

647 **Ali, W., Zhang, H., Mao, K., Shafeeque, M., Aslam, M.W., Yang, X., Zhong, L., Feng, X., Podgorski,**
648 **J., 2022. Chromium contamination in paddy soil-rice systems and associated human health risks**
649 **in Pakistan. Sci. Total Environ. 826,153910. <https://doi.org/10.1016/j.scitotenv.2022.153910>.**

650 **Amaral, D.C., Lopes, G., Guilherme, L.R.G., Seyfferth, A.L., 2017. A new approach to sampling**
651 **intact Fe plaque reveals Si-induced changes in Fe mineral composition and shoot as in rice.**
652 **Environ. Sci. Technol. 51, 38–45. <https://doi.org/10.1021/acs.est.6b03558>**

653 **Assimakopoulou, A., Kotsiras, A., Nifakos, K., 2013. Incidence of lettuce tipburn as related to**
654 **hydroponic system and cultivar. J. Plant Nutr. 36(9), 1383–1400.**
655 **<https://doi.org/10.1080/01904167.2013.793709>**

656 **Bali, A.S., Sidhu, G.P.S., Kumar, V., 2020. Root exudates ameliorate cadmium tolerance in plants: A**
657 **review. Environ. Chem. Lett. 18, 1243–1275. <https://doi.org/10.1007/s10311-020-01012-x>**

658 **Banakar, R., Fernandez, A.A., Díaz-Benito, P., Abadia, J., Capell, T., Christou, P., 2017.**

659 Phytosiderophores determine thresholds for iron and zinc accumulation in biofortified rice
660 endosperm while inhibiting the accumulation of cadmium. *J. Exp. Bot.* 68(17), 4983–
661 4995. <https://doi.org/10.1093/jxb/erx304>

662 Becker, M., Ngo, N.S., Schenk, M.K.A., 2020. Silicon reduces the iron uptake in rice and induces
663 iron homeostasis related genes. *Sci. Rep.* 10, 5079. <https://doi.org/10.1038/s41598-020-61718-4>

664 Briat, J.F., Ravet, K., Arnaud, N., Duc, C., Boucherez, J., Touraine, B., Cellier, F., Gaymard, F., 2010.
665 New insights into ferritin synthesis and function highlight a link between iron homeostasis and
666 oxidative stress in plants. *Ann. Bot.* 105, 811–822. <https://doi.org/10.1093/aob/mcp128>

667 Cao, Z.Z., Qin, M.L., Lin, X.Y., Zhu, Z.W., Chen, M.X., 2018. Sulfur supply reduces cadmium
668 uptake and translocation in rice grains (*Oryza sativa* L.) by enhancing iron plaque formation,
669 cadmium chelation vacuolar sequestration. *Environ. Pollut.* 238, 76–84.
670 <https://doi.org/10.1016/j.envpol.2018.02.083>

671 Chen, K., Li, B., He, G., 2000. High-yielding cultivation techniques for a new high-quality rice
672 variety Xiangzaoxian No. 31. *Crop Res.* 4, 43. <https://doi.org/10.16848/j.cnki.issn.1001-5280.2000.04.017>. [in Chinese]

673

674 Chen, Y.T., Wang, Y., Yeh, K.C., 2017. Role of root exudates in metal acquisition and tolerance.
675 *Curr. Opin. Plant Biol.* 39, 66–72. <https://doi.org/10.1016/j.pbi.2017.06.004>

676 Cheng, H., Wang, M., Wong, M.H., Ye, Z., 2014. Do radial oxygen loss and iron plaque formation
677 on roots alter Cd and Pb uptake and distribution in rice plant tissues? *Plant Soil* 375, 137–148.
678 <https://doi.org/10.1007/s11104-013-1945-0>

679 Coudert, Y., Périn, C., Courtois, B., Khong, N.G., Gantet, P., 2010. Genetic control of root
680 development in rice, the model cereal. *Trend Plant Sci.* 15(4), 219–226. <https://doi.org/10.1016/j.tplants.2010.01.008>.

681

682 Crowder, A.A., Coltman, D.W., 1993. Formation of manganese oxide plaque on rice roots in solution
683 culture under varying pH and manganese (Mn^{2+}) concentration conditions. *J. Plant Nutr.* 16 (4),
684 589–599. <https://doi.org/10.1080/01904169309364559>

685 Deng, D., Wu, S.C., Wu, F.Y., Deng, H., Wong, M.H., 2010. Effects of root anatomy and Fe plaque
686 on arsenic uptake by rice seedlings grown in solution culture. *Environ. Pollut.* 158, 2589–2595.

687 <https://doi.org/10.1016/j.envpol.2010.05.015>.

688 Eusterhues, K., Hädrich, A., Neidhardt, J., Küsel, K., Keller, T.F., Jandt, K.D., Totsche, K.U., 2014.

689 Reduction of ferrihydrite with adsorbed and coprecipitated organic matter: microbial reduction

690 by *Geobacter bremensis* vs. Abiotic reduction by Na-dithionite. *Biogeosciences* 11, 4953–4966.

691 <https://doi.org/10.5194/bg-11-4953-2014>

692 Frommer, J., Voegelin, A., Dittmar, J., Marcus, M.A., Kretzschmar, R., 2011. Biogeochemical

693 processes and arsenic enrichment around rice roots in paddy soil: results from micro-focused X-

694 ray spectroscopy. *Eur. J. Soil Sci.* 62, 305–317. [https://doi.org/10.1111/j.1365-](https://doi.org/10.1111/j.1365-2389.2010.01328.x)

695 [2389.2010.01328.x](https://doi.org/10.1111/j.1365-2389.2010.01328.x)

696 Fukao, T., Barrera-Figueroa, B.E., Juntawong, P., Peña-Castro, J.M., 2019. Submergence and

697 waterlogging stress in plants: a review highlighting research opportunities and understudied

698 aspects. *Front. Plant Sci.* 10, 340. <https://doi.org/10.3389/fpls.2019.00340>

699 Ge, T., Yuan, H., Zhu, H., Wu, X., Nie, S., Liu, C., Tong, C., Wu, J., Brookes, P., 2012. Biological

700 carbon assimilation and dynamics in a flooded rice–soil system. *Soil Biol. Biochem.* 48, 39–46.

701 <https://doi.org/10.1016/j.soilbio.2012.01.009>

702 Geng, Z., Wang, P., Fu, Y., Liu, W., Cui, Y., 2020. Bioaccessibility of chromium in rice and Its

703 human health risk assessment, *Asian J. Ecotoxicol.* (6), 205–211.

704 <https://doi.org/10.7524/AJE.1673-5897.20190610002>

705 Gojon, A., 2013. Inorganic Nitrogen acquisition and signalling. In: Eshel, A., Beekman, T. (Eds.),

706 Plant Roots. CRC Press, Boca Rotan, pp. 1–14.

707 Gu, D., Zhen, F., Hannaway, D.B., Zhu, Y., Liu, L., Cao, W., Tang, L., 2017. Quantitative

708 classification of rice (*Oryza sativa* L.) root length and diameter using image analysis. *PLoS One*

709 [12\(1\), e0169968. https://doi.org/10.1371/journal.pone.0169968.](https://doi.org/10.1371/journal.pone.0169968)

710 Gunnars, A., Blomqvist, S., Johansson, P., Andersson, C., 2002. Formation of Fe (III) oxyhydroxide

711 colloids in fresh water and brackish seawater, with incorporation of phosphate and calcium.

712 *Geochim. Cosmochim. Acta* 66, 745–758. [https://doi.org/10.1016/S0016-7037\(01\)00818-3](https://doi.org/10.1016/S0016-7037(01)00818-3)

- 713 Hayat, S., Khalique, G., Irfan, M., Wani, A.S., Tripathi, B.N., Ahmad, A., 2012. Physiological
714 changes induced by chromium stress in plants: an overview. *Protoplasma* 249, 599–611.
715 <https://doi.org/10.1007/s00709-011-0331-0>
- 716 Hepler, P.K., 2005. Calcium: A central regulator of plant growth and development. *Plant Cell*. 17(8),
717 2142–2155. <https://doi.org/10.1105/tpc.105.032508>
- 718 Holland, S.L., Avery, S.V., 2011. Chromate toxicity and the role of sulfur. *Metallomics* 3, 1119–1123.
719 <https://doi.org/10.1039/c1mt00059d>
- 720 Holzschuh, M.J., Carlos, F.S., Carmona, F.C., Bohnen, H., Anghinoni, I., 2014. Iron oxidation on the
721 surface of adventitious roots and its relation to aerenchyma formation in rice genotypes. *Revista*
722 *Brasileira de Ciência do Solo* 38 (1), 185–192. [https://doi.org/10.1590/S0100-](https://doi.org/10.1590/S0100-06832014000100018)
723 [06832014000100018](https://doi.org/10.1590/S0100-06832014000100018)
- 724 Hu, Y., Huang, Y.Z., Liu Y.X., 2014. Influence of iron plaque on chromium accumulation and
725 translocation in three rice (*Oryza sativa* L.) cultivars grown in solution culture. *Chem. Ecol.* 30
726 (1), 29–38. <https://doi.org/10.1080/02757540.2013.829050>
- 727 Jones, D.L., Hodge, A., Kuzyakov, Y., 2004. Plant and mycorrhizal regulation of
728 rhizodeposition. *New Phytol.* 163 (3), 459–480. [https://doi.org/10.1111/j.1469-](https://doi.org/10.1111/j.1469-8137.2004.01130.x)
729 [8137.2004.01130.x](https://doi.org/10.1111/j.1469-8137.2004.01130.x)
- 730 Kaiser, C., Kilburn, M.R., Clode, P.L., Fuchslueger, L., Koranda, M., Cliff, J.B., Solaiman, Z.M.,
731 Murphy, D.V., 2015. Exploring the transfer of recent plant photosynthates to soil microbes:
732 mycorrhizal pathway vs. direct root exudation. *New Phytol.* 205, 1537–1551.
733 <https://doi.org/10.1111/nph.13138>
- 734 Khan, F.H., Ambreen, K., Fatima, G. and Kumar, S., 2012. Assessment of health risks with reference
735 to oxidative stress and DNA damage in chromium exposed population. *Sci. Total Environ.* 430,
736 68–74. <https://doi.org/10.1016/j.scitotenv.2012.04.063>
- 737 Khan, N., Seshadri, B., Bolan, N., Saint, C.P., Kirkham, N.B., Chowdhury, S., Yamaguchi, N., Lee,
738 D.Y., Li, G., Kunhikrishnan, A., Qi, F., Karunanithi, R., Qiu, R., Zhu, Y.G., Syu, C.H., 2016.
739 Root iron plaque on wetland plants as a dynamic pool of nutrients and contaminants. *Adv. Agron.*

740 138, 1–96. <https://doi.org/10.1016/bs.agron.2016.04.002>

741 Li, J., Jia, Y., Dong, R., Huang, R., Liu, P., Li, X., Wang, Z., Liu, G., Chen, Z., 2019. Advances in the
742 mechanisms of plant tolerance to manganese toxicity. *Int. J. Mol. Sci.* 20(20), 5096.
743 <https://doi.org/10.3390/ijms20205096>

744 Li, Y., Zhao, J., Zjang, B., Liu, Y., Xu, X., Li, Y.F., Li, B., Gao, Y., Chai, Z., 2015. The influence of
745 iron plaque on the absorption, translocation and transformation of mercury in rice (*Oryza sativa*
746 L.) seedlings exposed to different mercury species. *Plant Soil* 398, 87–97.
747 <https://doi.org/10.1007/s11104-015-2627-x>

748 Liu, W.J., Zhu, Y.G., 2005. Iron and Mn plaques on the surface of roots of wetland plants. *Acta Ecol.*
749 *Sin.* 25 (2), 358–363. (In Chinese)

750 Liu, W.J., Zhu, Y.G., Smith, F.A., Smith, S.E., 2004. Do phosphorus nutrition and iron plaque alter
751 arsenate (As) uptake by rice seedlings in hydroponic culture? *New Phytol.* 162, 481–488.
752 <https://doi.org/10.1111/j.1469-8137.2004.01035.x>

753 Lombi, E., Susini, J., 2009. Synchrotron-based techniques for plant and soil science: opportunities,
754 challenges and future perspectives. *Plant Soil* 320, 1–35. [https://doi.org/10.1007/s11104-008-](https://doi.org/10.1007/s11104-008-9876-x)
755 [9876-x](https://doi.org/10.1007/s11104-008-9876-x)

756 Lu, L., Xie, R., Liu, T., Wang, H., Hou, D., Du, Y., He, Z., Yang, X., Sun, H., Tian, S., 2017. Spatial
757 imaging and speciation of Cu in rice (*Oryza sativa* L.) roots using synchrotron-based X-ray
758 microfluorescence and X-ray absorption spectroscopy. *Chemosphere* 175, 356–364.
759 <https://doi.org/10.1016/j.chemosphere.2017.02.082>.

760 Luo, Q., Wang, S., Sun, L., Wang, H., 2017. Metabolic profiling of root exudates from two ecotypes
761 of *Sedum alfredii* treated with Pb based on GC-MS. *Sci. Rep.* 7, 39878.
762 <https://doi.org/10.1038/srep39878>

763 Mariano Eduardo, D., Jorge Renato, A., Keltjens Willem, G., Marcelo, M., 2005. Metabolism and
764 root exudation of organic acid anions under aluminium stress. *Braz. J. Plant Physiol.* 17,
765 157–172. <https://doi.org/10.1590/S1677-04202005000100013>.

766 Montiel-Rozas, M.M., Madejón, E., Madejón, P., 2016. Effect of heavy metals and organic matter on
767 root exudates of herbaceous species: An assessment in sand and soil conditions under different

768 levels of contamination. Environ. Pollut. 216, 273–281.
769 <https://doi.org/10.1016/j.envpol.2016.05.080>

770 Nickens, K.P., Patierno, S.R. and Ceryak, S., 2010. Chromium genotoxicity: a double-edged sword.
771 Chem. Biol. Interact., 188(2), 276–288. <https://doi.org/10.1016/j.cbi.2010.04.018>

772 Nishiuchi, S., Yamauchi, T., Takahashi, H., Kotula, L., Nakazono, M., 2012. Mechanisms for coping
773 with submergence and waterlogging in rice. Rice 5, 2. <https://doi.org/10.1186/1939-8433-5-2>

774 Osmolovskaya, N., Dung, V.V., Kuchaeva, L., 2018. The role of organic acids in heavy metal
775 tolerance in plants. Bio. Comm. 63 (1), 9–16. <https://doi.org/10.21638/spbu03.2018.103>

776 Pathak, R.K., Singh, D.B., Sharma, H., Pandey, D., Dwivedi, S., 2021. Calcium uptake and
777 translocation in plants. In: Upadhyay, S.K. (Ed.), Calcium Transport Elements in Plants, 1st, ed.
778 Academic Press, New York, pp. 373–386.

779 Peng, C., Duan, D., Xu, C., Chen, Y., Sun, L., Zhang, H., Yuan, X., Zheng, L., Yang, Y., Yang, J.,
780 Zhen, X., Chen, Y., Shi, J., 2015. Translocation and biotransformation of CuO nanoparticles in
781 rice (*Oryza sativa* L.) plants. Environ. Pollut. 197, 99–107.
782 <https://doi.org/10.1016/j.envpol.2014.12.008>.

783 Pradas del Real, A.E., García-Gonzalo, P., Lobo, M.C., Pérez-Sanz, A., 2014. Chromium speciation
784 modifies root exudation in two genotypes of *Silene vulgaris*. Environ. Exp. Bot. 107, 1–6.
785 <https://doi.org/10.1016/j.envexpbot.2014.05.002>

786 Qin, Y., Zhu, H., Zhang, M., Zhang, H., Xiang, C., Li, B., 2016. GC-MS analysis of membrane-
787 graded fulvic acid and Its activity on promoting wheat seed germination. Molecules 21(10), 1363.
788 <https://doi.org/10.3390/molecules21101363>

789 Rashid, I., Murtaza, G., Zahir, Z.A., Farooq, M., 2018. Effect of humic and fulvic acid transformation
790 on cadmium availability to wheat cultivars in sewage sludge amended soil. Environ. Sci. Pollut.
791 Res. 25, 16071–16079. <https://doi.org/10.1007/s11356-018-1821-9>.

792 Ravel, B., Newville, M., 2005. Athena, Artemis, Hephaestus: data analysis for X-ray absorption
793 spectroscopy using IFEFFIT. J. Synchrotron Rad. 12, 537–541.
794 <https://doi.org/10.1107/S0909049505012719>

795 Saad, E.M., Sun, J., Chen, S., Borkiewicz, O.J., Zhu, M., Duckworth, O.W., Tang, Y., 2017.
796 Siderophore and organic acid promoted dissolution and transformation of Cr(III)-Fe (III)-(oxy)
797 hydroxides. *Environ. Sci. Technol.* 51 (6), 3223–3232. <https://doi.org/10.1021/acs.est.6b05408>

798 Seal, A.N., Haig, T., Pratley, J.E., 2004. Evaluation of putative allelochemicals in rice root exudates
799 for their role in the suppression of Arrowhead root growth. *J. Chem. Ecol.* 30, 1663–1678.
800 <https://doi.org/10.1023/B:JOEC.0000042075.96379.71>

801 Sebastian, A., Prasad, M.N.V., 2016. Iron plaque decreases cadmium accumulation in *Oryza sativa* L.
802 and serves as a source of iron. *Plant Biol.* 18 (6), 1008–1015. <https://doi.org/10.1111/plb.12484>.

803 Seyfferth, A.L., Webb, S.M., Andrews, J.C., Fendorf, S., 2010. Arsenic localization, speciation, and
804 co-occurrence with iron on rice (*Oryza sativa* L.) roots having variable Fe coatings. *Environ. Sci.*
805 *Technol.* 44, 8108–8113. <https://doi.org/10.1021/es101139z>

806 Somenahally, A.C., Hollister, E.B., Yan, W., Gentry, T.J., Loeppert, R.H., 2011. Water management
807 impacts on arsenic speciation and iron-reducing bacteria in contrasting rice-rhizosphere
808 compartments. *Environ. Sci. Technol.* 45, 8328–8335. <https://doi.org/10.1021/es2012403>

809 Tang, Y.Z., Michel, F.M., Zhang, L.H., Harrington, R., Parise, J.B., Reeder, R.J., 2010. Structural
810 properties of the Cr(III)-Fe(III) (oxy)hydroxide compositional series: Insights for a Nanomaterial
811 "solid solution". *Chem. Mat.* 22 (12), 3589–3598. <https://doi.org/10.1021/cm1000472>

812 Tao, Q., Zhao, J., Jinxing, L., Liu, Y., Luo, J., Yuan, S., Li, B., Li, Q., Xu, Q., Yu, X., Huang, H., Li,
813 T., 2020. Unique root exudate tartaric acid enhanced cadmium mobilization and uptake in Cd-
814 hyperaccumulator *Sedum alfredii*. 383, 121177. <https://doi.org/10.1016/j.jhazmat.2019.121177>

815 Tian, S., Lu, L., Yang, X., Webb, S.M., Du, Y., Brown, P.H., 2010. Spatial imaging and speciation of
816 lead in the accumulator plant *Sedum alfredii* by microscopically focused synchrotron X-ray
817 investigation. *Environ. Sci. Technol.* 44(15), 5920–5926. <https://doi.org/10.1021/es903921t>

818 Tripathi, R.D., Tripathi, P., Dwivedi, S., Kumar, A., Mishra, A., Chauhan, P.S., Norton, G.J.,
819 Nautiyal, C.S., 2014. Roles for root iron plaque in sequestration and uptake of heavy metals and
820 metalloids in aquatic and wetland plants. *Metallomics* 6, 1789–1800.
821 <https://doi.org/10.1039/c4mt00111g>

822 Uren, N.C., 2000. Types, amount, and possible functions of compounds released into the
823 rhizosphere by soil-grown plants. In: Pinton, R., Varanini, Z., Nannipieri, P. (Eds.), *The*
824 *Rhizosphere: Biochemistry and Organic Substances at the Soil–Plant Interface*. Marcel
825 Dekker, New York, pp. 19–40.

826 van Genuchten, C.M., Gadgil, A.J., Peña, J., 2014. Fe (III) nucleation in the presence of bivalent 12
827 cations and oxyanions leads to subnanoscale 7 Å polymers. *Environ. Sci. Technol.* 48, 11828–
828 11836. <https://doi.org/10.1021/es503281a>

829 Wang, Y., Yang, J., Han, H., Hu, Y., Wang, J., Feng, Y., Yua, B., Xia, X., Darma, A., 2021.
830 Differential transformation mechanisms of exotic Cr(VI) in agricultural soils with contrasting
831 physio-chemical and biological properties. *Chemosphere* 729, 130546
832 <https://doi.org/10.1016/j.chemosphere.2021.130546>

833 Wang, Y., Yang, R., Zheng, J., Shen, Z., Xu, X., 2019. Exogenous foliar application of fulvic acid
834 alleviate cadmium toxicity in lettuce (*Lactuca sativa* L.). *Ecotoxicol. Environ Saf.* 167,10–19.
835 <https://doi.org/10.1016/j.ecoenv.2018.08.064>.

836 Williams, P.N., Santner, J., Larsen, M., Lehto, N.J., Oburger, E., Wenzel, W., Glud, R.N., Davison,
837 W., Zhang, H., 2014. Localised flux maxima of arsenic, lead, and iron around root apices in
838 flooded lowland rice. *Environ. Sci. Technol.* 48 (15), 8498–8506.
839 <https://doi.org/10.1021/es501127k>

840 Wirth, J., Chopin, F., Santoni, V., Viennois, G., Tillard, P., Krapp, A., Lejay, L., Daniel-Vedele, F.,
841 Gojon, A., 2007. Regulation of root nitrate uptake at the NRT2.1 protein level in *Arabidopsis*
842 *thaliana*. *J. Biol. Chem.* 282, 23541–23552. <https://doi.org/10.1074/jbc.M700901200>

843 Wu, C., Ye, Z., Li, H., Wu, S., Deng, D., Zhu, Y., Wong, M., 2012. Do radial oxygen loss and
844 external aeration affect iron plaque formation and arsenic accumulation and speciation in rice? *J.*
845 *Exp. Bot.* 63, 2961–2970. <https://doi.org/10.1093/jxb/ers017>.

846 Xiao, W., Ye, X., Zhu, Z., Zhang, Q., Zhao, S., Chen, D., Gao, N., Hu, J., 2021. Continuous flooding
847 stimulates root iron plaque formation and reduces chromium accumulation in rice (*Oryza sativa*
848 L.). *Sci. Total Environ.* 788,147786. <https://doi.org/10.1016/j.scitotenv.2021.147786>

- 849 Xiao, W., Zhang, Q., Zhao, S., Chen, D., Gao, N., Huang, M., Ye, X., 2023. Citric acid
850 secretion from rice roots contributes to reduction and immobilization of Cr(VI) by
851 driving microbial sulfur and iron cycle in paddy soil. *Sci. Total Environ.* 16,158832.
852 <https://doi.org/10.1016/j.scitotenv.2022.158832>.
- 853 Xu, B., Wang, F., Zhang, Q., Lan, Q., Liu, C., Guo, X., Cai, Q., Chen, Y., Wang, G., Ding, J., 2018.
854 Influence of iron plaque on the uptake and accumulation of chromium by rice (*Oryza sativa* L.)
855 seedlings: Insights from hydroponic and soil cultivation. *Ecotoxicol Environ. Saf.* 162, 51–58.
856 <https://doi.org/10.1016/j.ecoenv.2018.06.063>
- 857 Xu, B., Yu, S., 2013. Root iron plaque formation and characteristics under N₂ flushing and its effects
858 on translocation of Zn and Cd in paddy rice seedlings (*Oryza sativa*). *Ann. Bot.*, 111(6):1189–
859 1195. doi:10.1093/aob/mct072
- 860 Xu, M., Gao, P., Wu, J., Ma, J., Zhang, X., Yang, G., Long, L., Chen, C., Song, C., Xiao, Y., 2022.
861 Biochar promotes arsenic sequestration on iron plaques and cell walls in rice roots. *Chemosphere*
862 288, 132422. <https://doi.org/10.1016/j.chemosphere.2021.132422>
- 863 Yamaji, N., Ma, J.F., 2007. Spatial distribution and temporal variation of the rice silicon transporter
864 Lsi1. *Plant Physiol.* 143, 1306–1313. <https://doi.org/10.1104/pp.106.093005>
- 865 Yang, J., Xia, X., Liu, J., Wang, J., Hu, Y., 2020. Molecular mechanisms of chromium (III)
866 immobilization by organo–ferrihydrite co-precipitates: The significant roles of ferrihydrite and
867 carboxyl. *Environ. Sci. Technol.* 54 (8), 4820–4828. <https://doi.org/10.1021/acs.est.9b06510>
- 868 Yang, J., Zhu, S., Zheng, C., Sun, L., Liu, J., Shi, J., 2015. Impact of S fertilizers on pore-water Cu
869 dynamics and transformation in a contaminated paddy soil with various flooding periods. *J.*
870 *Hazard. Mater.* 286, 432–439. <https://doi.org/10.1016/j.jhazmat.2015.01.035>
- 871 Yang, L.T., Jiang, H.X., Qi, Y.P., Chen, L.S., 2012. Differential expression of genes involved in
872 alternative glycolytic pathways, phosphorus scavenging and recycling in response to aluminium
873 and phosphorus interactions in citrus roots. *Mol. Biol. Rep.* 39 (5), 6353–6366.
874 <https://doi.org/10.1007/s11033-012-1457-7>.
- 875 Yang, L.T., Qi, Y.P., Jiang, H.X., Chen, L.S., 2013. Roles of organic acid anion secretion in

876 aluminium tolerance of higher plants. *Biomed. Res. Int.* 2013, 173682.
877 <https://doi.org/10.1155/2013/173682>

878 Yang, S., Zhao, J., Chang, S.X., Collins, C., Xu, J., Liu, X., 2019a. Status assessment and
879 probabilistic health risk modeling of metals accumulation in agriculture soils across China: A
880 synthesis. *Environ. Int.* 128, 165–174. <https://doi.org/10.1016/j.envint.2019.04.044>

881 Yang, Y., Yang, Z., Yu, S., Chen, H., 2019b. Organic acids exuded from roots increase the available
882 potassium content in the rhizosphere soil: a rhizobag experiment in *Nicotiana tabacum*. *Hort. Sci.*
883 54, 23–27. <https://doi.org/10.21273/HORTSCI13569-18>

884 Yang, Y.Y., Jung, J.Y., Song, W.Y., Suh, H.S., Lee, Y., 2000. Identification of rice varieties with
885 high tolerance or sensitivity to lead and characterization of the mechanism of tolerance. *Plant*
886 *Physiol.* 124, 1019–1026. <https://doi.org/10.1104/pp.124.3.1019>

887 Ye, Z.H., Cheung, K.C., Wong, M.H., 2001. Copper uptake in *Typha latifolia* as affected by iron and
888 manganese plaque on the root surface. *Can. J. Bot.* 79, 314–320. <https://doi.org/10.1139/b01-012>

889 Yu, X.Z., Lu, M.R., Zhang, X.H., 2017. The role of iron plaque in transport and distribution of
890 chromium by rice seedlings. *Cereal Res. Commun.* 45 (4), 598–609.
891 <https://doi.org/10.1556/0806.45.2017.040>

892 Yu, Y., 2018. *History of Chinese Rice Varieties (Hunan Conventional Rice Rolls)*, first ed. China
893 Agriculture Press, China.

894 Yuan, H., Zhu, Z., Liu, S., Ge, T., Jing, H., Li, B., Liu, Q., Lynn, T.M., Wu, J., Kuzyakov, Y., 2016.
895 Microbial utilization of rice root exudates: ¹³C labeling and PLFA composition. *Biol. Fertil.*
896 *Soils* 52, 615–627. <https://doi.org/10.1007/s00374-016-1101-0>

897 Zandi, P., Yang, J., Darma, A., Bloem, E., Xia, X., Wang, Y., Li, Q., Schnug, E., 2022. Iron plaque
898 formation, characteristics, and its role as a barrier and/or facilitator to heavy metal uptake in
899 hydrophyte rice (*Oryza sativa* L.). *Environ. Geochem. Health.* [https://doi.org/10.1007/s10653-](https://doi.org/10.1007/s10653-022-01246-4)
900 [022-01246-4](https://doi.org/10.1007/s10653-022-01246-4).

901 Zandi, P., Yang, J., Xia, X., Barabasz-Krasny, B., Możdżeń, K., PuŁa, J., Elke, B., Wang, Y.,
902 Hussain, S., Hashemi, S.M., Rózanowski, B., Qian, L., 2021. Sulphur nutrition and iron plaque
903 formation on roots of rice seedlings and their consequences for immobilisation and uptake of

904 chromium in solution culture. *Plant Soil* 462, 365–388. [https://doi.org/10.1007/s11104-021-](https://doi.org/10.1007/s11104-021-04870-8)
905 04870-8

906 Zandi, P., Yang, J.J., Xin, X., Yu, T., Li, Q., Możdżeń, K., Barabasz-Krasny, B., Yaosheng, W., 2020.
907 Do sulfur addition and rhizoplane iron plaque affect chromium uptake by rice (*Oryza sativa* L.)
908 seedlings in culture solution? *J. Hazard. Mater.* 2020, 121803.
909 <https://doi.org/10.1016/j.jhazmat.2019.121803>

910 Zeng, F., Chen, S., Miao, Y., Wu, F., Zhang, G., 2008. Changes of organic acid exudation and
911 rhizosphere pH in rice plants under chromium stress. *Environ. Pollut.* 155 (2), 284–289.
912 <https://doi.org/10.1016/j.envpol.2007.11.019>

913 Zeng, F., Zhou, W., Qiu, B., Ali, S., Wu, F., Zhang, G., 2011. Subcellular distribution and chemical
914 forms of chromium in rice plants suffering from different levels of chromium toxicity. *J. Plant*
915 *Nutr. Soil Sci.* 174, 249–256. <https://doi.org/10.1002/jpln.200900309>

916 Zhang, Q., Liu, J., Lu, H., Zhao, S., Wang, W., Du, J., Yan, C., 2015. Effects of silicon on growth,
917 root anatomy, radial oxygen loss (ROL) and Fe/Mn plaque of *Aegiceras corniculatum* (L.)
918 Blanco seedlings exposed to cadmium. *Environ. Nanotechnol. Monitor. Manag.* 4, 6–11.
919 <https://doi.org/10.1016/j.enmm.2015.04.001>

920 Zhang, Z., Shi, W., Ma, H., Zhou, B., Li, H., Lü, C., He, J., 2020. Binding mechanism between fulvic
921 acid and heavy metals: integrated interpretation of binding experiments, fraction
922 characterizations, and models. *Water Air Soil Pollut.* 231,184. [https://doi.org/10.1007/s11270-](https://doi.org/10.1007/s11270-020-04558-2)
923 020-04558-2

924 Zhao, F., Ma, Y., Zhu, Y.G., Tang, Z., Mcgrath, S.P., 2015. Soil contamination in China, current
925 status and mitigation strategies. *Environ. Sci. Technol.* 49 (2), 750–759.
926 <https://doi.org/10.1021/es5047099>

1 **Table Captions**

2 **Table 1** Cr and Fe concentrations and percentage distributions in different organs of the rice
3 plant

4 **Table 2** $\delta^{13}\text{C}$ values (‰), percentage of non-isotopic carbon and ^{13}C abundance for
5 labelled/unlabelled rice shoot and root (with or without iron plaque) samples

6 **Table 1**

Treatments	DCB extracts (iron plaque)				Roots				Shoots			
	Concentration		Distribution		Concentration		Distribution		Concentration		Distribution	
	(mg kg ⁻¹)		(%)		(mg kg ⁻¹)		(%)		(mg kg ⁻¹)		(%)	
	Cr	Fe	Cr	Fe	Cr	Fe	Cr	Fe	Cr	Fe	Cr	Fe
Fe80-CK	0.00b ±0.00	41.26b ±2.80	-	90.7	0.00b ±0.00	1.95ab ±0.43	-	4.3	0.00b ±0.00	0.40a ±0.04	-	5.0
Fe80-Cr(III)	1.89a ±0.14	62.73a ±2.60	37.3	88.7	2.66a ±0.14	3.87a ±0.65	53.0	5.3	0.04a ±0.00	0.34a ±0.01	9.7	6.0
LSD %	0.60	20.74	9.41	8.72	0.61	4.66	16.16	4.30	0.01	0.21	7.59	5.17

7 *Notes.* Data are means ± SE (n=3); DCB, dithionite–citrate–bicarbonate, CK and Cr (III) represent 0 and 1.0 mg L⁻¹
8 CrCl₃ · 6H₂O, respectively; Fe80 represents 80 mg L⁻¹ FeSO₄ · 7H₂O; data are means of 3 replications; different small
9 letters indicate a significant difference at *p* < 0.05 according to the LSD test.

10 **Table 2**

Plant Sample (PS)	* $\delta^{13}\text{C}$ (‰)	**C% ($\mu\text{g C g}^{-1}$ of a PS) $\times 100$	^{13}C abundance ($\mu\text{g } ^{13}\text{C g}^{-1}$ PS C)
CK-root	-30	46.09	1.08
^{13}C -root	515	45.54	1.67
Fe- ^{13}C -root	456	23.25	1.61
CK-shoot	-32.99	43.05	1.08
^{13}C -shoot	1968	44.47	3.23

11 *Note.* * - [(molar ratio of $^{13}\text{C}/^{12}\text{C}$ in samples divided by the carbonate-based VPDB standards) -1×1000]; CK-12 unlabelled (^{12}C) plant samples; ** - denotes the mass content percentage of C in plant samples.

1 **Figure captions**

2 **Fig. 1.** The concentrations of Fe (a) and Cr (b) in root tip and mature root regions before (in iron
3 plaque) and after (in root tissues) DCB extraction in *Oryza. sativa* L. at the seedling stage. Bars
4 labelled with different lowercase letters are considered significant at $p < 0.05$. Data points and bars
5 represent means \pm SE (n=3).

6 **Fig. 2.** (a)-Microscale distribution (μ -XRF mapping) of Cr ($a_{1,4}$), Fe ($a_{2,5}$), and Ca ($a_{3,6}$) on the
7 epidermal surface of mature and tip regions of rice roots with iron plaque, and under Cr(III) treatment.
8 (b)-Correlation between the intensities of Cr with Fe ($b_{1,4}$) and Ca ($b_{2,5}$) as well as Fe with Ca ($b_{3,6}$)
9 within maps of the root tip and mature sections quantified by μ -XRF analysis. Scale bars ranging from
10 dark blue (low counts) to dark red (high counts) colours for each element were acquired from
11 fluorescence intensities. Each image reports the relative distribution map of individual elements.

12 **Fig. 3.** Two-dimensional μ -XRF elemental distribution maps for cross-sections of the root tip and
13 mature root regions in rice seedlings after Fe80-Cr(III) treatment. Hot spot regions are marked by red
14 “X” and labelled in both the root tip (1, 2) and mature (1, 2) root cross-sections. Red boxes in the
15 upper images show where μ -XRF maps were obtained. The selected regions with relatively higher
16 concentrations of Cr are referred to those of positions subjected to μ -X-ray absorption near-edge
17 spectroscopy (μ -XANES) spectra collection. Scale bars representing different colours (dark blue-low
18 counts to dark red-high counts) for each element were acquired from fluorescence intensities. Each
19 image reports the relative distribution map of individual elements.

20 **Fig. 4.** Chromium (Cr) K-edge XANES spectra (a) and their first derivative spectra (b) from Cr
21 hotspots (in Fig. 3 a_{1-2}) in the root tip (T) and mature (M) root cross-sections, as well as the Cr
22 reference standards (Cr(III) bound to ferrihydrite (Fh) or fulvic acid (FA, referred to as organo-Cr(III)
23 complexes) and a Cr(III) compound ($\text{Cr}(\text{CH}_3\text{COO})_3$). The linear combination fitting (LCF) results are

24 shown in (c). The experimental and fitting XANES spectra in the subgraph (c) are shown as solid and
25 dashed lines, respectively. R factor represents a goodness-of-fit parameter.

26

27 **Fig. 5.** Elemental maps of $^{12}\text{C}^{14}\text{N}$, $^{13}\text{C}^{14}\text{N}$, $^{52}\text{Cr}^{16}\text{O}$, and $^{56}\text{Fe}^{16}\text{O}$ and corresponding RGB maps,
28 measured by NanoSIMS, illustrating the overlapping of Cr, Fe and ^{13}C hotspots (C-green, Cr -red, Fe-
29 blue) in cross-sections of mature root (white dotted circles in image a) and root tip (white arrows in
30 image b) regions in rice seedlings after Fe80-Cr(III) treatment. ^{13}C -labelled spots in bioimaging of
31 root cross-sections reflect the active nano-scaled spot of root exudates (phyto-metabolites) secreting
32 from root epidermis.

33

34 **Fig. 6.** The concentration ratio of Fe/Cr to the calcium (Ca) in the iron plaque of different root
35 sections during several days after Fe80-Cr (III) treatment. Markers labelled with different lowercase
36 letters are considered significant at $p < 0.05$. Error bars represent \pm SD (n=2). (Fe/Ca and Cr/Ca ratios
37 were calculated to minimise the impact of varied root weights on the determined Fe and Cr
38 concentrations at the corresponding harvesting time).

Figure 1

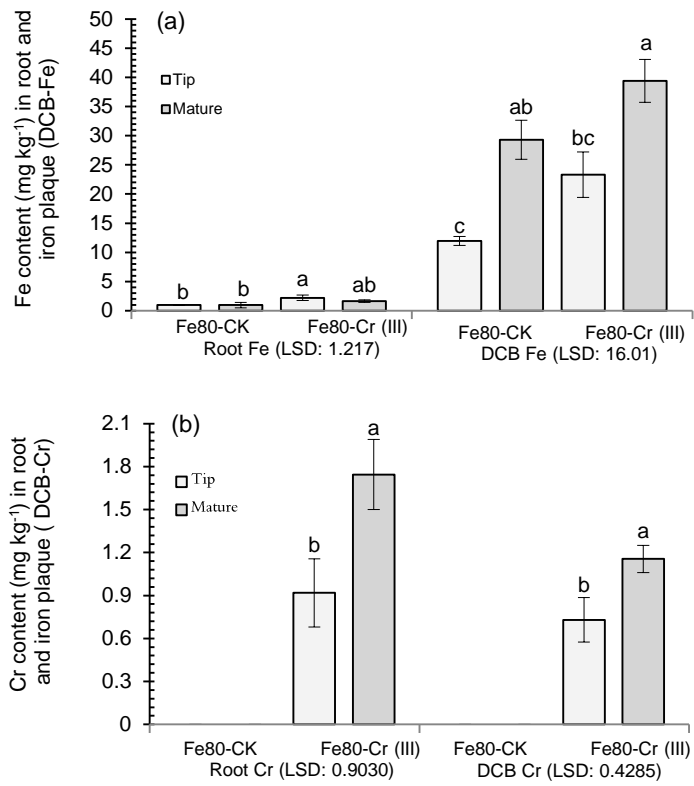


Figure 2

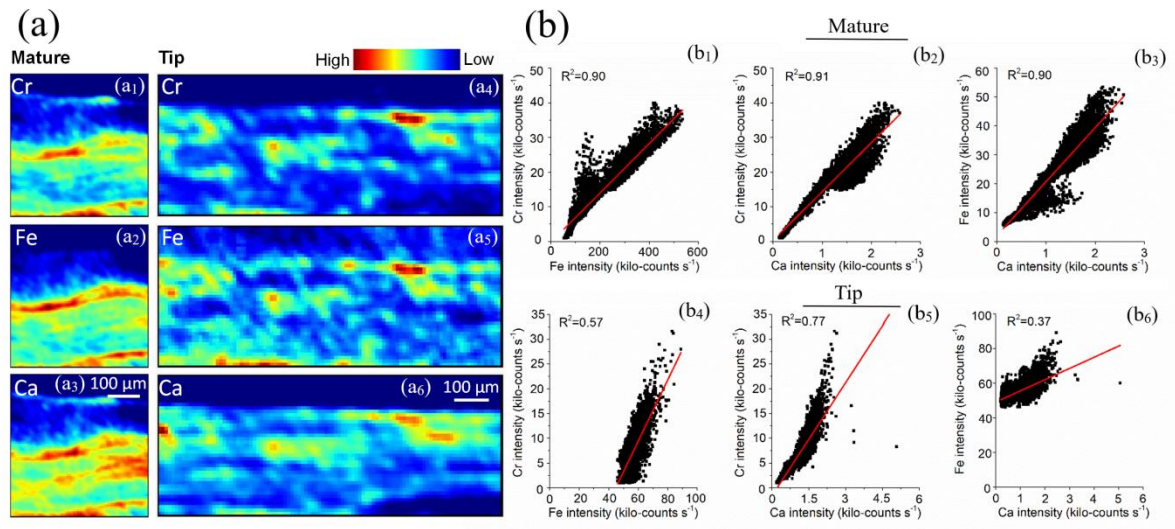


Figure 3

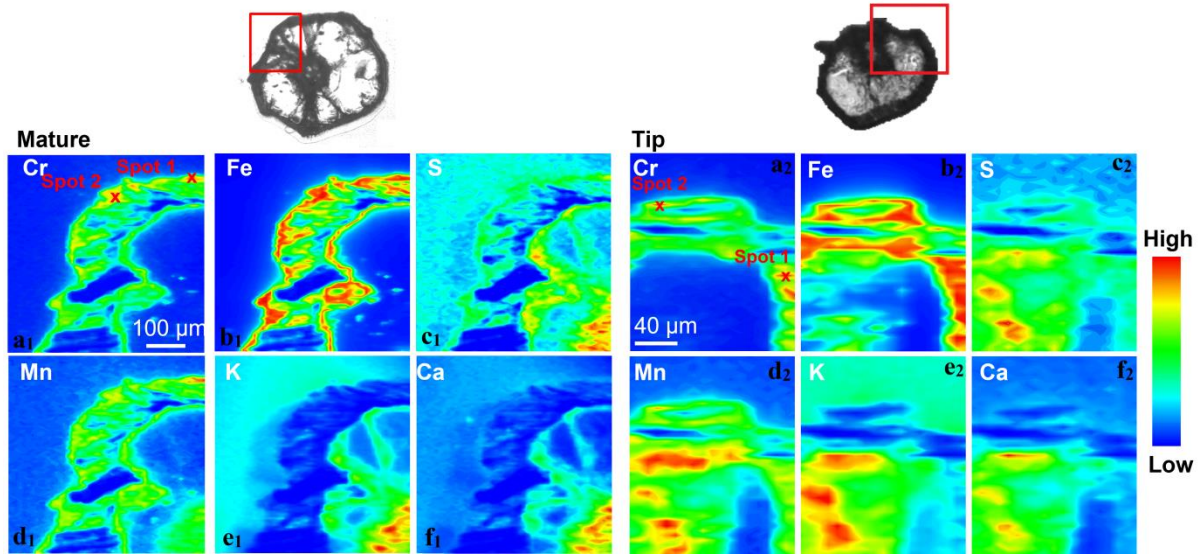


Figure 4

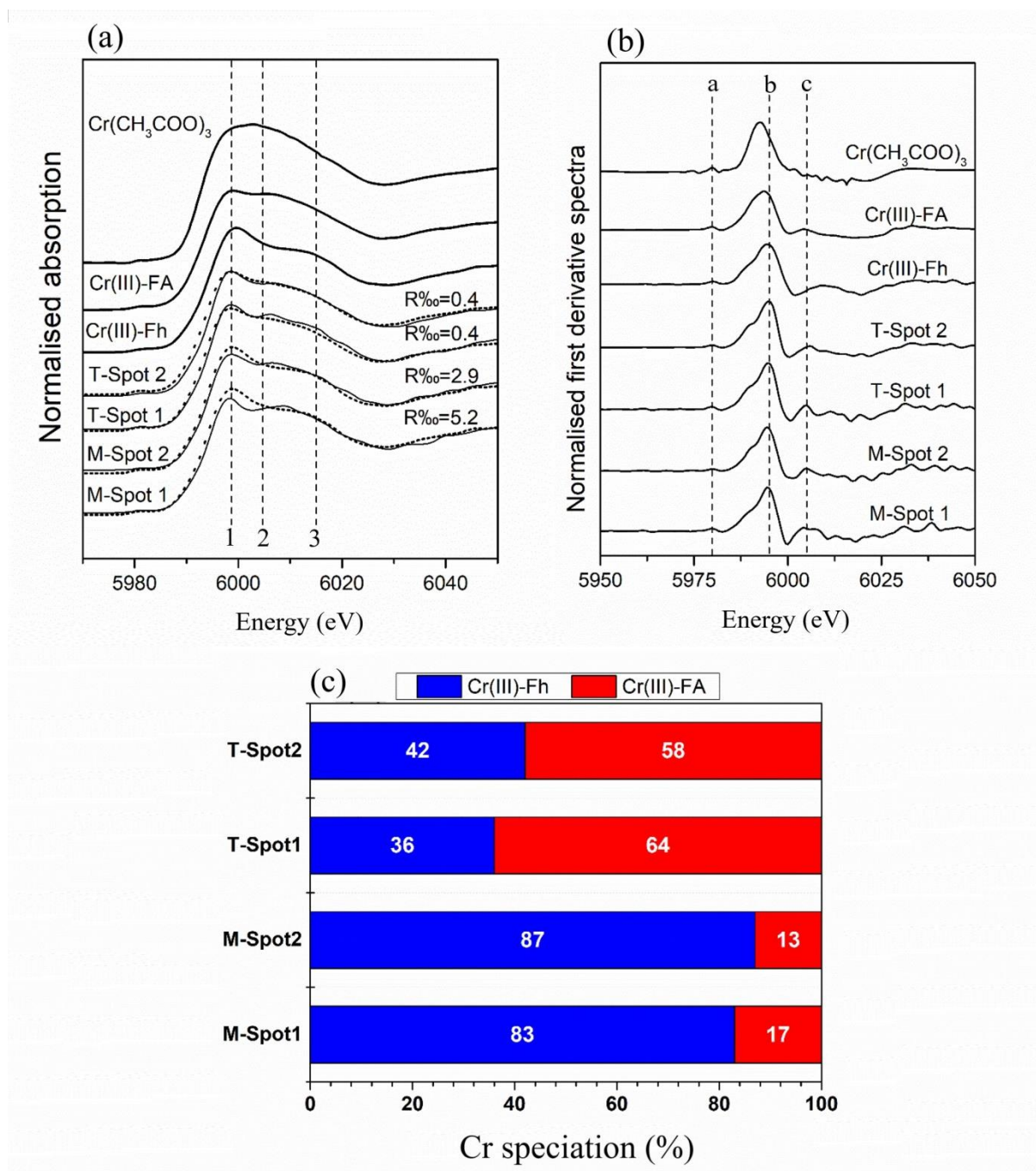


Figure 5

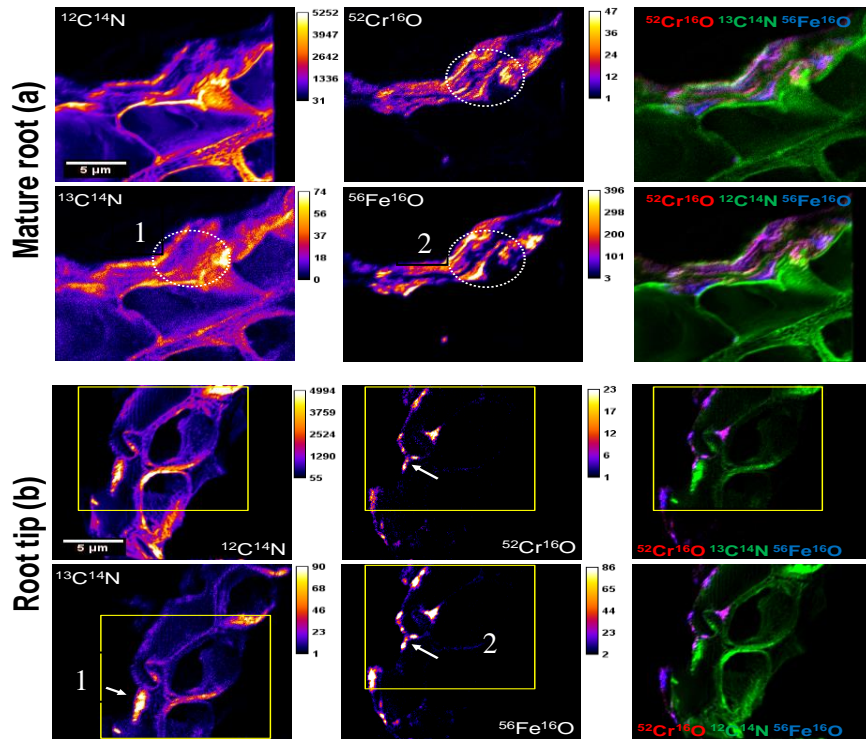
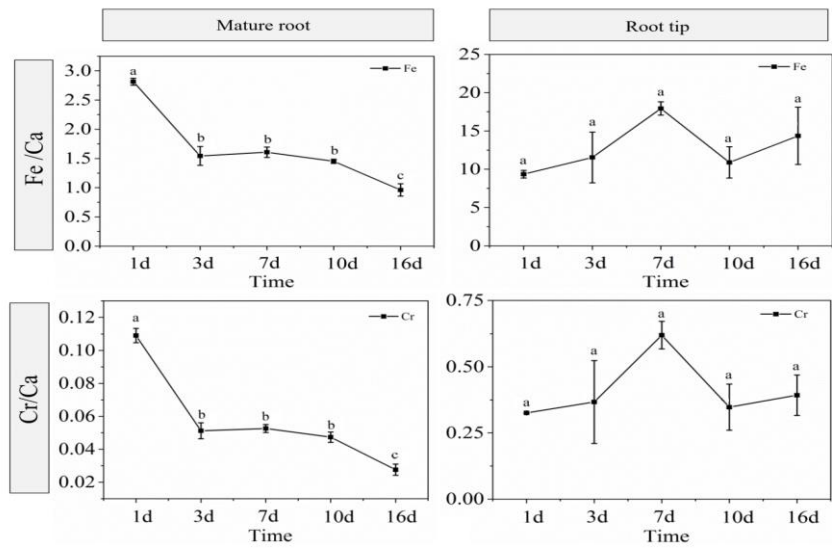


Figure 6





Click here to access/download
Supplementary Material
Supporting information (SI).docx



CRedit authorship contribution statement

#XX and PZ equally contributed to this work.

JY: designed the experiments. **XX** and **PZ**: performed the lab experiments with the kind guidance of **JY**. **JY**, **XX** and **PZ**: performed the XRF, XANES and SEM measurements and data analysis. **JY**, **JL**, **RL** and **CR**: conducted the NanoSIMS experiments. **JY**, **JL** and **XX**: performed the NanoSIMS data analysis. **PZ**, **XX**, **JY** and **JL**: analysed the data and drafted the manuscript. **JY**, **PZ**, **BE**, **ES** and **BBK**: participated in the interpretation of results. **JY**, **CR**, **RL**, **PZ**, **BE**, **ES** and **BBK**: improved the grammar and corrected spelling mistakes. **PZ**, **JY**, **XX**, **BE**, **BBK** and **ES**: edited and thoroughly revised the manuscripts. All authors read, corrected and approved the final submitted version of the manuscript.

Declaration of interests

The authors declare that they have no known competing financial interests or personal relationships that could have appeared to influence the work reported in this paper.

The authors declare the following financial interests/personal relationships which may be considered as potential competing interests: